

Cryo-electron tomographic and genetic analysis
of the actin-like MamK cytoskeleton during
magnetosome chain assembly and division of
Magnetospirillum gryphiswaldense

Dissertation
der Fakultät für Biologie
der
Ludwig-Maximilians-Universität München



vorgelegt von
Emanuel Katzmann
aus Sondershausen
München 2012

Die vorliegende Doktorarbeit wurde im Zeitraum von Oktober 2007 bis April 2012 an der Ludwig-Maximilians-Universität München und dem Max-Planck-Institut für Biochemie in Martinsried durchgeführt.

1. Gutachter: Prof. Dr. Dirk Schüler (Ludwig-Maximilians-Universität München)
2. Gutachter: Prof. Dr. Marc Bramkamp (Ludwig-Maximilians-Universität München)

Tag der Disputation: 16. Juli 2012

Publications originating from this thesis

CHAPTER 2

E. Katzmann, A. Scheffel, M. Gruska, J. M. Plitzko, D. Schüler (2010) Loss of the actin-like protein MamK has pleiotropic effects on magnetosome formation and chain assembly in *Magnetospirillum gryphiswaldense*. Mol Microbiol 77: 208.

CHAPTER 3

E. Katzmann, F. D. Müller, C. Lang, M. Messerer, M. Winklhofer, J. M. Plitzko, D. Schüler (2011) Magnetosome chains are recruited to cellular division sites and split by asymmetric septation. Mol Microbiol 82: 1316.

- Titel cover of Mol. Microbiol. magazine vol. 82
- Research highlight: Splitting a bacterial magnet. 2011. Nature 480: 416-417

Co-author publications

I

R. Uebe, K. Junge, V. Henn, G. Poxleitner, E. Katzmann, J. M. Plitzko, R. Zarivach, T. Kasama, G. Wanner, M. Pósfai, L. Böttger, B. Matzanke, D. Schüler (2011) The cation diffusion facilitator proteins MamB and MamM of *Magnetospirillum gryphiswaldense* have distinct and complex functions, and are involved in magnetite biomineralization and magnetosome membrane assembly. Mol Microbiol 82: 818.

II

A. Lohße, S. Ullrich, E. Katzmann, S. Borg, G. Wanner, M. Richter, B. Voigt, T. Schweder, D. Schüler (2011) Functional Analysis of the Magnetosome Island in *Magnetospirillum gryphiswaldense*: The *mamAB* Operon Is Sufficient for Magnetite Biomineralization. PLoS ONE 6: 1.

III

S. Kolinko, C. Jogler, E. Katzmann, G. Wanner, J. Peplies, D. Schüler (2011) Single-cell analysis reveals a novel uncultivated magnetotactic bacterium within the candidate division OP3. Environ Microbiol Ahead of Print: 1.

IV

I. Kolinko, C. Jogler, E. Katzmann, D. Schüler (2011) Frequent mutations within the genomic magnetosome island of *Magnetospirillum gryphiswaldense* are mediated by RecA. J Bacteriol 193: 5328.

V

R. Uebe, B. Voigt, T. Schweder, D. Albrecht, E. Katzmann, C. Lang, L. Böttger, B. Matzanke, D. Schüler (2010) Deletion of a fur-like gene affects iron homeostasis and magnetosome formation in *Magnetospirillum gryphiswaldense*. J Bacteriol.

VI

C. Jogler, W. Lin, A. Meyerdierks, M. Kube, E. Katzmann, C. Flies, Y. Pan, R. Amann, R. Reinhardt, D. Schüler (2009) Toward Cloning of the Magnetotactic Metagenome: Identification of Magnetosome Island Gene Clusters in Uncultivated Magnetotactic Bacteria from Different Aquatic Sediments. Appl Environ Microbiol 75: 3972.

Contributions to publications presented in this thesisCHAPTER 2:

E. Katzmann performed all experiments i. e. constructed the *M. gryph.* $\Delta mamK$ mutant, analyzed the mutant by cryo-electron tomography and transmission electron microscopy, performed biochemical analysis and wrote the manuscript together with D. Schüler.

CHAPTER 3:

E. Katzmann performed all experiments except for initial steps during time-lapse microscopy and cephalixin inhibitor concentration determination. E. Katzmann wrote the manuscript together with D. Schüler.

Co-author contributions**I**

E. Katzmann performed transmission electron microscopy analysis and cryo-electron tomography on $\Delta mamM$ and $\Delta mamB$ strains.

II

E. Katzmann performed transmission electron microscopy analysis and cryo-electron tomography on all mutant strains and constructed the $\Delta A15$ ($\Delta mamJKL$) mutant.

III

E. Katzmann performed transmission electron microscopy analysis on environmental samples.

IV

E. Katzmann performed transmission electron microscopy analysis on $\Delta recA$ mutant strain.

V

E. Katzmann performed transmission electron microscopy analysis on Δfur strain.

VI

E. Katzmann performed transmission electron microscopy analysis on magnetic enriched bacteria from an environmental sample.

Index

Publications originating from this thesis	I
<i>Co-author publications</i>	<i>I</i>
<i>Contributions to publications presented in this thesis</i>	<i>II</i>
Index	IV
Abbreviations	VI
Summary	1
Zusammenfassung	3
CHAPTER 1	5
Introduction	5
1.1 <i>Magnetotactic bacteria</i>	5
1.1.2 <i>Magnetospirillum gryphiswaldense</i> and <i>Magnetospirillum magneticum</i>	7
1.2 <i>Cell biology of magnetosome formation</i>	8
1.2.1 Structure and formation of magnetosome membrane (MM) vesicles	8
1.2.2 Magnetite biomineralisation	10
1.2.3 Magnetosome chain assembly	11
1.2.4 Genetics of magnetosome chain assembly	13
1.2.4.1 The magnetosome island and MamJ	13
1.2.4.2 MamK is a member of the actin-like protein family	15
1.3 <i>Cell division in bacteria</i>	20
1.4 <i>Cryo-electron tomography</i>	21
CHAPTER 2	24
2.1 <i>Manuscript:</i>	24
<i>Loss of the actin-like protein MamK has pleiotropic effects on magnetosome formation and chain assembly in Magnetospirillum gryphiswaldense</i>	24
2.1.1 Supporting information	42
CHAPTER 3	50
3.1 <i>Manuscript:</i>	50

<i>Magnetosome chains are recruited to cellular division sites and split by asymmetric septation</i>	50
3.1.1 Supporting information	65
CHAPTER 4	73
Discussion	73
4.1 <i>Temperature and oxidative stress affect chain formation</i>	73
4.2 <i>M. gryph. grows from midcell and divides into asymmetric daughter cells.</i>	74
4.3 <i>MamK participates in magnetosome chain recruitment and segregation</i>	76
4.4 <i>Cleavage, midcell-recruitment and relocalisation of the magnetosome chain is mediated by MamK.</i>	78
4.5 <i>Magnetosome chain and magnetosome filament are cleaved by asymmetric septation and snapping</i>	79
4.6 <i>Ultrastructural analysis of the magnetosome</i>	81
4.7 <i>An improved model of magnetosome chain assembly</i>	83
Outlook	86
References	88
Acknowledgements	97
Eidesstattliche Erklärung	99

Abbreviations

3D	<u>3</u> <u>d</u> imensional, 3 rd dimension
aa	<u>A</u> mino <u>a</u> cid
Alp	<u>A</u> ctin- <u>l</u> ike <u>p</u> rotein
<i>M. magnet.</i>	<i>Magnetospirillum magneticum</i> , strain AMB-1
ATP	<u>A</u> denosine-5'- <u>t</u> riphosphate
CAR	<u>C</u> entral <u>a</u> cidic <u>r</u> epeated (repeat, domain)
CDF	<u>C</u> ation <u>d</u> iffusion <u>f</u> acilitator (protein family)
CET	<u>C</u> ryo- <u>e</u> lectron <u>t</u> omography
CM	<u>C</u> ytoplasmic <u>m</u> embrane
CP	<u>C</u> ytoplasm
DIC	<u>D</u> ifferential <u>i</u> nterference <u>c</u> ontrast
et al.	et alii (lat.: and others)
FRET	<u>F</u> luorescence <u>r</u> esonance <u>e</u> nergy <u>t</u> ransfer
GTP	<u>G</u> uanosine-5'- <u>t</u> riphosphate
(e)GFP	(<u>e</u> nhanced) <u>G</u> reen <u>f</u> luorescent <u>p</u> rotein
LM	<u>L</u> ight <u>m</u> icroscopy
MTB	<u>M</u> agnetotactic <u>b</u> acteria
<i>M. gryph.</i>	<i>Magnetospirillum gryphiswaldense</i> , strain MSR-1
MS-1	<i>Magnetospirillum magnetotacticum</i> , strain MS-1
Mam(<i>mam</i>)	<u>M</u> agnetosome <u>m</u> embrane <u>a</u> ssociated
mms	<u>M</u> agnetosome <u>m</u> embrane <u>s</u> pecific
MAI	<u>M</u> agnetosome <u>i</u> sland
MC	<u>M</u> agnetosome <u>c</u> hain
MipZ	<u>M</u> id cell <u>p</u> ositioning of FtsZ
MV-1	<i>Magnetic vibrio</i>
MMP	<u>M</u> agnetic <u>m</u> ulticellular <u>p</u> rookaryote
MM	<u>M</u> agnetosome <u>m</u> embrane
Mb	<u>M</u> ega <u>b</u> yte
Mre	<u>M</u> ecillinam <u>r</u> esistance, actin-like protein
Nm	<u>N</u> anometer

ORF	<u>O</u> pen <u>r</u> eading <u>f</u> rame
PAGE	<u>P</u> oly <u>a</u> crylamid gel <u>e</u> lectrophoresis
Par	<u>P</u> artitioning
Pbp	<u>P</u> enicillin <u>b</u> inding <u>p</u> rotein
PDZ	Protein domain in <u>P</u> SD95, <u>D</u> lg1, <u>Z</u> o-1
pH	Negative decadic logarithm of proton concentration
PHB	<u>P</u> oly <u>h</u> ydroxy <u>b</u> utyrate, bacterial storage compound
pN	<u>P</u> ico <u>n</u> ewton
TEM	<u>T</u> ransmission <u>e</u> lectron <u>m</u> icroscopy
Tol-Pal	<u>T</u> olerant, transporter of group A colicin - <u>p</u> eptidoglycan <u>a</u> ssociated <u>l</u> ipoprotein; complex
WT	<u>W</u> ildtyp

Summary

Magnetotactic bacteria (MTB) possess the unique ability to align along geomagnetic field lines. This is possible due to intracellular magnetite particles biomineralised within vesicles. The entity of magnetite and vesicle forms the magnetosome which is the basic unit of the complex sub cellular structure the magnetosome chain. This magnetosome chain in turn aligns the individual magnetic moments of the magnetosomes to generate a torque sufficient to orientate the entire cell along the geomagnetic field. In this work one major constituent of the magnetosome chain, the magnetosome filament of *Magnetospirillum gryphiswaldense* was identified and characterised by use of special ultrastructural examination methods like the cryo-electron tomography (CET) and conventional transmission electron microscopy (TEM).

First, deletion mutagenesis of the actin-like MamK, which was hypothesised to form the magnetosome filament, resulted in $\Delta mamK$ cells with a lowered magnetic orientation behaviour and short (19 particles) magnetosome chains randomly localised within the cell. This is in contrast to the central, long (30 particles) chain in *M. gryph.* WT, which frequently showed neighboured (parallel chains) magnetosomes. CET examination of $\Delta mamK$ cells revealed that filaments could only be detected when *mamK* was expressed from a plasmid. This confirmed that the magnetosome filament is composed out of MamK proteins.

Since delocalised magnetosome chains were found in $\Delta mamK$ *M. gryph.* it was argued if MamK has a role in positioning of the magnetosome chain towards the cell centre. For this, a second detailed analysis to investigate the *M. gryph.* cell cycle and magnetosome chain formation was conducted. Here first time-lapse light microscopy data on *M. gryph.* showed an asymmetric cell elongation from midcell, which resulted in 15% length difference between the offspring. In consultation with previous observations (3) a cell buckling at the constriction site was observed. CET analysis of cells in different states of division showed an asymmetric septum formation at the centre of the magnetosome chain in *M. gryph.* so far unknown in bacteria. This septum started to constrict the entire cell and progression in division formed a wedge-like indenter on one site, opposite the magnetosome chain. Together with the resulting buckling of the entire cell and on-going asymmetric constriction the magnetosome filament (MamK) became split and the chain

thus divided into two equal parts. This was interpreted as a new mechanism to overcome the strong magnetic interaction forces within the magnetosome chain.

In order to study the fate of the divided, polar sub chains in the daughter cells, iron induction experiments on cell division arrested *M. gryph.* WT and $\Delta mamK$ cell were carried out. Surprisingly, these studies revealed that magnetosome chains concatenate at the arrested division sites in WT but not in $\Delta mamK$, once the magnetosome crystals have reached their mature size. This led to the hypothesis that MamK actively concatenates and assembles the magnetosomes to chains and recruits them to midcell in order to guarantee an equal distribution of the magnetic trait during cell division. In this thesis evidence is also given by initial bacterial Two-Hybrid studies, that indicated a link between proteins of the division machinery and the magnetosome chain.

Zusammenfassung

Magnetotaktische Bakterien (MTB) besitzen die einzigartige Fähigkeit sich entlang geomagnetischer Feldlinien auszurichten. Diese Eigenschaft wird ermöglicht durch intrazelluläre Magnetit-Teilchen, die innerhalb von Vesikeln biomineralisiert werden. Die Einheit aus Magnetit und Vesikel bildet das Magnetosom, welches die grundlegende Komponente der komplexen, subzellulären Struktur - der Magnetosomenkette ist. Diese Magnetosomenkette summiert die einzelnen magnetischen Momente der Magnetosomen so, dass es ausreicht um die gesamte Zelle entlang des Erdmagnetfeldes auszurichten.

Als Hauptbestandteil dieser Arbeit sollte die Magnetosomenkette und das Magnetosomenfilament in *Magnetospirillum gryphiswaldense* durch die Verwendung spezieller Untersuchungsmethoden wie der Kryo-Elektronen-Tomographie (engl. CET) und konventioneller Transmissionselektronenmikroskopie (TEM) identifiziert und charakterisiert werden.

Zuerst wurde Deletionsmutagenese an dem Aktin ähnlichen Protein MamK von *M. gryph.* durchgeführt, von dem angenommen wurde, dass es das Magnetosomenfilament bildet. In $\Delta mamK$ *M. gryph.* Zellen wurde ein verringertes magnetisches Orientierungsverhalten und mehrere, kurze (19 Partikel) Magnetosomenketten, zufällig innerhalb der Zelle lokalisiert, aufgefunden. Dies steht im Gegensatz zu der zentralen, langen (30 Partikel) Kette des *M. gryph.* WT, die außerdem häufig benachbarte (parallele) Ketten aufwies. CET Untersuchungen an $\Delta mamK$ Zellen zeigten, dass nur dann Filamente detektiert werden konnten, wenn *mamK* von einem Plasmid exprimiert wurde. Dies bestätigte, dass das Magnetosomenfilament in *M. gryph.* aus MamK Proteinen besteht. Darüber hinaus wurden weniger Vesikel in der $\Delta mamK$ Mutante gefunden als im WT, was Anhaltspunkte für eine mögliche Verbindung zwischen MamK und der Magnetosomenbildung gab. Da $\Delta mamK$ *M. gryph.* delokalisierte Magnetosomenketten aufweist, konnte eine dynamische Funktion von MamK bei der Positionierung der Magnetosomenkette in Richtung Zellemitte vermutet werden.

Eine zweite, detaillierte Analyse untersucht in dieser Arbeit den Zusammenhang des *M. gryph.* Zellzyklus mit der Magnetosomenketten Bildung. Hierfür wurde zum ersten Mal

Zeitkurs Lichtmikroskopie an *M. gryph.* durchgeführt und es zeigte sich ein asymmetrisches Wachstum von der Zellmitte, welches einen 15% Längenunterschied zwischen den Nachkommen zur Folge hatte. In Einklang mit früheren Beobachtungen (3), dass *M. gryph.* Zellen im Bereich der Teilungsebene einknicken, wurde eine weitergehende, gründliche ultrastrukturelle Analyse von Zellen in verschiedenen Stadien der Teilung mittels CET durchgeführt. Diese zeigte eine asymmetrische Ausbildung des Teilungsseptums in der Mitte der Magnetosomenkette von *M. gryph.* Dieses Septum verengte die gesamte Zelle in der Mitte und bei fortschreitender Zellteilung bildete sich eine keilförmige Peptidoglykaneinstülpung auf der gegenüberliegenden Seite der Magnetosomenkette aus. Zusammen mit dem Einknicken des gesamten Zellkörpers und der asymmetrischen Verengung wurde das Magnetosomenfilament (MamK) und damit die Kette in zwei gleiche Hälften geteilt. Die beobachtete Asymmetrie wurde als ein neuer Mechanismus interpretiert, um die starken magnetische Wechselwirkungen innerhalb der Magnetosomenkette zu überwinden. Zur Untersuchung des Schicksals der geteilten, polaren Subketten in den Tochterzellen, wurden Experimente mittels Eiseninduktion an in der Zellteilung gehemmten *M. gryph.* WT und $\Delta mamK$ Zellen durchgeführt. Überraschenderweise zeigten diese Studien, dass die Magnetosomenketten an den Teilungsebenen im WT lokalisierten, sobald die Magnetosomenkristalle ihre reife Größe erreicht hatten, dies aber nicht in der $\Delta mamK$ geschah. Das führte zu der Vermutung, dass MamK aktiv die Magnetosomen in der Zellmitte sammelt und verkettet, um eine gleichmäßige Verteilung der magnetischen Eigenschaften während der Zellteilung zu gewährleisten. In dieser Arbeit wurden auch Hinweise durch anfängliche Studien mittels bakteriellem Zwei-Hybrid Experimenten gegeben, die auf eine Verbindung zwischen Proteinen des Teilungsapparates und der Magnetosomenkette schließen lassen.

CHAPTER 1

Introduction

1.1 Magnetotactic bacteria

Antoni van Leeuwenhoek built the first light microscope in the 17th century able to observe bacterial cells (4). With that he laid the foundation to study bacterial structures. Over the following centuries, different prokaryotic morphologies (e. g. cocci, spirilla and rods) were discovered. However, only very recently it became evident that bacteria are not simple bags of enzymes and contain functional units like the flagella and by increase of resolution in microscopy techniques, organelles and a cytoskeleton.

One particularly intriguing example of bacterial organelles is found in the group of magnetotactic bacteria (MTB). This diverse group was first described in 1963 by Salvatore Bellini (5) and independently rediscovered by Richard Blakemore (6). Both observed bacteria which accumulated under the microscope at only one site of the sample when exposed to an external magnetic field. MTB comprise a group of physiologically and morphologically heterogeneous prokaryotes and belong to different phyla like Proteobacteria, Nitrospirae and the uncultivated candidate division OP3 (7). The natural habitats of MTBs are aquatic environments and their preferred ecological niches are neutral or weak alkaline with microoxic or anoxic conditions as well as the presence of a soluble iron pool (8, 9). On-going ultrastructural and biochemical examination revealed that many of these bacteria possess intracellular membrane enveloped bacterial organelles with natural ferrimagnetic magnetite (Fe_3O_4) crystals – the magnetosomes. The morphology of the magnetite crystal depends on the species and most common types are cuboctahedric, elongated-prismatic and bullet-shaped crystals. These magnetite crystals were mostly found to be assembled into a chain, thereby enabling the MTB to passively align along the geomagnetic field lines (10, 11) (Figure 1).

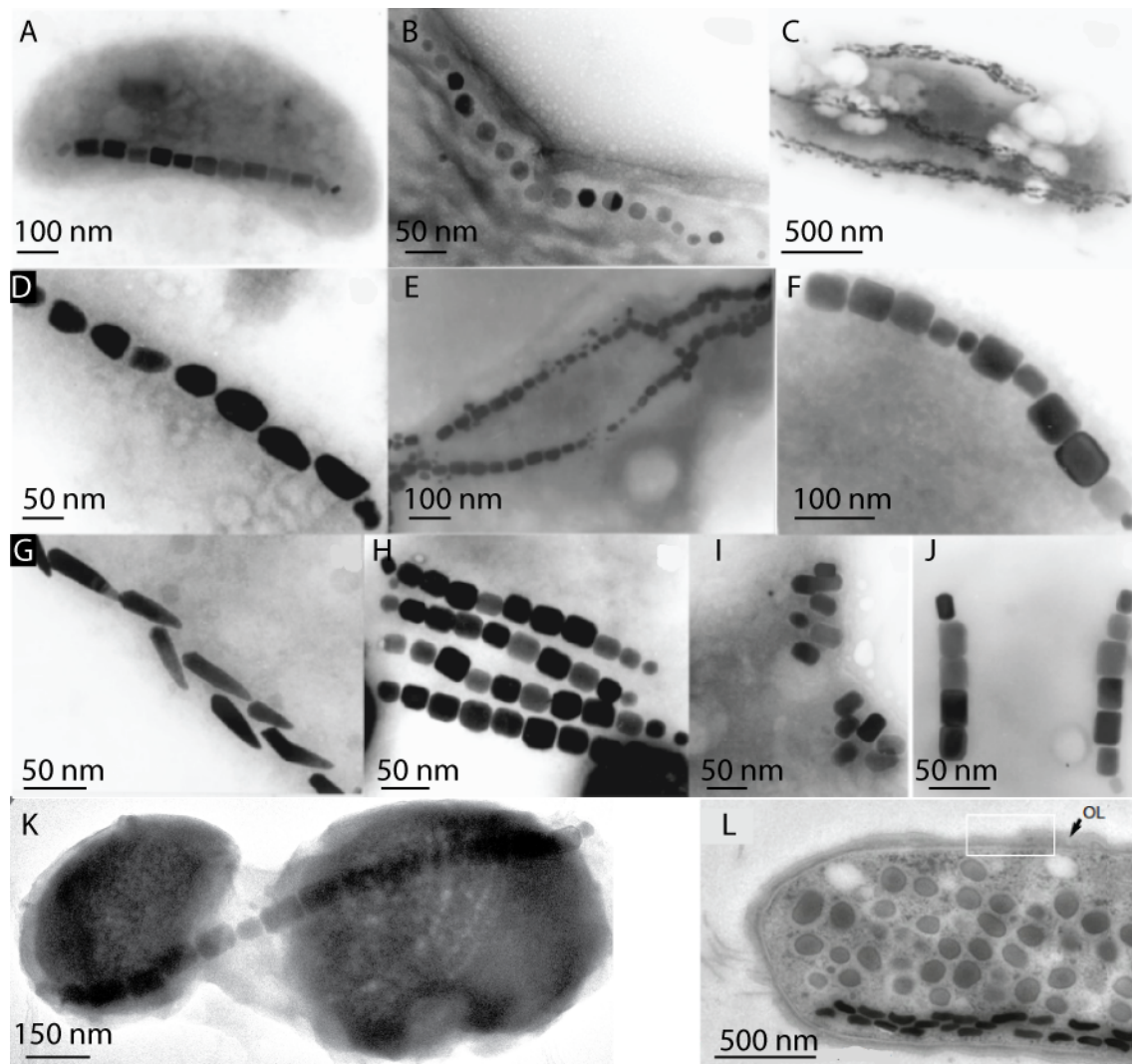


Figure 1: TEM micrographs of various magnetosome chain configurations. Most prominent crystal shapes in MTBs are elongated prisms (A, E, F, H, I, J, K), cubo-octahedral (B), and bullet-shaped morphologies (C, D, G, L). Crystals can be arranged in single or multiple chains. Modified from (12). Magnetic enrichment of cocci melon-shaped cell (K) (7) and *Magnetobacterium bavaricum* (L) adapted from (13).

This magnetic orientation reduces the dimensionality of the chemo-aerotactic navigation and efficiently allows MTB to migrate towards their favoured habitat (14).

Genetic analysis of magnetosome formation became possible only during the last 10 years, however, today draft and complete genome sequences are available from five MTBs. This information paved the way to gather detailed knowledge of the structure and function of these microorganisms at a molecular level. Despite their heterogeneity, MTB seem to share a common set of genes organised in a single genomic region, the magnetosome island (MAI), which encodes the major proteins involved in magnetosome biogenesis and chain formation (15, 16).

Recently, some of the functions these proteins have in the formation of the bacterial organelles were elucidated (17, 18). However, little was known about the dynamic

processes governing the formation and partition of magnetosome chains during cytokinesis (3, 19).

1.1.2 *Magnetospirillum gryphiswaldense* and *Magnetospirillum magneticum*

To study magnetosome chain formation only a few cultivable MTB like the magnetospirilla strains are available. Most of what is known originates from studies of two strains which can be genetically manipulated. *M. gryph.* was isolated from the sediment of the river Ryck near Greifswald (Germany) in 1990 (20) and can be cultured in the laboratory up to high densities (21). This gram-negative alphaproteobacterium is spirilla-shaped and bipolar monotrichously flagellated. It is 3-5 μm in length and on average 500 nm in diameter (Figure 2). *M. gryph.* grows chemo-organoheterotrophically and utilises different organic acids with oxygen or nitrogen as terminal electron acceptor (22).

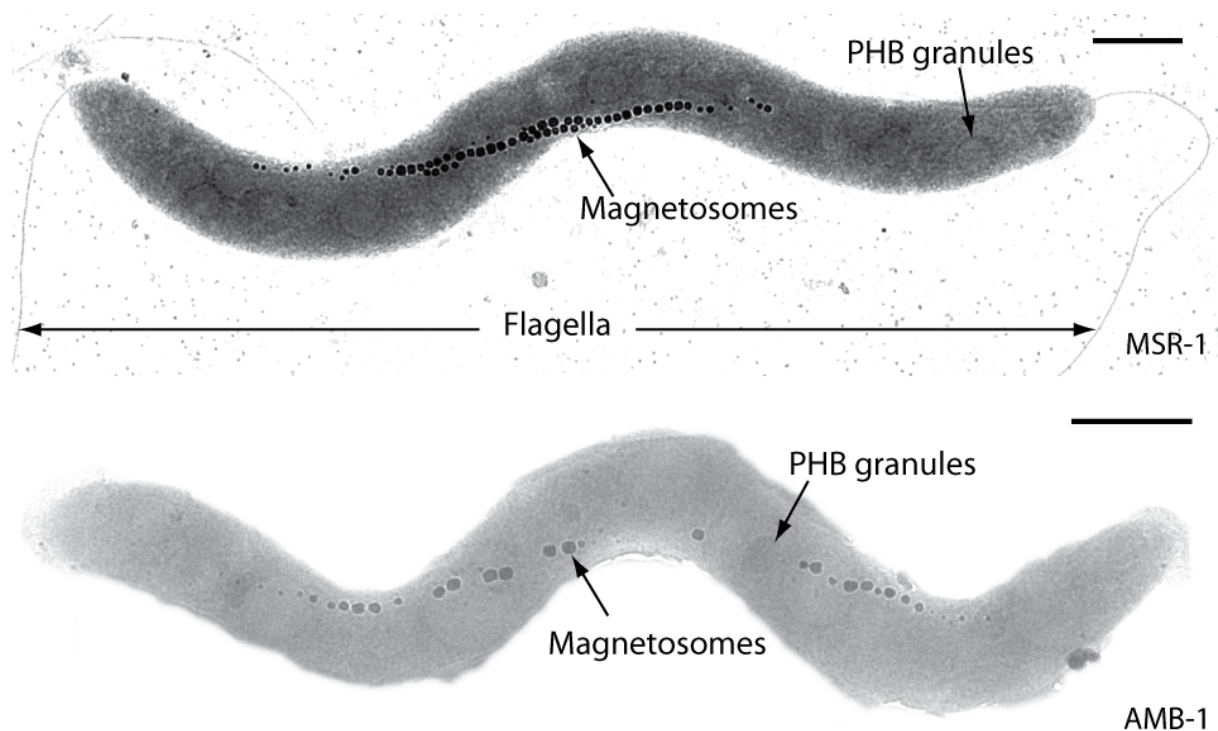


Figure 2: A: *Magnetospirillum gryphiswaldense* MSR-1 cell, PHB: polyhydroxybutyrate. B: *Magnetospirillum magneticum* AMB-1 cell. Scale bar, 500 nm.

The magnetite crystals of *M. gryph.* are cuboctahedric and assemble into a chain, which comprises 30 - 40 magnetosomes. The arrangement into chains sums up the magnetic moments of the individual magnetosomes and enhances the magnetic orientation.

The draft genome of *M. gryph.* has 4268 predicted open reading frames (ORF) and is 4.26 Mb in size (23). A genetic system was developed, which enabled genetic manipulation of *M. gryph.* (24, 25). Although still tedious, this allows chromosomal insertions, deletion mutagenesis as well as recombinant protein expression. Up to date ~26 single gene deletions and ~18 gene fragment or cluster mutants of *M. gryph.* were generated in this and other laboratories. The second well-characterised strain is *Magnetospirillum magneticum* (Figure 2B), which shares 52% of the annotated ORFs of *M. gryph.* Despite their morphological similarities, both organisms differ in certain aspects: (i) *M. magnet.* is non-motile (95% of culture) (26), (ii) it exhibits larger crystals (48 nm in *M. magnet.* vs. 35 nm in *M. gryph.*) (27, 28) and (iii) it has a more widely spaced magnetosome distribution than observed for *M. gryph.*

1.2 Cell biology of magnetosome formation

Formation of functional magnetosome chains includes three key steps: (i) invagination of the magnetosome vesicle from the cytoplasmic membrane (CM), (ii) transport and biomineralisation of the magnetite in the magnetosome membrane (MM) vesicles and the (iii) assembly of crystals into a coherent linear chain. In the following, knowledge on all steps will be described with major focus on the assembly of magnetosomes into chains, as it is the central aim of this work.

1.2.1 Structure and formation of magnetosome membrane (MM) vesicles

Organelles are defined as compartments bounded by a biological membrane with dedicated specialised biochemical functions. Magnetosomes are an entity of magnetite crystal and lipid bilayer, thus can be considered as true organelles within a bacterial cell (29).

Freeze-etching experiments and subsequent TEM analysis on cells of *Magnetospirillum magnetotacticum* MS-1 revealed convex protrusions and cup-shaped depressions which were interpreted to be the magnetosome lipid bilayer encapsulating the magnetite crystal. The thickness of the vesicle membranes was 3 - 4 nm and thus within the size of the cytoplasmic membrane (CM), where this lipid bilayer was speculated to originate from (30). A recent study in *Desulfovibrio magneticum* RS-1 argued that the bullet-shaped crystals contain no MM at all, since they were not able to detect a crystal

enveloping structure (31). However, an earlier study investigating MM fractions of RS-1 (32) revealed a couple of magnetosome membrane (Mam) specific proteins like MamA, MamK and MamM. On the other hand, a sheath-like structure surrounding the magnetosomes was described in various uncultivated MTB strains. This magnetosomal matrix was speculated to be a semicrystalline gel and between 20 - 70 nm in thickness depending on the strain. Several functions were assigned to the matrix e.g. as a template for precipitation of pre-magnetite, to chelate Fe^{2+} or in controlling the chemiosmotic properties of the solution around the crystal (33, 34). However, the existence of this matrix has not been confirmed yet by ultrastructural examination or other visualisation methods. Biochemical analysis of the MM, CM, cytoplasm (CP) and outer membrane (OM) of *M. gryph.* revealed a similar phospholipid composition between MM and CM and a set of at least 18 specific proteins which are magnetosome membrane associated (16, 35). Mössbauer spectroscopy studies in MS-1 already suggested that magnetosomes might originate from the inner membrane by 'invagination' (36). Later, iron starved *M. magnet.* cells analysed by cryo-electron tomography (CET) clearly showed vesicles, which were associated with the cytoplasmic membrane (CM) and showed bulb-like budding of the inner membrane towards the cytoplasm harbouring either mature or immature magnetite crystals (Figure 3)(1).

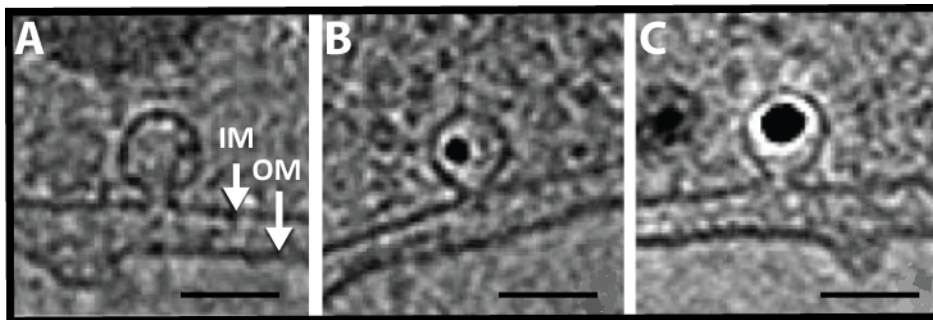


Figure 3: X-y projections of cryo-electron tomogram sections of *M. magnet.* cell membranes. (A-C): Membrane bound vesicles of *M. magnet.* tomogram section adapted from (1). IM and OM: inner and outer membrane, respectively. Scale bar, 50 nm

Extensive mutagenesis studies in *M. magnet.* led to a more detailed model for step-wise assembly of the magnetosomes in which the first step describes the invagination controlled by the four proteins MamI, MamL, MamQ and MamB (also present in *M. gryph.*)(17). MamB is a protein belonging to the cation diffusion facilitator (CDF) transporter superfamily. MamQ has some similarity to LemA, which has unknown

functions. MamI and MamL are MTB specific, but no homologues were found in other bacteria with known functions.

Tomograms of the *M. gryph.* triple $\Delta mamJKL$ ($\Delta A15$) mutant, generated earlier in this study, were devoid of magnetosome vesicles, which led to the conclusion that MamL is necessary for vesicle genesis in *M. gryph.* too (18, 37). MamL was neither detected in the proteomic analysis of the magnetosome membrane in *M. magnet.* nor *M. gryph.* possibly due to its small size of 91 amino acids (aa). However, a MamL-GFP fusion expressed in *M. magnet.* was suggested to be transiently associated with the magnetosomes and 15 amino acids of the MamL C-terminal are predicted to form a helix. Membrane bending is suggested to occur by interaction via the positively charged residues of MamL with the cytoplasmic site of the inner membrane. The control of vesicle size and shape in MTB is unknown although $\Delta mms6$ and $\Delta mamGFDC$ operon mutants showed defects in crystal as well as vesicle size in *M. gryph.* (18, 27). In *M. magnet.* MamY may have tubulation effects on the vesicle shape and might be involved in the pinch-off of the vesicles, however, in *M. gryph.* a *mamY* deletion did not interfere with the vesicle formation or morphology instead, surprisingly, affected the magnetosome chain localisation (24, 38).

1.2.2 Magnetite biomineralisation

Magnetotactic bacteria contain > 3% iron as measured per dry weight, which is several orders of magnitude higher than in non-magnetotactic bacteria (39). Magnetite is preferentially formed under alkaline (pH > 8) and slightly reducing ($E^0 \sim -0.2$ to -0.4) conditions (40). To provide these conditions, biomineralisation occurs within magnetosome vesicles, since the physiological properties of the cytoplasm and periplasm are unlikely for iron supersaturation and thus magnetite formation. In order to initialise magnetite biomineralisation in *M. gryph.* a low O_2 partial pressure of 20 mbar and addition of 15 - 20 μM iron for saturating concentrations is required (21, 41). High amounts of iron are suggested to be taken up by three different systems in an energy dependent or independent process (42-45).

Several proteins were implicated in magnetite biomineralisation and beside MamB another CDF transporter protein MamM is necessary. Both, MamM and MamB were shown to be crucial for magnetite formation, where MamM stabilises MamB and this in addition is required for vesicle formation (46).

MamE is a putative trypsin-like serine protease with a PDZ protein interaction domain participating in magnetosome protein recruitment. MamN, a putative H^+ - antiporter

involved in vesicle pH regulation, and MamO, a speculated serine protease, seem to affect magnetite crystal formation (29, 47).

The proteins MamGFDC, Mms6 and MamPRST control magnetite size and preliminary experiments include MamH, MamH-like and MamX proteins to affect magnetite and magnetosome formation in *M. gryph.* (17, 18, 24, 27).

1.2.3 Magnetosome chain assembly

Why do MTB align their individual crystals into chains? First assumptions explained chain-like magnetosome alignment in bacteria with an advantage over other bacteria in order to find their specific habitat and nutrition. This is accomplished by a passive torque which results from the interaction of the geomagnetic field with the intracellular magnetosome chain (MC) and aligns the bacterial cell to give it a swimming direction (6, 48-50).

There is a variety of chain configurations found within MTBs ranging from a single chain, two chains per cell to multiple rosetta-like bundles and magnetosome clusters (13, 51-55) (Figure 1). The MCs typically extend along the long axis of the cell body. Their position with respect to cell diameter, however, largely depends on the individual cell shape, but is usually close to the inner membrane (Figure 1 and 2).

The physical properties of the magnetosomes were examined to understand how a line up of magnetosomes into a chain is possible. Assembly into chains sums up their magnetic moments and generates a sufficient strong magnetic dipole to align MTB parallel along the geomagnetic field. (53). This results in permanent natural magnetisation approaching the saturation magnetisation. Further, Frankel *et al.* (1980) observed that a chain of 22 cuboctahedric 50 nm^3 magnetosomes would have a magnetic dipole moment sufficient for cell orientation along the geomagnetic field at ambient temperature (11, 56). Later, Simpson determined by electron holography 10 magnetosomes in a chain to be sufficient for magnetic navigation in *M. gryph.* based on the same modelling according to the Langevin function (57). Magnetite crystals of *M. gryph.* with a diameter of $\sim 30 \text{ nm}$ are single domain crystals and the magnetic moment of the equant crystal will be parallel along one of the [111] axes i. e. the easy direction of magnetisation. This direction gives the magnet the largest net magnetic moment per volume possible (53). TEM holography studies revealed that in magnetospirilla mature magnetosome crystals are flanked by immature superparamagnetic (below 20 nm)

magnetite crystals. These small crystals became magnetised by their larger neighbours and recruited towards the ends thus assembling the magnetosomes into a chain (55).

A recent study suggested a further level of chain assembly, where individual magnetite particles had to be biologically controlled arranged in a certain orientation within the MC in order to generate the magnetic dipole (52). Another prerequisite to transmit the torque exerted by the magnetic field is the fixation of the entire MC within the cell. Initial Mössbauer spectroscopy experiments on magnetosome dynamics, which measured the translational motion (position change) and free rotation within whole MS-1 cells, suggested that the magnetosomes must be tightly anchored by biological structures (58).

1.2.4 Genetics of magnetosome chain assembly

1.2.4.1 The magnetosome island and MamJ

Two genes are known to contribute in magnetosome chain assembly: MamJ is part of the magnetosome island (MAI) and encoded by the *mamAB*-operon.

The only part of the MAI essential for magnetite biomineralisation is the *mamAB*-operon, whereby the *mamGFDC*-operon is involved in size control of the magnetite and the *mms6*-operon in crystal shape (18, 27).

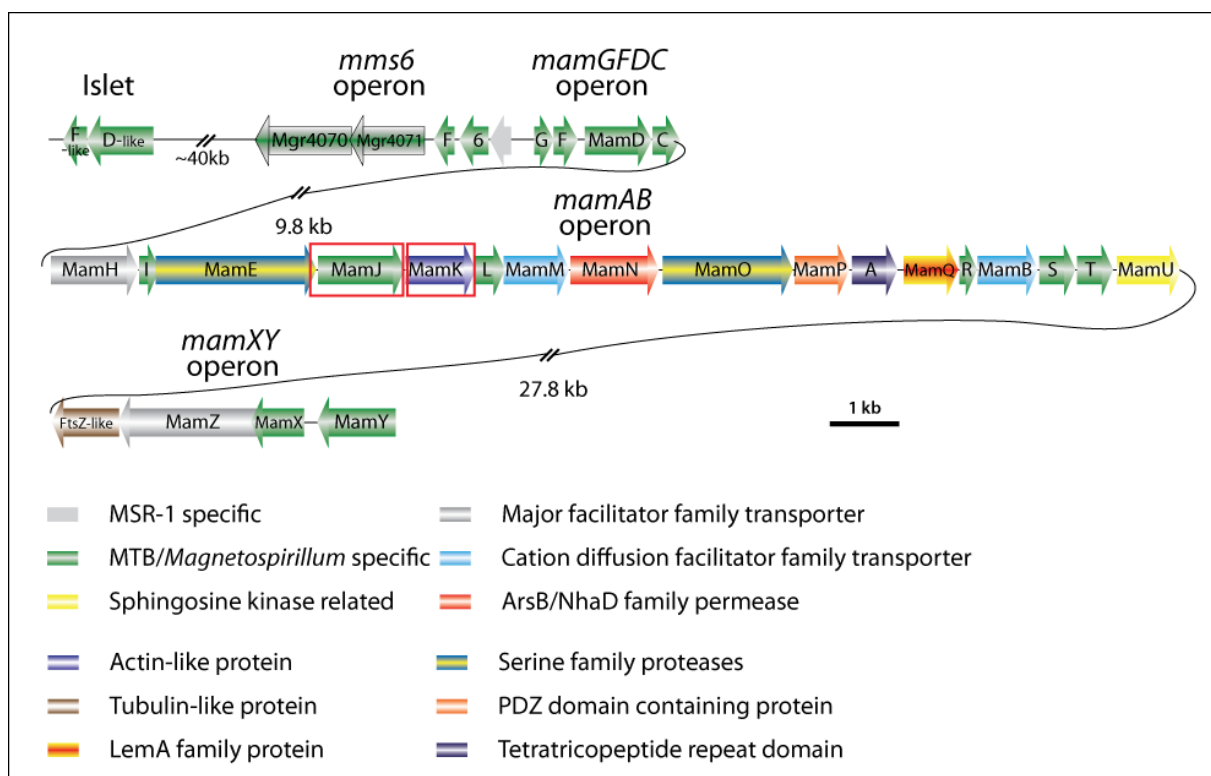


Figure 4: Schematic overview of the magnetosome island (MAI) in *M. gryph.* Gene organization is depicted by arrows and individual colours represent corresponding protein families. Red boxes highlight the MamJ and MamK proteins.

The *mamAB*-operon consists of 17 genes, but only a few of them are characterised in detail. Other members of the *mamAB*-operon have only assigned or putative functions in *M. gryph.*, but bioinformatic sequence analysis classified them into different protein families (Figure 4). In addition, an islet outside the MAI of *M. magnet.* comprising seven

genes with homology to *mamK*, *D*, *L*, *Q*, *E*, *F* and *mamJ* was recently detected in *M. magnet.* (59) and smaller in *M. gryph.* (R. Uebe, personal communication).

MamJ has an acidic isoelectric point (pI) value of 4.1 and a molecular weight of 44.3 kDa. It was previously thought to be involved in magnetite formation, but instead found to be essential for the line-up of magnetosomes in *M. gryph.* (2). MamJ is 426 amino acids (aa) in length and comprises a suspicious central acidic repetitive (CAR) domain containing Glu- and Pro-rich motives (ncbi protein id: CAE12033.1), followed by an Ala-rich and Gly-rich domain at the C-terminus. Deletion of *mamJ* in *M. gryph.* resulted in clusters of magnetosomes randomly arranged within the cell (Figure 5B), whereas the number and size of the magnetite crystals was not affected (2). Several truncations of MamJ revealed that only the first 45 N-terminal aa, 25 aa in between the Ala- and Gly-rich domain and 40 aa of the C-terminal end were essential to restore WT-like MC formation in Δ *mamJ*. Deletion of the suspicious CAR domain, surprisingly, had no effect on MC formation when expressed in Δ *mamJ* mutant (60). So far homologos of MamJ proteins have been only indentified in other magnetospirilla: two MamJ proteins are present in MS-1 (Magn03009039 and Magn03008112) and three in *M. magnet.*: MamJ (misannotated as TonB, amb0964), LimJ (amb1003, a moderately conserved MamJ paralogue) and a MamJ-like (position 440939 - 439811 in NC_007626.1)(59, 61). Both MamJ orthologues of MS-1 and *M. magnet.* display a high similarity (MamJ_{*M. magnet.*}/Magn03009039 and LimJ/Magn03008112), whereas MamJ-like of *M. magnet.* is more closely related to the MamJ of *M. gryph.* Furthermore, all six MamJ proteins share two common domains: the N-terminal DXWX₂LLX₂SPWS and the C-terminal VPVEX₄GXFX₂AXSA. MamJ_{*M. gryph.*} is assumed to interact direct or in case of MamJ_{*M. magnet.*} more indirect with the actin-like MamK protein (60, 61).

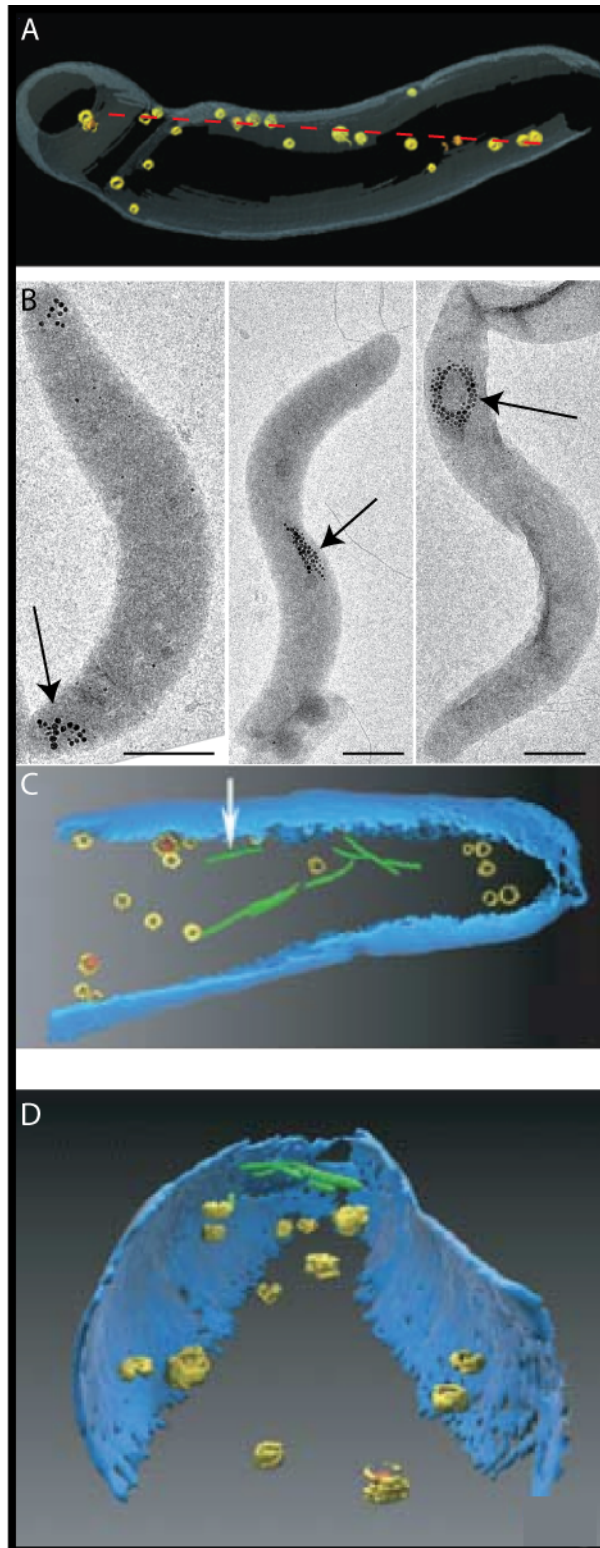


Figure 5: Micrographs and segmented tomograms of $\Delta mamJ$ *M. gryph.* and $\Delta mamK$ *M. magnet.* (A) Segmented tomograms of $\Delta mamK$ *M. magnet.* adapted from (1), dashed red line indicates uniaxial magnetosome localisation. (B) TEM micrographs of $\Delta mamJ$ *M. gryph.* cells, arrows indicate rings and clusters of aggregated magnetosomes. Scale bar 500 nm. (C and D) CET tomograms of $\Delta mamJ$ *M. gryph.* adapted from (2). Green: filaments, yellow: vesicles, red: magnetite, blue/grey: cell envelope.

1.2.4.2 MamK is a member of the actin-like protein family

The second gene participating in magnetosome chain assembly is located directly downstream of *mamJ* and termed *mamK*. MamK of *M. gryph.* is 348 aa in length with a molecular weight of 37.6 kDa and a pI of 5.4. This protein family branches within the family of actin-like proteins (Alps) (62, 63), is highly conserved in magnetotactic alphaproteobacteria and homologous are present in all MTB (Figure 6). Some MTBs even possess multiple MamK proteins, as described for *M. magnet.* (59). The homology of MamK to Alps like MreB, the major component of the bacterial cytoskeleton involved in cell elongation, cell shape control and division, made it a likely candidate for studying chain assembly and integrity.

To investigate MamK function *M. magnet.* and *M. gryph.* cells were examined by cryo-electron tomography (CET) in two independent studies (1, 2). The *mamK* gene was first deleted in *M. magnet.* and resulted in an absence of filamentous structures, which were found in WT cells running in parallel to 4 - 5 magnetosomes with a length of 200 - 250 nm. The deletion of *mamK* led to scattered or

loosely arranged magnetosomes in groups of 2 - 3 individual particles, however, the groups can still be aligned along an imaginary common axis in the data presented (1) (Figure 5A, red dashed line). In a parallel CET study on *M. gryph.* by Scheffel *et al.* (2006) (Figure 5C-D) filamentous structures were also revealed in WT and $\Delta mamJ$ cells. These filaments were 3 - 4 nm in diameter and speculated to be formed by MamK which supposedly acts as cytoskeletal scaffold of the magnetosome chain (MC) to which MamJ might attach the magnetosomes (2). Based on the results by Komeili *et al.* and Scheffel *et al.* (2006) two different models of MC formation for *M. gryph.* and *M. magnet.* were postulated.

In *M. magnet.* the magnetosome vesicles invaginate from the inner membrane and the magnetite crystals form within the attached vesicle (Figure 3). These vesicles are already aligned into a chain independent of iron presence and stay in continuous contact with the inner cytoplasmic membrane.

In the *M. gryph.* model of MC formation empty vesicles are scattered throughout the entire cell and then aligned into a chain-like structure, whereby the fate of the vesicles (membrane bound or not) remained uncertain. Scheffel *et al.* (2006) were not able to detect membrane bound vesicles in their study, thus the invagination hypothesis was not experimentally proven for *M. gryph.* Once small vesicles have formed, on-going magnetite biomineralisation in individual, scattered magnetosomes results in their MamJ mediated chain-like arrangement along MamK filaments. How this arrangement is accomplished in *M. gryph.* is a subject matter and one question of this work.

A first fusion of MamK to GFP in *M. gryph.* was analysed by Schübbe *et al.* (64), where a linear signal was detected and speculated to be magnetosome associated. Linear MamK-GFP signals were also detected in other MTB like *M. magnet.* or in the non-magnetic mutant *M. gryph.* MSR-1B. Pradel *et al.* (2007) concluded that MamK is able to form filaments in *E. coli* and in areas without magnetosomes of *M. magnet.* Time-lapse studies of dual fluorescently labelled MamK expressed in *E. coli* demonstrated further that MamK nucleates at multiple sites and assembles into mosaic filaments *in vivo* (65). Moreover, they showed that MamK undergoes dynamic polymerisation and that one end co-localizes with the *Shigella* outer membrane protein and polar marker IcsA (VirG) in spherical $\Delta mreB$ *E. coli* cells (66). In another study by Taoka *et al.* (2007) experiments with a MamK antiserum revealed a cytosolic localisation. *In situ* and *in vitro* studies showed a polymerisation of MamK into filamentous bundles of 8 - 18 nm in diameter (Figure 6C). These bundles were composed of MamK protofilaments with 6 nm in

diameter. Addition of γ -ATP to MamK was required for this polymerisation, whereas the presence of ATP only generated stable monomers i. e. non-dynamic filaments (59, 67). The protein has 5 ATP binding sites: T33, D174, D181, E232 and G302 (CDD analysis of annotated MamK (68)). The overall abundance of MamK molecules in *M. magnet.* was determined to be 5 times higher than for MreB (26.000 vs. 5000 copies per cell) (67). Prediction of MamK_{*M. gryph.*} molecule structure in this study based on homology revealed similarity to the structure of MreB from *Thermotoga maritima* (Figure 6D).

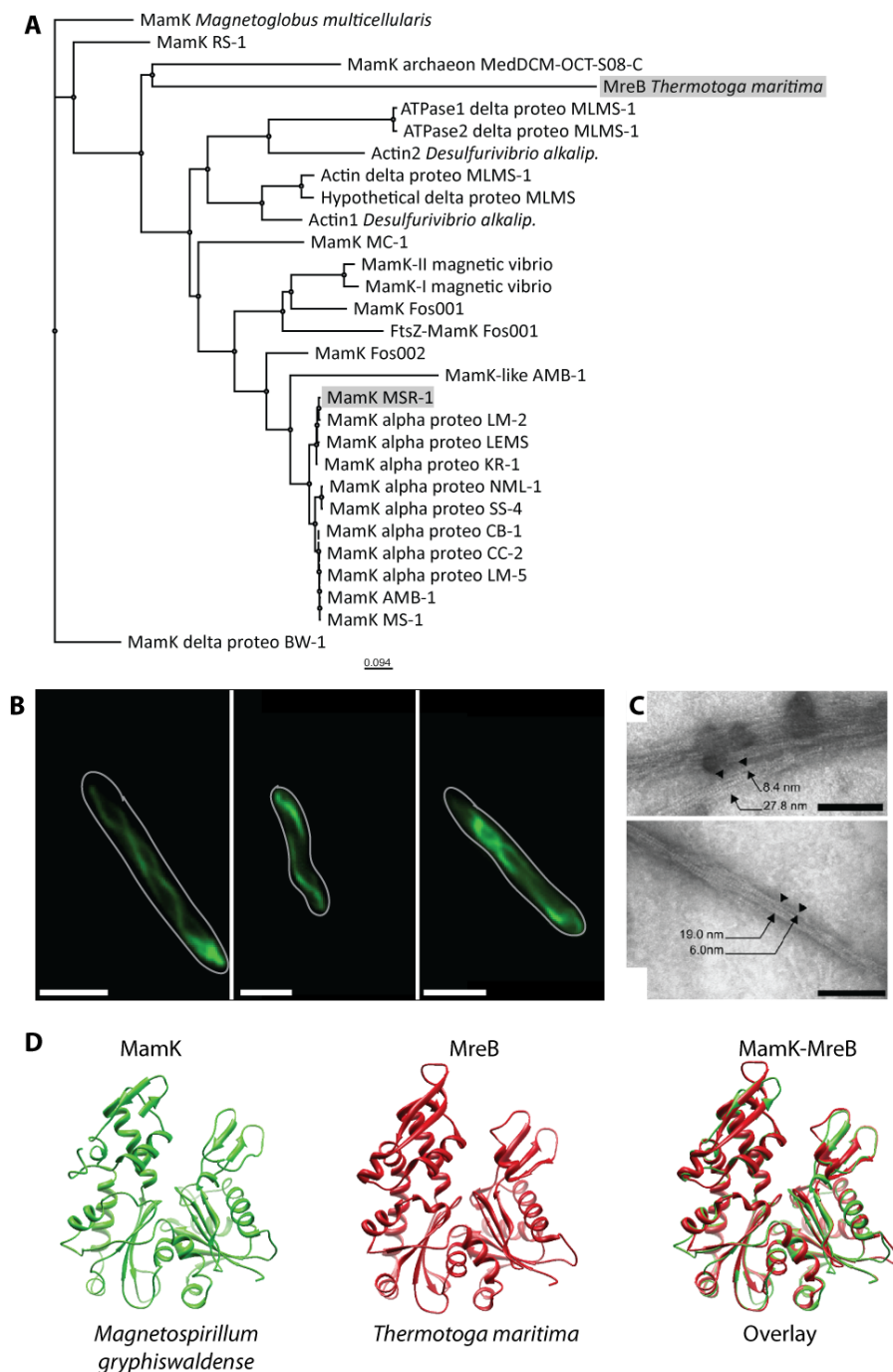


Figure 6: (A): Phylogenetic tree of MamK and MamK-like protein sequences of MTB and actin-like proteins of related organisms (from ncbi) together with MreB based on PHYLIP neighbour joining method. Distance matrix model: Jones-Taylor-Thornton. (B): TEM micrographs of *in vitro* polymerised MamK of *M. magnet.*, scale bar, 100nm, adapted from (59). (C): Fluorescence images of eGFP labelled MamK heterologous expressed in Δ *mamK* strain of *M. gryph.* Scale bar, 1 μ m. (D): Homology-based 3D model generated with 3D-JIGSAW on MreB matrix of *T. maritima*.

MamK is one member of the actin-like proteins (Alps) family and to understand putative functions of MamK two of the best studied Alps MreB and ParM will be introduced in more detail.

Analysis of a mecillinam resistant (Mre) *E. coli* mutant revealed an intriguing morphological change from rod to spherical cell shape (69). The deleted protein MreB shares the conserved regions with eukaryotic actin and from its structure it was suggested to be the bacterial precursor of actin (70, 71). Polymerised MreBs form multi-layered sheets of interwoven filaments and this MreB polymers appear to be a single-stranded helical filament instead of the linear protofilament as observed for the MreB crystal structure (72). MreB proteins are best characterised in *E. coli*, *B. subtilis* and *C. crescentus*, where they were thought to form helical cables which are dynamic by a treadmilling-like mechanism (73). However, this is controversially discussed, since recent CET studies on rod shaped bacteria could not detect helical MreB structures (74). Moreover, TIRF revealed that MreB in *B. subtilis* assembles into discrete patches that move progressively along peripheral tracks perpendicular to the cell axis and were likely to be misinterpreted as helical filaments (75, 76). MreB was shown to be associated with the cell membrane in *E. coli* and *Thermotoga maritima* and was able to induce membrane curvature when expressed *in vitro* (77). However, MreB acts together with the proteins MreC, MreD, RodA and Pbp2 in order to maintain cell shape. (78). All Mre proteins are encoded within a *mreBCD*-operon at the *E. coli* chromosome which is also present in *M. gryph.*

The second well characterised bacterial Alp belongs to the partitioning (Par) family. This group first described a system for equipartition and segregation of the *E. coli* F plasmid during cytokinesis (79). The sequence identity between ParM and actin is low (< 15%) although both are similar in size and share conserved regions around their nucleotide-binding sites, which is also confirmed by their corresponding crystal structures.

In brief the par system comprises one *cis*-acting, centromere-like region *parC* and two *trans*-acting elements: the DNA binding protein ParR and the actin-like filamentous protein ParM. Together, the ParMRC module is responsible for chromosome segregation

during cytokinesis, whereupon the actin-like ParM filaments push the plasmids to opposite cell poles through interaction with the DNA bound ParR-*parC* complex (80). The ParM protein forms a dynamic filament by coupling nucleotide binding and hydrolysis to polymerisation and thus allows pushing and pulling of structures attached to its ends described as 'cytomotive' action (81). ParM filaments extend at both ends instead of one as described for actin. Assembly into filaments occurs by a nucleation and condensation reaction, which begins with monomers and ATP hydrolysis at the ends. This leads to the formation of a ParM seed with ADP bound monomers accumulated at its centre and elongation through further ATP hydrolysis results in the final filament. Together with its catastrophic disassembly, when an ATP cap is missing or the filament is plasmid unbound, this enables ParM to spontaneously form short filaments and randomly search the plasmid-bound ParR-*parC* complex within the cell (80, 82).

1.3 Cell division in bacteria

The bacterial cell is challenged with the task of generating two identical daughter cells comprising the steps of (i) chromosome and organelle segregation, (ii) cell wall elongation with subsequent constriction and (iii) final cell division. Magnetotactic bacteria like *M. gryph.* face the additional challenge of dividing and equipartitioning the magnetosome chain (MC) preferably to pass on the selective advantage of magnetotaxis to both daughter cells. The even segregation of the MC to maintain magnetic navigation was already noted in 1980 by Frankel and Blakemore (11). To ensure proper distribution of the chain it has to be positioned at the cellular division site, where it will be split against the magnetostatic interaction forces of nascent magnetosomes.

A filamentous temperature sensitive (fts) mutant of *E. coli* was described by Hirota *et al.* (83) and later Bi and Lutkenhaus (84) discovered that the protein FtsZ assembled at the cell centre into the so called Z-ring which is contractile and the basic unit of the divisome. FtsZ belongs to the group of tubulin-like proteins and depending on the cell cycle either localises filamentous or ring-like within the cell (85). The entire molecular division machinery comprises, up to now, 20 proteins in *Caulobacter crescentus* (86) and beside the Z-ring also the cytoskeleton (e.g. Mre proteins, see above) as well as the Tol-Pal complex (87) are involved in cytokinesis. The divisome has to be localised at the cell centre in order to guarantee equal sized progeny cells. A gradient of negative regulators was found to achieve this within the cell either by oscillation or static mode of action. In *C. crescentus*, which is closely related to *M. gryph.*, binary fission results in two different-sized progeny cells and instead of the MinCDE system for *E. coli* the protein MipZ fulfilled the task of divisome positioning. MipZ delays Z-ring formation until chromosome segregation is accomplished in *C. crescentus* (88) and a homologue is also present in the *M. gryph.* genome.

Analogous to magnetospirilla, which have to split the magnetosome chain and evenly segregate it to the progeny cells, organelle segregation is another important task, which has to be performed prior to division in bacteria. The carboxysomes of cyanobacteria were detected to evenly segregate between daughter cells by the filamentous ParA and MreB protein (89). Another example of prokaryotic organelle segregation was described by Galán *et al.* (2010). They analyzed a Δ *phaF* (phasinF) mutant of *Pseudomonas putida* which had agglomerated polyhydroxyalkanoate (PHA) granules at one cell pole instead

of the needle-like arrangement at the cross section regularly observed for the WT. Moreover, an interaction of PhaF and the chromosome could be detected leading to the hypothesis of chromosome segregation mediated PHA distribution between the daughter cells (90).

1.4 Cryo-electron tomography

Filamentous structures were rarely seen by conventional TEM techniques in bacteria. Cryo-electron tomography (CET) has proven powerful in identification of cytoskeletal elements and to resolve electron permeable, fragile structures like vesicles and membranes, which makes it suitable to examine magnetosome chains of *M. gryph*. (1, 2, 91-96).

CET is based on conventional transmission electron microscopy, but differs from this by the tiltable sample holder (goniometer), the frozen state of the samples as well as computer-based reconstruction of the 3-dimensional (3D) tomogram. This leads to an increased resolution of $\sim 2 - 8$ nm in all three directions without losses or distortions between sections. CET is therefore the highest resolution technique available today to image biological specimen like bacterial cells.

For CET a close to *in vivo* sample preparation is achieved by amorphous ice. The frozen specimen is transferred into the microscope and tilted within the electron beam usually between $\pm 65^\circ$. At defined angle increments (usually every 1° to 2°) an image of the sample is captured and the resulting images are aligned and assembled via the weighted back-projection method (Figure 7). The generated 3D volume or tomogram of the cell possesses much more details than a conventional 2D image and the individual projections can be segmented in order to reveal the spatial orientation of individual cell components. However, drawbacks of this technique are the missing wedge and thus information loss due to the restricted tilt angle, the specimen thickness, which should not exceed 500 nm and the size of the detector (CCD camera).

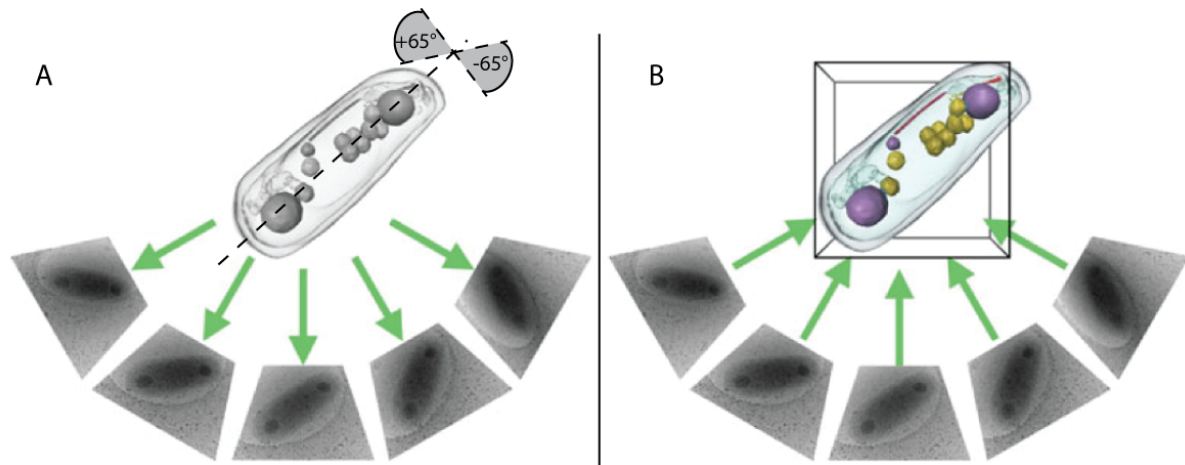


Figure 7: Schematic illustration of the cryo-electron tomography principle. (A) The specimen (bacterial cell) is tilted around a defined angle ($\pm 65^\circ$) and with an 1 or 2° increment images are acquired. (B) Individual projections are aligned to a stack by weighted-back projection and cellular components are segmented to reveal their 3D orientation in the tomogram. Adapted and modified from (96).

CET analyses of magnetospirilla confirmed the invagination hypothesis and showed for the first time where the vesicles form within *M. magnet.* cells. In addition, first components of the magnetosome chain ultrastructure like filaments associated with magnetosomes could be resolved. The position and orientation of the magnetosome chain with respect to the 3D cell body could be visualized also specific parameters like vesicle size, membrane thickness, filament diameter and length were determined for the first time within intact cells. However, questions regarding the identity, entire length and anchoring of the filamentous structures in *M. gryph.* could not be answered. Cell envelope organization and magnetosome chain segregation during *M. gryph.* cell cycle were not described at an ultrastructural level by CET before.

1.5 Aim of this work

Preliminary work had implicated the MamK and MamJ proteins in the assembly of functional magnetosome chains. The deletion of *mamJ* in *M. gryph.* resulted in clustered magnetosomes whereas deletion of *mamK* in the closely related *M. magneticum* caused the loss of magnetosome filaments and abolished chain formation (1, 2). This led to a model in which the actin-like MamK was suggested to provide a rigid cytoskeletal scaffold to which magnetosome vesicles are attached by the acidic MamJ protein, thereby mechanically stabilizing the chain against its immanent tendency to collapse. However, more recent observations in both organisms were not fully consistent with this generalised model.

The aim of this study was to reconcile conflicting observations and to further analyse the role of genetic and abiotic factors in assembly, positioning and cleavage of the magnetosome chain during cell cycle.

In chapter 2, the analysis of a MamK mutant generated in *M. gryph.* by cryo-electron tomography is described. This revealed that MamK forms cytoskeletal structures involved in magnetosome organization, although unexpectedly not being absolutely essential for the assembly of shorter magnetosome chains.

The second part, described in chapter 3 of the work aimed to analyse the role of MamK in magnetosome chain formation and segregation during *M. gryph.* cytokinesis. Examination of synchronised and division-inhibited cells by time-lapse imaging and cryo-electron tomography demonstrated a key role of MamK in dynamic magnetosome chain assembly, positioning and segregation during an asymmetric process of cell division.

CHAPTER 2

2.1 Manuscript:

Loss of the actin-like protein MamK has pleiotropic effects on magnetosome formation and chain assembly in *Magnetospirillum gryphiswaldense*

Loss of the actin-like protein MamK has pleiotropic effects on magnetosome formation and chain assembly in *Magnetospirillum gryphiswaldense*

Emanuel Katzmann,^{1,2} André Scheffel,^{3†}
Manuela Gruska,² Jürgen M. Plitzko² and
Dirk Schüler^{1*}

¹Ludwig-Maximilians-Universität München, Department Biologie I, Bereich Mikrobiologie, Biozentrum der LMU, D-82152 Martinsried, Germany.

²Max Planck Institute of Biochemistry, Department of Molecular Structural Biology, Am Klopferspitz 18, D-82152 Martinsried, Germany.

³Max Planck Institute for Marine Microbiology, Celsiusstr. 1, D-28359 Bremen, Germany.

Summary

Magnetotactic bacteria synthesize magnetosomes, which are unique organelles consisting of membrane-enclosed magnetite crystals. For magnetic orientation individual magnetosome particles are assembled into well-organized chains. The actin-like MamK and the acidic MamJ proteins were previously implicated in chain assembly. While MamK was suggested to form magnetosome-associated cytoskeletal filaments, MamJ is assumed to attach the magnetosome vesicles to these structures. Although the deletion of either *mamK* in *Magnetospirillum magneticum*, or *mamJ* in *Magnetospirillum gryphiswaldense* affected chain formation, the previously observed phenotypes were not fully consistent, suggesting different mechanisms of magnetosome chain assembly in both organisms. Here we show that in *M. gryphiswaldense* MamK is not absolutely required for chain formation. Straight chains, albeit shorter, fragmented and ectopic, were still formed in a *mamK* deletion mutant, although magnetosome filaments were absent as shown by cryo-electron tomography. Loss of MamK also resulted in reduced numbers of magnetite crystals and magnetosome vesicles and led to the mislocalization of MamJ. In addition, extensive analysis of

wild type and mutant cells revealed previously unidentified ultrastructural characteristics in *M. gryphiswaldense*. Our results suggest that, despite of their functional equivalence, loss of MamK proteins in different bacteria may result in distinct phenotypes, which might be due to a species-specific genetic context.

Introduction

The ability of magnetic navigation in magnetotactic bacteria (MTB) is based on the synthesis of magnetosomes, which are complex intracellular organelles. In *Magnetospirillum gryphiswaldense* MSR-1 (in the following referred to as MSR) and related magnetospirilla magnetosomes comprise cubo-octahedral nanocrystals of magnetite (Fe₃O₄) that are enveloped by vesicles of the magnetosome membrane (MM) (Gorby *et al.*, 1988; Schüler, 2004a). Previous studies revealed that the MM is a phospholipid bilayer, which is associated with a set of about 20 specific proteins (Gorby *et al.*, 1988; Grünberg *et al.*, 2001; 2004). In *M. magneticum* AMB-1 (in the following referred to as AMB) it was shown that the MM originates via invagination from the cytoplasmic membrane (CM) (Komeili *et al.*, 2006).

For maximum sensitivity of magnetic orientation, magnetosomes are organized within single or multiple chains, which represent one of the highest structural levels found in a prokaryotic cell. However, a string of magnetic dipoles has an immanent tendency of collapsing to lower its magnetostatic energy unless it is properly stabilized (Kirschvink, 1982; Kobayashi *et al.*, 2006). Recently, it has been found that the assembly and maintenance of magnetosome chains are governed by dedicated cellular structures. Two complementary studies investigated chain formation in the two related magnetic bacteria MSR and AMB by cryo-electron tomography (CET) (Komeili *et al.*, 2006; Scheffel *et al.*, 2006). CET has emerged as a powerful technology for bridging the gap between protein–protein interactions and cellular architecture (Lučić *et al.*, 2005; Li and Jensen, 2009; Milne and Subramaniam, 2009). In CET, cells are embedded in vitreous ice in a close-to-native state, thereby avoiding artefacts typically

Accepted 3 May, 2010. *For correspondence. E-mail dirk.schueler@lrz.uni-muenchen.de; Tel. (+49) 89 21 80-74502; Fax (+49) 89 21 80-74515. †Present address: School of Chemistry and Biochemistry, Georgia Institute of Technology, Atlanta, GA 30332-0400, USA.

associated with conventional electron microscopy. CET analysis of MSR and AMB demonstrated a cytoskeletal network of filaments, 3–4 nm in diameter, which traverse the cells adjacent to the CM. Magnetosomes were closely arranged along this magnetosome-associated cytoskeleton, which has been tentatively referred to as 'magnetosome filament' (MF) (Frankel and Bazylinski, 2006). It was speculated that MFs might be encoded by the *mamK* gene because of its sequence similarity to other cytoskeletal proteins (Grünberg *et al.*, 2004; Schüler, 2004a), which together with other genes relevant for magnetosome formation is part of the large *mamAB* operon in all analysed MTB (Grünberg *et al.*, 2001; Jogler and Schüler, 2009; Nakazawa *et al.*, 2009; Jogler *et al.*, 2009a; Murat *et al.*, 2010). MamK proteins form a distinct and coherent branch within the large superfamily of prokaryotic actin-like proteins (Alps), which perform diverse functions in cell shape determination, establishment of polarity, cell division, chromosome segregation and plasmid partition (Carballido-Lopez, 2006; Derman *et al.*, 2009).

Because of the difficulties with genetic manipulation of MTB, a *mamK* deletion mutant has so far been available only in AMB (Komeili *et al.*, 2006). *AMBΔmamK* cells had lost their coherent chain-like structure. Instead, groups of few (two to three) neighbouring magnetosomes were separated by large gaps and appeared dispersed throughout the cell (Komeili *et al.*, 2006). Cytoskeletal MFs could no longer be identified in tomograms of mutant cells, indicating that MamK in fact might be the structural element of the magnetosome-associated cytoskeleton. Similar to MreB and other Alps, MamK fusions to GFP displayed a filament-like organization *in vivo* and appeared as spiral or straight lines in cells of AMB (Dye *et al.*, 2005; Pradel *et al.*, 2006). MamK-GFP of AMB expressed in *Escherichia coli* formed straight filaments, which were structurally and functionally distinct from the known MreB and ParM filaments (Carballido-Lopez and Errington, 2003; Pradel *et al.*, 2006). Recombinant MamK of *Magnetospirillum magnetotacticum* MS-1 (in the following referred as MS) *in vitro* polymerized into long straight filamentous bundles in the presence of a non-hydrolyzable ATP analogue (Taoka *et al.*, 2007). In the related magnetic bacterium MSR MamK was shown to interact with the acidic repetitive MamJ protein, which was demonstrated to be another key player of magnetosome chain assembly (Scheffel *et al.*, 2006; Scheffel and Schüler, 2007). A deletion mutant of *mamJ* did no longer produce straight magnetosome chains, but magnetite crystals were found arranged in compact clusters (Scheffel *et al.*, 2006; Scheffel and Schüler, 2007), whereas empty vesicles and immature crystals are scattered throughout the cytoplasm and detached from the MFs, which were still present within *MSRΔmamJ* cells.

One obvious model that was suggested from these data is that MamJ connects magnetosomes to the cytoskeletal MF formed by MamK, which mechanically stabilizes the magnetosome chain and prevents it from collapsing (Komeili, 2007a,b; Scheffel and Schüler, 2007). According to this model, loss of either MamK or MamJ should result in an essentially identical phenotype, which is the abolishment of chain formation and agglomeration of magnetosome particles. However, the reported phenotypes of the MamJ deletion in MSR (agglomerated magnetosomes) and the MamK deletion in AMB (dispersed magnetosomes) were strikingly distinct. This raised the question, whether the MamJ and MamK proteins perform different or additional functions in different species of MTB, and whether the observed phenotypic differences are due to species-specific modes of chain formation caused by different genetic control in the two strains used in the two studies (Jogler and Schüler, 2007; Komeili, 2007b). In a very recent study, a second actin-like protein was discovered in the genome of AMB that shares 54.4% identity with MamK and is encoded within a genomic islet outside the MAI (Rioux *et al.*, 2010). Like MamK, this MamK-like protein was also demonstrated to form filaments both *in vivo* and *in vitro*, and it was speculated that the presence of this second *mamK*-like gene might account for the variable phenotype of the *ΔmamK* mutant in AMB (Rioux *et al.*, 2010).

To reconcile these conflicting observations and to further clarify the role of MamK, we characterized in detail a *mamK* deletion mutant of MSR by transmission electron microscopy (TEM) and CET. We show that in contrast to AMB, MamK of MSR is not required for chain formation. However, the absence of MFs results in a pleiotropic phenotype displaying shorter and fragmented chains that are displaced from their usual midcell localization. In addition, mutants are also impaired in magnetite formation. Our results suggest that MamK has a role in magnetosome chain positioning and MM vesicle formation, and loss of MamK may have distinct effects in different bacteria depending on the genetic context.

Results

Characterization of an unmarked, in-frame ΔmamK mutant of M. gryphiswaldense

We generated an unmarked, in-frame *mamK* deletion mutant of *M. gryphiswaldense* (MSR), in the following referred to as *MSRΔmamK*. Under standard conditions (microaerobic, 30°C) cells of *MSRΔmamK* strain exhibited morphology (Fig. 1), as well as growth and motility apparently identical to the wild type (WT). Whereas single crossover insertants of pEK32 were deficient in magnetite crystal formation, *MSRΔmamK* cells formed magneto-

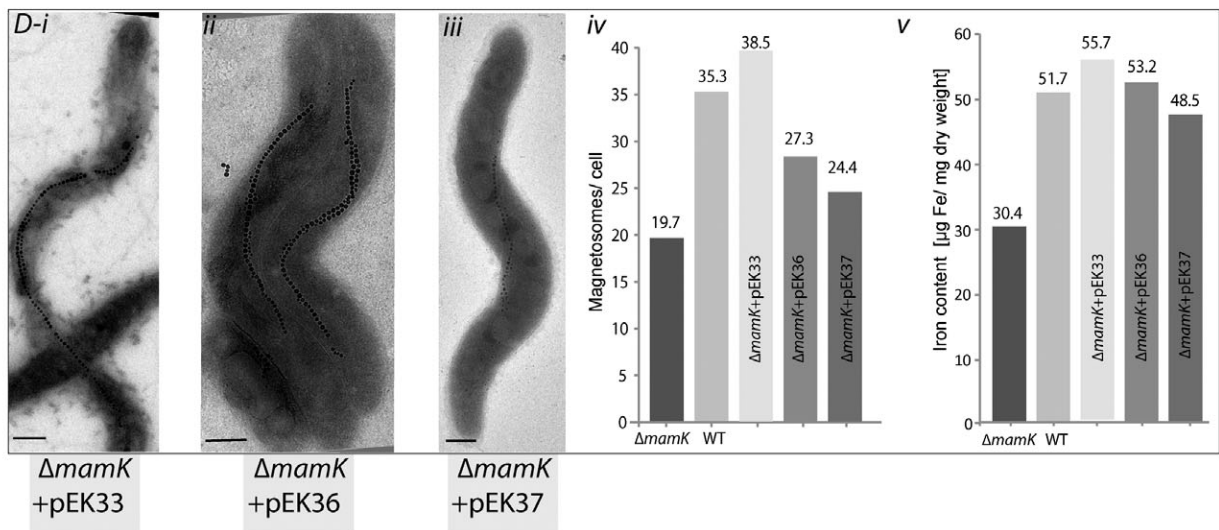
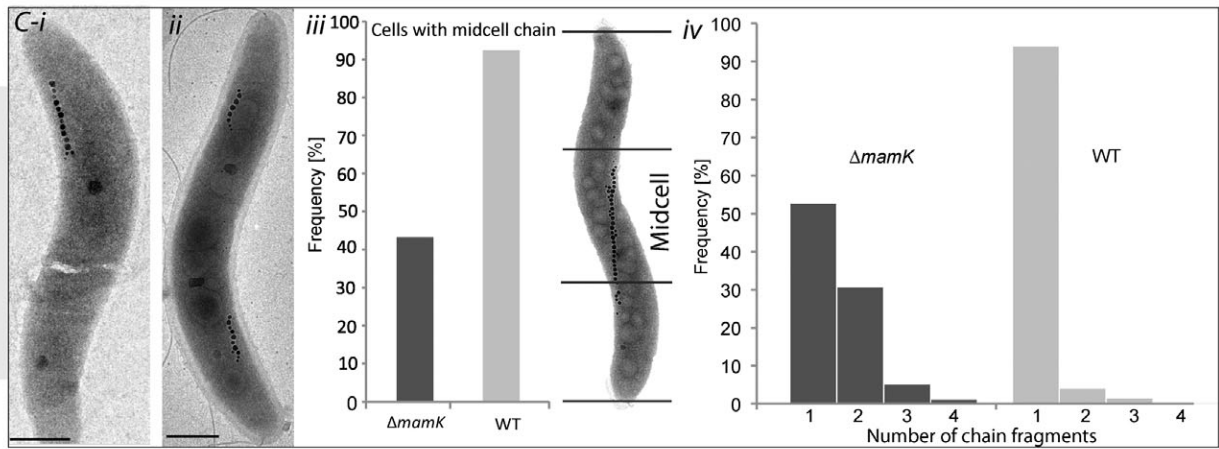
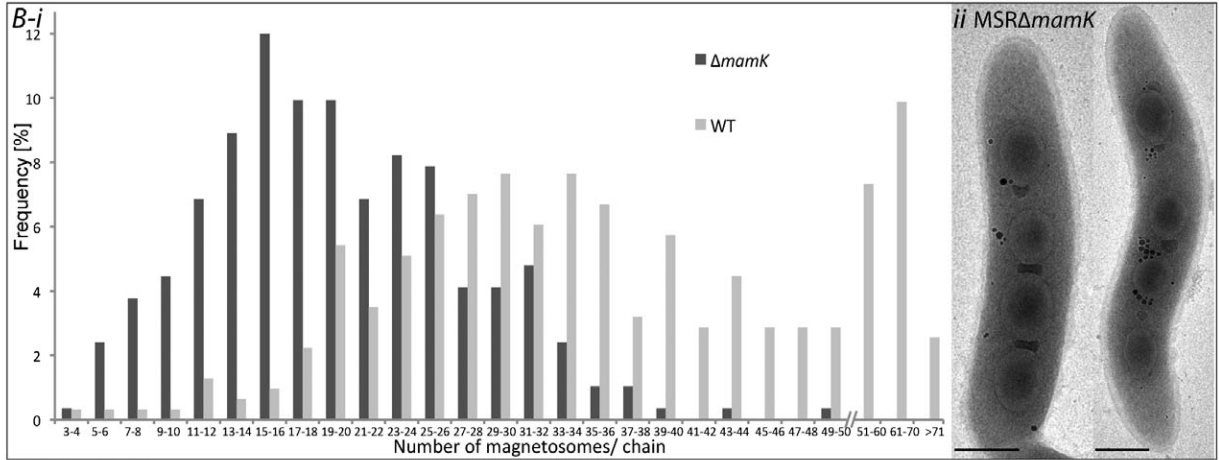
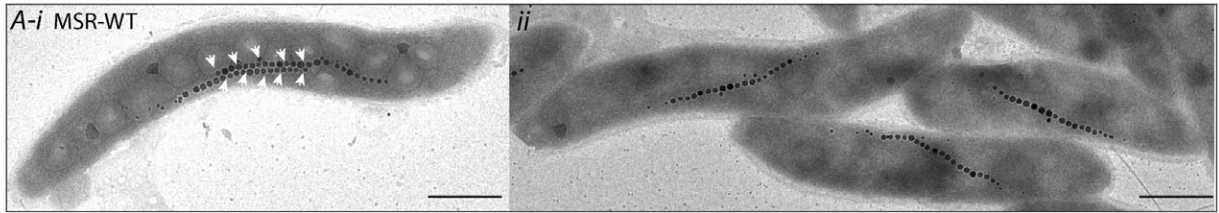


Fig. 1. Overview of morphologies and magnetosome chain organizations found in MSR Δ *mamK* cells and WT. A. TEM micrographs of MSR WT cells. White arrows indicate parallel chains. Bi. Statistical analysis of magnetosome particles per chain and micrographs of MSR Δ *mamK* cells displaying dispersed magnetosomes (Bii). Ci–ii. Micrographs of MSR Δ *mamK* cells displaying ectopic chain localization, and statistical analysis of chain position (iii), and chain numbers (iv) in MSR Δ *mamK*. Di–iii. TEM micrographs of transcomplemented MSR Δ *mamK* cells with various plasmids. Magnetosome numbers and iron contents of the strains are shown in (Dv–vi). Scale bars 500 nm.

somes and aligned to magnetic fields. However, magnetic orientation of mutant cultures was markedly weaker than the WT as indicated by lower C_{mag} values (1.08 vs. 1.44 in the WT). Measurement of ~590 magnetosomes from ~30 cells revealed that the magnetite crystals were unaffected in shape and size, and the mean crystal diameter of 34 nm was essentially identical to that of the WT (33 nm). However, on average MSR Δ *mamK* cells contained substantially fewer magnetosomes (19.7 crystals) per cell than WT cells (35.3 crystals) (Fig. 1D–iv) grown under identical conditions, which was also consistent with a reduced iron accumulation of mutant cells (30.4 $\mu\text{g mg}^{-1}$ vs. 51.7 $\mu\text{g mg}^{-1}$ dry weight in the WT, Fig. 1D–v).

Chain formation was assessed by TEM with respect to the average number of chains per cells, the average length (i.e. the number of particles), and the average distance between neighbouring particles. A chain was defined empirically by a minimum number of 10 magnetosomes that showed a linear alignment, and which were interspaced by not more than ~50 nm from each other. Within this distance magnetic crystals are known to interact magnetically, whereas single particles spaced by about > 200 nm are magnetically uncoupled and behave as independent magnetic dipoles (Simpson, 2008; Li *et al.*, 2009). Around 70% of WT magnetosome chains had between 19 and 44 particles, were 0.6–2.5 μm in length, tightly spaced (10.9 nm interparticle distance, 50.2 nm center-to-center distance), with smaller, apparently growing, and more widely spaced magnetite particles at the ends. In 92% of the cells straight, long and continuous chains were positioned at midcell (Fig. 1C–iii). Ectopic (e.g. terminal) chain localization or fragmented chains (6%) were found only occasionally. However, in about 17% of the WT cells 2–3 parallel chains were observed (Fig. 1A).

In contrast, MSR Δ *mamK* cells displayed a distinct and much more inconsistent pattern of magnetosome chain configurations. A fraction of cells had lost their coherent, tightly spaced chain-like structure, but instead magnetosomes were dispersed along a linear axis throughout the cells and spaced by distances up to ~920 nm (Fig. 1B and C). However, this pattern, which was somewhat reminiscent to the described phenotype of Δ *mamK* in AMB (Komeili *et al.*, 2006) was found in only 18% of the cells (Fig. 1B–ii). Instead, the major fraction of cells still formed single or multiple tightly spaced chains. A minor fraction (5%) of the MSR Δ *mamK* cells exhibited chains similar to those in the WT (i.e. one single, tightly spaced chain with

> 10 magnetosome positioned at midcell; Fig. 1C–iii). In the majority of cells, however, chains were aberrant with respect to their number, length and position. For example, the occurrence of fragmented chains with multiple (up to 4) subchains was increased (average 1.38 chains per MSR Δ *mamK* cell) compared with the WT (1.19 per cell). Individual fragmented chains on average were significantly shorter (14.2 particles in MSR Δ *mamK* vs. 26.1 in the WT), and 29% of the cells had chains with fewer than 10 particles, compared with only 2% in the WT. Notably, parallel chains that were frequently present in WT cells, were never observed in MSR Δ *mamK* cells. The position of magnetosome chains within cells was estimated by dividing the cells into three equal sectors to distinguish between midcell and terminal localization. A midcell localization of the chain was observed in only 43% of MSR Δ *mamK* cells (WT: 92%), whereas in the majority of mutant cells the chains were located closely to the cell poles (Fig. 1C–i–ii).

We and others had observed previously that purified magnetosome particles from WT cells tend to form chains *in vitro* as long as the particles are enveloped by an intact MM (Grünberg *et al.*, 2004; Kobayashi *et al.*, 2006; Schefel *et al.*, 2006; Taoka *et al.*, 2007; Li *et al.*, 2009). To test whether the loss of MamK, which is associated with the MM of MSR (Fig. S1), had an effect on the integrity of the MM, and consequently, on chain formation *in vitro*, magnetosome particles purified from mutant and WT cells were investigated by TEM. Isolated mutant and WT magnetite crystals were surrounded by a MM-like organic layer of identical thickness (8–12 nm) and appearance as reported previously (Gorby *et al.*, 1988; Schüller, 2004b; Taoka *et al.*, 2006) with junctions that interconnected the individual particles (Fig. S2). Similar like WT magnetosomes, isolated mutant magnetosomes had a tendency to form chains as observed before (Grünberg *et al.*, 2004) (Fig. S2–i–iv).

Complementation analysis: *MamK_{MSR}* and *MamK_{AMB}* are functionally equivalent

Immunodetection revealed that MamM and MamB, whose genes are located 338 and 7192 bp downstream of *mamK* within the *mamAB* operon, respectively, were expressed at WT levels in the mutant strains (data not shown), indicating that *mamK* deletion had no polar effects. To further preclude second-site mutations, we analysed cells

transcomplemented with a functional *mamK* gene. Cloning and expression of the 1044 bp *mamK*_{MSR} gene under control of the native P_{*mamAB*} promoter (Lang *et al.*, 2009) in pEK36 resulted in MamK expression comparable to WT levels (data not shown) upon transfer into MSRΔ*mamK*. In addition, also magnetite formation, iron accumulation and chain formation were restored, albeit to a lower extent than in the WT (Figs 1D-iv–v and 4D).

To answer the question whether observed differences in WT and Δ*mamK* phenotypes between AMB and MSR might be due to sequence divergence of MamK orthologs, we also tested transcomplementation by *mamK*_{AMB}, and in addition by *mamK*_{MS} (*M. magnetotacticum* MS-1). Plasmids pEK37 and pEK35 carrying *mamK*_{AMB} and *mamK*_{MS}, respectively, were conjugated into MSRΔ*mamK*. Magnetosome numbers, iron accumulation, C_{mag} and chain formation were restored by MSRΔ*mamK* + pEK35 (data not shown) and MSRΔ*mamK* + pEK37 (Fig. 1D-iii–v) at comparable levels, indicating that *mamK*_{MS} and *mamK*_{AMB} are functionally equivalent to *mamK*_{MSR} and can substitute its function in MSRΔ*mamK* cells. We also investigated the effect of MamK overexpression by cloning of *mamK*_{MSR} on pEK33 under control of the strong MSR promoter *pmamDC* (Lang *et al.*, 2009). Transmission electron micrographs revealed long, straight WT-like magnetosome chains in MSR cells expressing *mamK* from pEK33, and filaments of similar abundance, length and thickness were visible within 3D maps. Likewise, cells displayed similar magnetosome numbers (Fig. 1D-i–v) and magnetic orientation (WT C_{mag} = 1.47, WT + pEK33 C_{mag} = 1.50), indicating that moderate overexpression of *mamK* has only minor effects on magnetosome chain formation (Fig. S3).

Intracellular localization of MamK

Plasmids harbouring various MamK-EGFP fusions were expressed in WT and several mutant backgrounds. Functionality of fusions was verified by partial restoration of WT-like phenotype upon expression of pAS_K, pAS_K1, pAS_K2 and pEK42 in MSRΔ*mamK*. Fluorescence microscopy revealed distinct localization patterns from linear-to-helical filaments in all tested MamK-EGFP fusions. However, the respective patterns were dependent on the length of the linker between EGFP and MamK: Expression of pAS_K1 harbouring a C-terminal MamK-GSI-EGFP (Fig. 2A and B) fusion, and pAS_K2 harbouring an N-terminal EGFP-SAI-MamK fusion (data not shown) resulted in a linear fluorescence signal of about half the cell length that was restricted to midcell in *E. coli* and MSR, similar as observed in other studies (Pradel *et al.*, 2006). In contrast, WT + pAS_K harbouring a N-terminal EGFP-LCLQGE-MamK displayed a linear-to-helical fluorescence pattern spanning from pole to pole

throughout the entire cell, and occasionally forming loops (Fig. 2A). A similar pattern was also observed if pAS_K and pEK42 were expressed in MSRΔ*mamK*, the non-magnetic mutant strain MSR-1B lacking most magnetosome genes by deletion (Schübbe *et al.*, 2003; Ullrich *et al.*, 2005), and *E. coli* (Fig. 2A–H). Previous experiments indicated that MamK interacts with the acidic MamJ protein (Scheffel *et al.*, 2006; Scheffel and Schüler, 2007), but the filamentous localization of MamK was independent from MamJ (as demonstrated by expression in Δ*mamJ* strain) and other magnetosome genes (as demonstrated by expression in MSR-1B) (Scheffel *et al.*, 2006). Therefore, we asked whether localization of MamJ was on the other hand dependent on the presence of MamK. Expression of pAS_J harbouring a MamJ-EGFP fusion in MSRΔ*mamK* abolished its filamentous localization, but instead resulted in a punctual, cytoplasmic fluorescence signal, similar as the localization of MamJ-EGFP previously detected in MSR-1B (Scheffel *et al.*, 2006) (Fig. 2A–J). This indicates that proper MamJ localization requires the presence of MamK. Because the linear-to-helical localization of EGFP-MamK (pAS_K, pEK42) was also observed in *E. coli* and *M. gryphiswaldense* MSR-1B backgrounds (Fig. 2E–H), this demonstrates that the filamentous localization is an intrinsic property of EGFP-MamK_{MSR}, which does not require the presence of other magnetosome proteins. Expression of pAS_K in AMB resulted in the same filamentous signal pattern; however, spiral localization was absent (Fig. 2J).

Spontaneous formation of spheroplasts ('coccol bodies') can be regularly observed in aging cells of *M. gryphiswaldense* and other magnetospirilla (Balkwill *et al.*, 1980; Schüler and Köhler, 1992). Interestingly, in such spheroplast cells EGFP-MamK (pAS_K) did no longer localize within linear filaments, but instead yielded a ring-like fluorescence signal closely beneath the cell periphery, which is consistent with the peripheral ring-like, bent appearance of the magnetosome chains in such a cell as shown by fluorescence microscopy and TEM (Fig. 2J–M).

CET

Previous CET analyses of magnetosome chain topology in AMB and MSR were limited to only single or a few cells (Komeili *et al.*, 2006; Scheffel *et al.*, 2006). Therefore, we analysed chain assembly and MFs in greater detail in a larger number of WT and MSRΔ*mamK* cells of MSR. Filaments accompanying the magnetosome chains were identified in 16 of 28 of all analysed tomographic volumes from WT cells (Fig. 3), and 2 of 10 analysed MSRΔ*mamK* cells complemented with pEK42 (*mamK*_{MSR}, Fig. 4A) and pEK34 (*mamK*_{AMB}). As tomograms at the recorded magnification are limited in the field of view, they represent only a fraction of the whole cell. Moreover, some information is

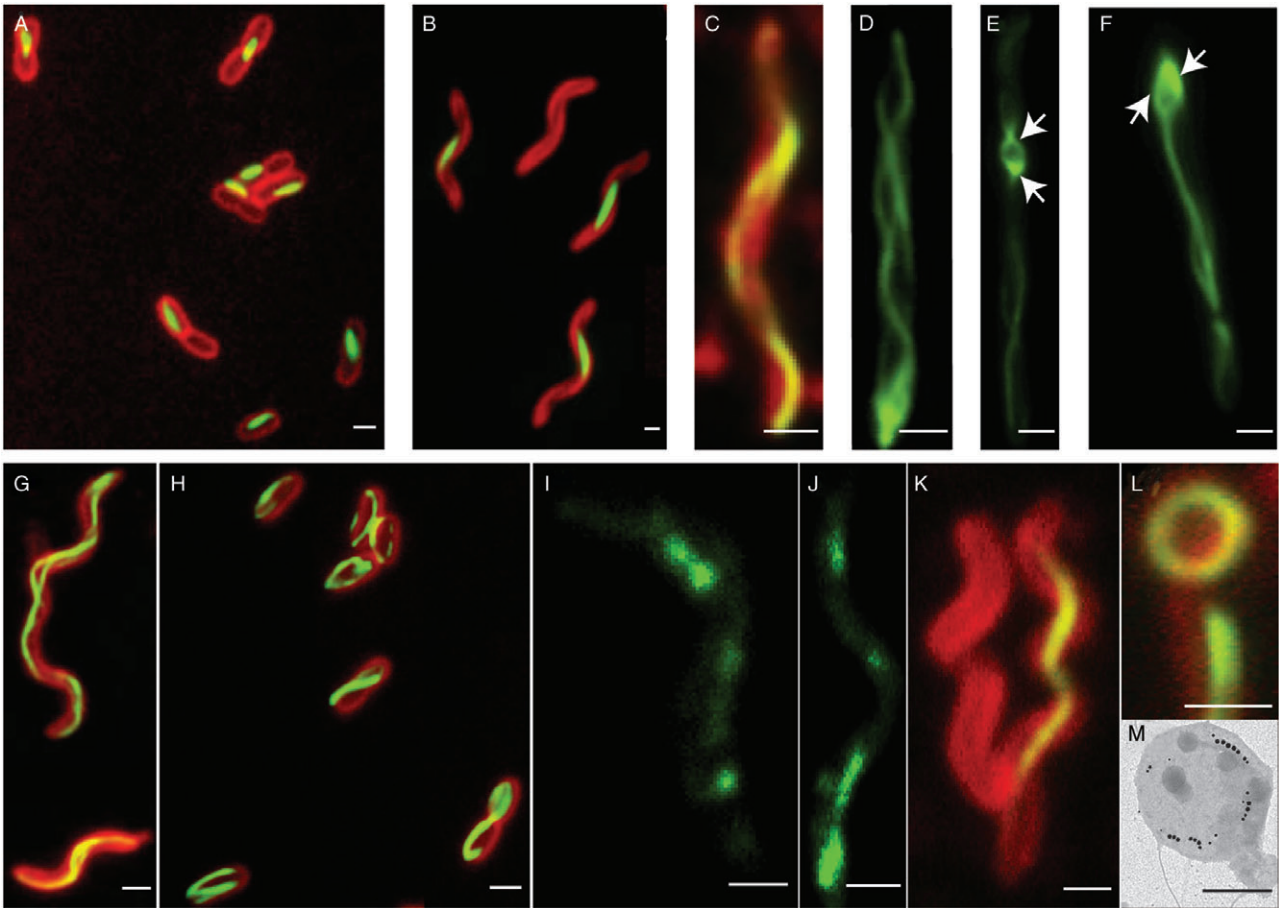


Fig. 2. Fluorescence micrographs of *E. coli*, MSR (and MSR-1B) and AMB expressing different EGFP fusions.
 A. Overlay of FM4-64 (red) and *egfp* (green) recombinant *E. coli* expressing pAS_K1. Localization pattern of MamK_GSI_eGFP.
 B. pAS_K1 expressed in non-magnetic mutant MSR-1B.
 C. MSR WT expressing pAS_K.
 D–F. MSR Δ *mamK* mutant of MSR-1 expressing pAS_K (eGFP_LCLQGE_MamK) resulting in loop-shaped or spiral localization patterns. Loop-like structures are observed at midcell (white arrows).
 G. pAS_K expressed in MSR-1B exhibiting helical filaments.
 H. Overlay of FM4-64 and *egfp* image of recombinant *E. coli* expressing pAS_K. Helical filaments are visible.
 I–J. MSR Δ *mamK* mutant expressing eGFP fused MamJ (pAS_J).
 K. Overlay of FM4-64 and *egfp* of AMB WT expressing pAS_K resulting in a long filamentous localization throughout the entire cell.
 L. MSR Δ *mamK* mutant expressing pAS_K in MSR Δ *mamK* in a spheroplast cell.
 M. TEM micrograph of a spheroplast cell. Scale bars 500 nm.

not accessible due to the limited tilt range and the resulting missing wedge. Therefore, it is possible that filaments in the other WT and transcomplemented cells escaped detection if localized perpendicular to the tilt-axis. Individual filaments, which were 3–6 nm in diameter and 0.5–1 μ m in length, occasionally formed bundles of 2–4 filaments that were ~20 nm in diameter and approximately 1 μ m long (Movie S1). However, as filaments were not always within the same z-plane, their total dimensions can only be roughly estimated. Detected filaments were localized within the cytoplasm in close proximity to MM vesicles. Although the magnetosome chains were predominantly found at midcell, empty vesicles and filaments were also present in 100–300 nm vicinity to the inner membrane of

the cell pole. However, we were unable to detect direct connections or discern distinct structures where filaments insert into the polar membrane. This was partially due to the presence of complex ordered structures resembling arrays of chemoreceptors (Briegel *et al.*, 2009), which were located closely beneath the polar membrane (Fig. 3E–H). Analysis of different CET datasets determined an array length of ~28 nm and a lattice distance of ~11 nm (Fig. 3E, insets). Notably, in some cells filaments seemed to be connected laterally to the CM.

A couple of WT and transcomplemented cells were tomographed in state of early (Fig. 3A–E), and late division (Fig. 4A). According to those tomograms, the MF traverse the entire cell before septum formation, which

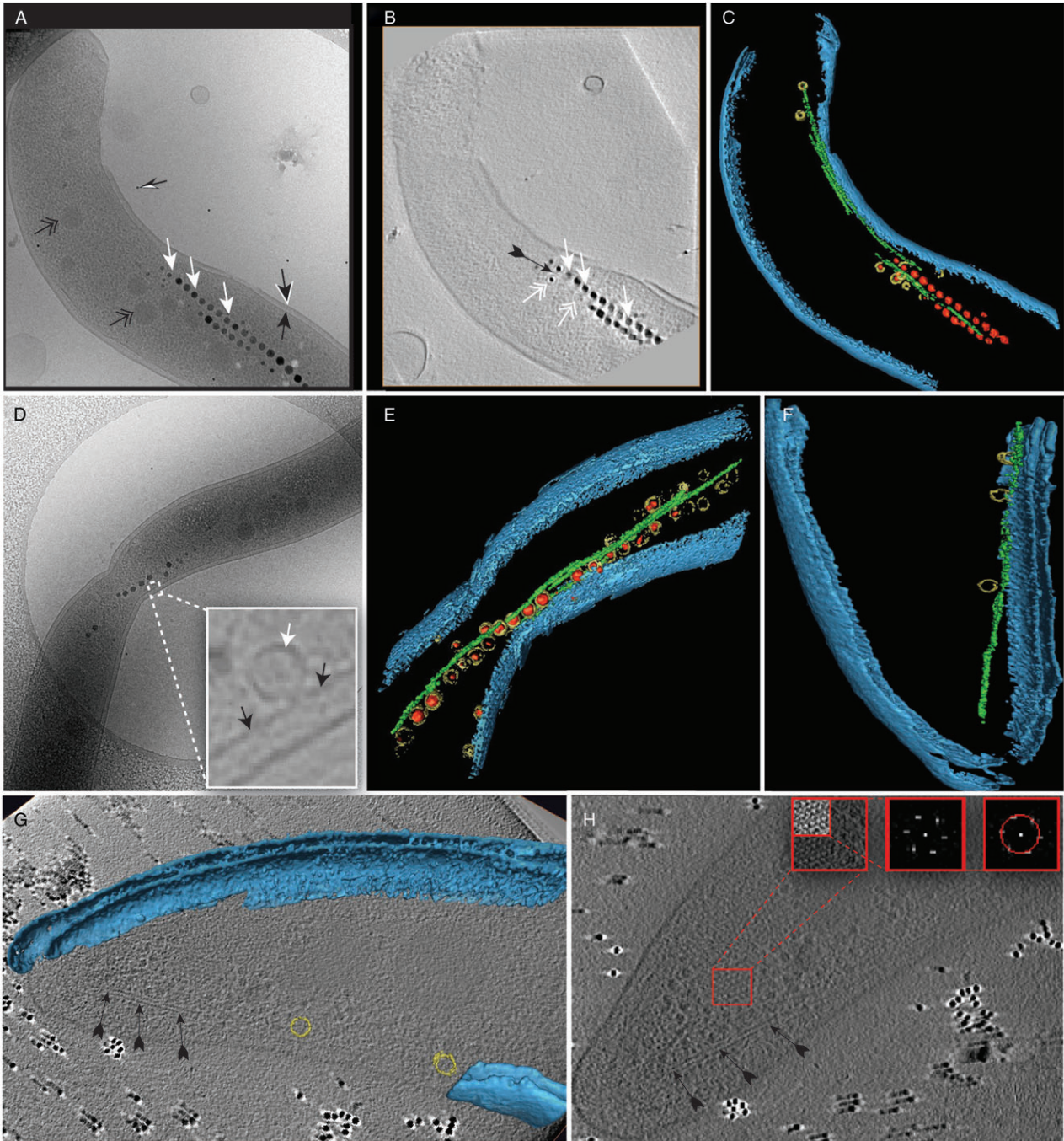


Fig. 3. Cryo-electron micrographs and tomograms of MSR WT.

A. Cryo-electron micrograph of a WT cell after the acquisition of a tilt series in vitrified ice.

B. x-y slice of a tomogram from (A).

C. Surface rendered volume the WT cell. Depicted are the cell membrane (blue), magnetite crystals (red), vesicles (yellow) and filaments (green).

D. Cryo-electron micrograph of WT cell in early division state after acquisition of a tilt series. Inset D: MM vesicle from *iv* invaginating from the CM (black arrows CM, white arrow MM).

E. Surface rendered volume of cell shown in (D).

F. Surface rendered pole of MSR WT cell exhibiting filaments close to the pole membrane.

G–H. x-y slices of WT tomogram (F). (Insets of H): power spectra of a putative chemoreceptor array, lattice distance 10.5 nm. Arrow tips; black: CM and black with white rim OM, black-white: fiducial gold marker (15 nm), white: magnetite crystals, double-white (B): vesicle membrane, black with fletching: filament, double-black: PHB granules.

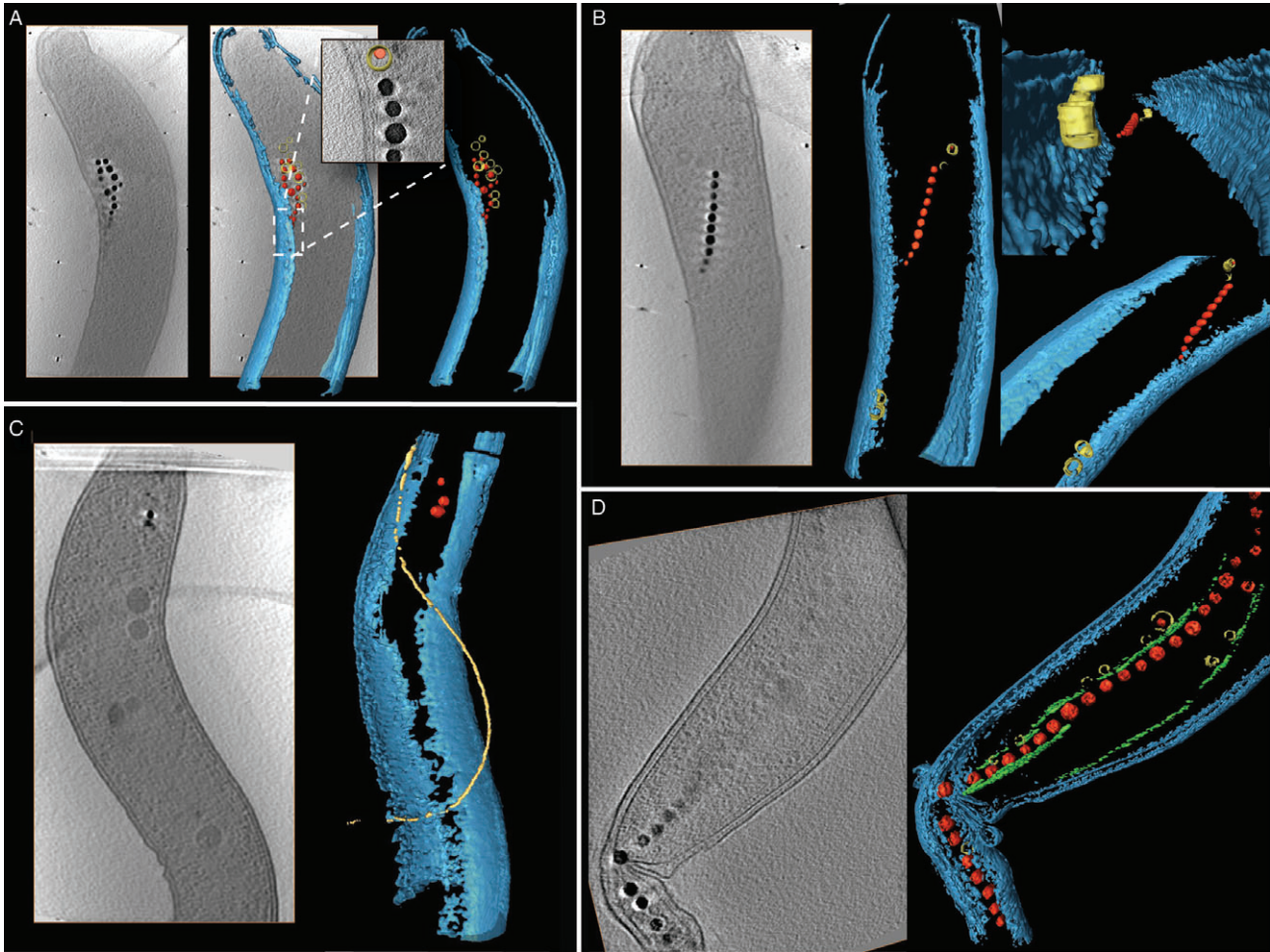


Fig. 4. Cryo-electron tomograms of $MSR\Delta mamK$ in early stationary phase grown under standard conditions (30°C, FSM), flagella (yellow) in (C).

D. Transcomplemented $MSR\Delta mamK$ mutant in late division state expressing *mamK* from pEK42. Surface-rendered representation of a segment of the cells showing vesicles (yellow) and magnetite crystals (red). Different three-dimensional orientations show the variety of the pleiotropic phenotypes (membrane in blue) of $MSR\Delta mamK$ mutants. The apparent absence of MM (vesicles, yellow) from mature magnetite crystals (red) is due to the adverse effect of variable diffraction contrast during tilting as a result of the crystalline magnetite.

remarkably might occur asymmetrically from only one side (Fig. 4A). During later division the magnetosome chain, and likely also the MF may be split into two parts (Figs 3A–E and 4D). However, due to the potential risk of technical artefacts these observations require future verification. Interestingly, two distinct filaments were detected in Fig. 4A within this cell. This was not observed in the analysed WT cells and might be the result of *mamK* expression from pEK42.

As in conventional micrographs, tomograms of WT cells frequently showed two parallel chains of particles that were aligned opposite to each other along the filaments (Figs 1A–i and 3A–E). In contrast, we failed to detect parallel chains in any of the 15 analysed $MSR\Delta mamK$ tomograms, which always contained only one linear string of crystals per analysed section.

Sometimes filaments with association to the CM were detected, where magnetosomes were absent or sparse (Fig. 3A). Whereas the number of magnetite crystals was significantly lower in $MSR\Delta mamK$, the proportion of empty versus filled vesicles per tomographed area was not increased. Even though the absolute enumeration of vesicles per cell is not possible due the limited analysed area and technical limitations (e.g. limited tilt range, missing wedge), the total number of MM vesicles (empty or filled) per viewed section was also decreased in the mutant. If all tomograms of central sections at identical magnification were taken into account under the assumption that they may represent comparable, randomly chosen areas at midcell from the WT (15 cells) and $MSR\Delta mamK$ (8 cells) cells, the average number of all vesicles were 21.6 (WT) versus 14.8 in the mutant,

respectively, implying that the formation of MM vesicles is affected in the mutant.

Magnetosome membrane vesicles were predominantly found in close contact with the CM. In several cells, empty MM vesicles were detected that were invaginating from the CM, apparently with the MM forming a continuum with the CM (Fig. 3A, inset). The size of empty or partially filled vesicles varied between 13.4 and 33.5 nm. However, vesicle dimensions were not strictly correlated with the presence or absence of growing immature crystallites, as larger vesicles (18–33.5 nm) devoid of crystals as well as smaller vesicles harbouring small crystallites were apparent in the analysed tomograms.

Effect of MSR Δ mamK on dynamic assembly of magnetosome chains

Deletion of *mamK* did not result in agglomeration of magnetosomes, but mutant cells still maintained a chain-like configuration. We therefore reasoned that instead merely providing a backbone or scaffold that mechanically stabilizes the magnetosome chain, the primary function of MamK might be rather in the control of the dynamic positioning and concatenating the individual particles during chain assembly and cell division as speculated before (Frankel and Bazylynski, 2006; Pradel *et al.*, 2006). For clarification, we undertook a growth experiment in which magnetite synthesis was induced in growing MSR Δ *mamK* and WT cells by the addition of iron to previously non-magnetic, iron-starved cells. As shown in Fig. 5, both WT and MSR Δ *mamK* cells started to form magnetite after addition of 50 μ M Fe(III)-citrate, and small (10–20 nm) crystallites could be first detected after 30 min. As in previous induction experiments (Scheffel *et al.*, 2006; Faivre *et al.*, 2007), initiation of magnetosome formation took place usually at few locations close to the cell periphery and scattered throughout the cell in WT and MSR Δ *mamK*. During the first 80 min magnetite biomineralization proceeded at similar rates in both strains. After about 100 min, magnetite formation of the mutant then lagged behind the WT, resulting in a lower magnetic orientation for the MSR Δ *mamK* over the remaining 200 min (Fig. 5). After 90 min irregular chains of magnetosomes became apparent at different loci in both mutant and WT cells. However, while WT cells formed the typical linear, and sometimes parallel chain fragments already located at midcell, chains in induced MSR Δ *mamK* mutant cells were displaced, short and more distorted than in those WT cells. After 120 and 300 min, further development of WT chains resulted in gradual extension and midcell localization, whereas in MSR Δ *mamK* cells fragmented, displaced chains were formed.

Discussion

Previous studies had suggested that the actin-like protein MamK is required for magnetosome chain assembly of AMB by aligning these organelles within the cell (Komeili *et al.*, 2006; Pradel *et al.*, 2006). However, the phenotype of a Δ *mamK* mutant of MSR generated in this study argues against an essential role in chain formation in this organism, as in spite of the absence of filamentous structures mutant cells are still able to form linear and coherent chains, albeit with reduced lengths and ectopic positions. For the assembly of a functional magnetosome chain, individual magnetite crystals have to be (i) aligned along a common linear axis, (ii) concatenated (i.e. by bringing newly synthesized particles to the nascent, tightly spaced magnetosome chain), and finally (iii) chains have to be positioned properly at their usual midcell localization. Instead merely providing a backbone or scaffold that mechanically stabilizes magnetosome chain, our data support speculations that MamK might be involved in sorting, concatenating and intracellular positioning of the magnetosome chain (Pradel *et al.*, 2006; Jogler and Schüler, 2009). On the other hand, the fact that a small percentage of Δ *mamK* cells still form long chains does not necessarily indicate that MamK has no scaffolding role at all, but just could mean that it cannot be the only factor promoting chains.

Our induction experiments show that MSR Δ *mamK* cells are also still able to assemble short, but coherent chains from dispersed magnetosome particles if challenged with the *de novo* synthesis of magnetite particles in non-magnetic, iron-starved cells undergoing cell division. This raises the question of how these chains are maintained in MSR Δ *mamK* mutants against their immanent tendency to agglomerate. Several mechanisms for chain formation have been suggested. In AMB chain initiation starts with the simultaneous formation of multiple, adjacent magnetosomes (Komeili *et al.*, 2004; Li *et al.*, 2009). In marked difference, magnetite biomineralization in MSR is initiated at multiple sites dispersed over the entire cell (Scheffel *et al.*, 2006) before eventually becoming concatenated into the mature coherent chains located at midcell, which suggests a control over dynamic localization and intracellular positioning of magnetosomes in this organism. When magnetic crystals continue to grow, increasing magnetostatic interactions between adjacent particles force them into close contact, which is then further stabilized by interactions through MM constituents. In the absence of the 'bead-on-a-string' like alignment along the MamK filaments, connections between the invaginating MM vesicles and the CM may be sufficient to maintain the linear arrangement of subchains in MSR Δ *mamK*. In addition to the cytoskeletal MF, an elusive sheath-like structure has been postulated that may hold magnetosome

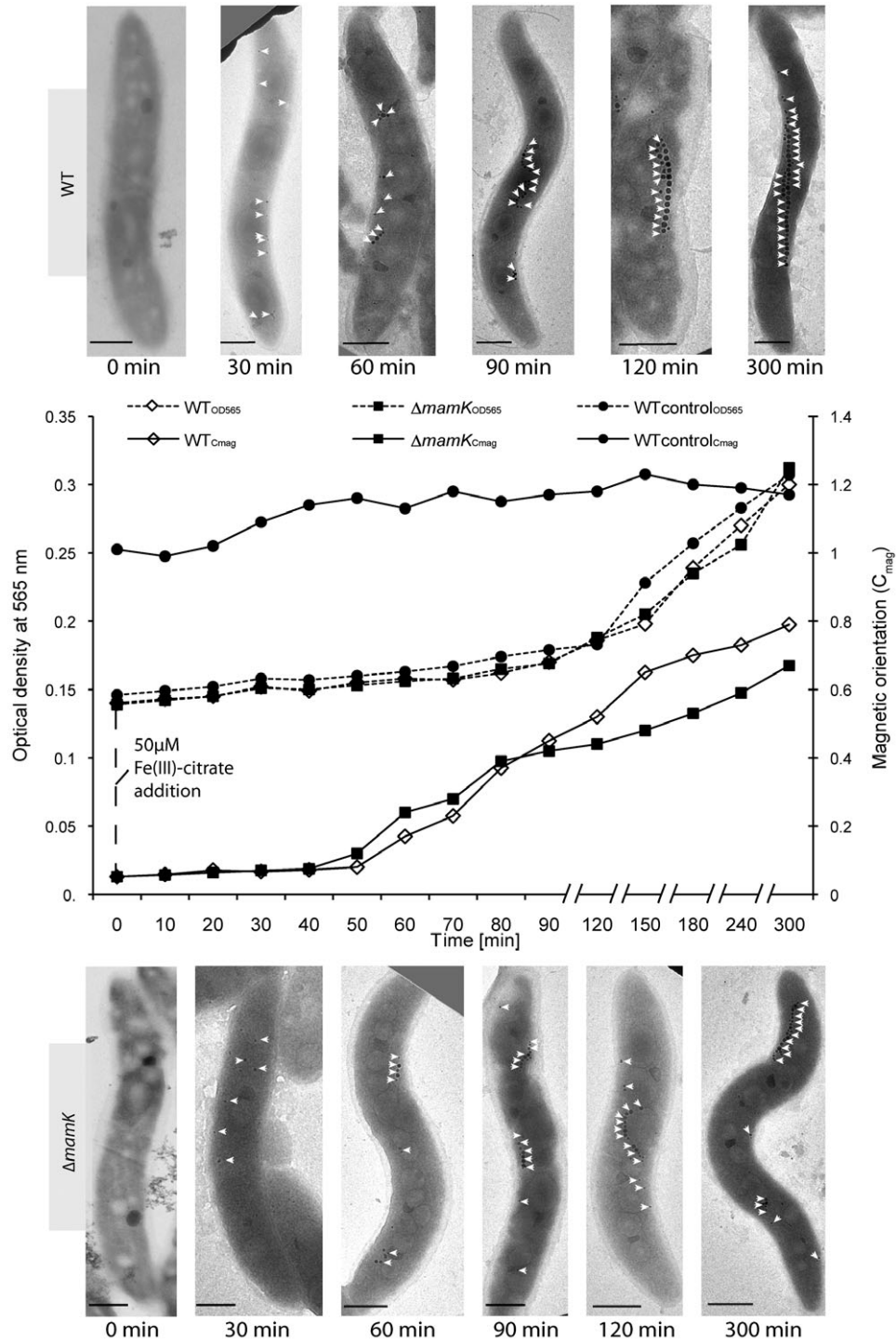


Fig. 5. Time course of magnetosome synthesis and chain assembly after iron induction in *M. gryphiswaldense* WT and MSR Δ mamK. Non-magnetic cells were cultured for 300 min in low iron media. 50 μ M Fe(III)-citrate was added at 0 min and growth (dashed line) was analysed by optical density at 565 nm. WT control cells were cultured under standard un-induced growth conditions in 50 μ M Fe(III)-citrate FSM. Solid lines: magnetic orientation (C_{mag}). Electron micrographs of cells from aliquots taken at various time points are shown. Scale bars 500 nm.

chains together and in place within the cell (Kobayashi *et al.*, 2006; Taoka *et al.*, 2006). However, in our extensive CET studies we failed to detect any indications for the existence of such an intracellular structure.

Like in AMB, deletion of the *mamK* gene resulted in the complete absence of MFs. In addition, we were unable to detect any other filament-like structures in MSR Δ *mamK* cells. This is interesting, as MSR Δ *mamK* cells are likely to contain further cytoskeletal structures formed by other filamentous proteins, such as MreB and FtsZ, which are encoded in the genome of MSR. In a study on *Caulobacter crescentus*, in which the formation of MreB filaments was inhibited by A22 treatment, similar filaments, which were speculated to be FtsZ, were still detectable by CET (Li *et al.*, 2007). Our failure to detect them thus might indicate that other cytoskeletal structures are way less abundant than MamK filaments within the cell.

Complementation of the MSR Δ *mamK* mutant not only with *mamK*_{MSR}, but also with *mamK*_{AMB} and *mamK*_{MS} did restore chain formation and the presence of magnetosomal filaments, indicating that these *mamK* alleles have equivalent functions and can substitute each other. However, despite the morphological and ultrastructural resemblance of the two organisms, the phenotypes of *mamK* mutants are distinct between MSR and AMB. Whereas the effect on chain assembly is less pronounced in MSR Δ *mamK* than in AMB1 Δ *mamK*, in which the mutant lacked the long, highly organized chains seen in WT (Komeili *et al.*, 2006), loss of MamK in MSR has several additional, pleiotropic effects. These differences do not result from different growth conditions, as MSR grown in magnetic spirillum growth medium (i.e. the genuine AMB medium) displayed the same morphology and magnetosome organization as in FSM (Flask Standard Medium, see *Experimental procedures*) (data not shown). On the other hand, WT AMB cells grown in FSM under identical conditions as MSR display a distinct chain configuration that is characterized by fairly loose, widely spaced chains that may extend through the entire cell (Fig. S4), compared with the midcell localization of densely spaced MSR chains (Fig. 1A), and it has been recently argued by Rioux *et al.* that the fraction of misaligned magnetosome chains in AMB1 Δ *mamK* may be well within the variability usually observed in the WT strain (Rioux *et al.*, 2010). This relatively weak phenotype and the differences between MSR and AMB might be explained by the fact that only 52% of all genes are shared between the two strains (Richter *et al.*, 2007). In fact, in the recent study by Rioux *et al.* a second *mamK*-like gene was discovered outside the MAI in an islet together with six additional magnetotaxis-related genes (Rioux *et al.*, 2010). These findings support the idea that the observed differences between AMB and MSR and their *mamK* mutants are due to a different genomic

context. Therefore, only a double deletion mutant of the *mamK*-like gene in addition to Δ *mamK* will reveal a more conclusive picture about MamK function in AMB.

One of the various effects of the *mamK* deletion in MSR is the formation of multiple, fragmented chains, which are strongly reminiscent to the subchains observed by Li *et al.* in experiments, in which magnetite formation was induced in aerobically grown non-magnetic cells of AMB by a shift to microaerobic incubation (Li *et al.*, 2009). Each of these subchains behaved as an ideal uniaxial single-domain particle with extremely weak magnetostatic interactions between subchains (Li *et al.*, 2009). Another distinctive feature of the MSR mutant is that the chains are displaced from their usual midcell location, which indicates that MamK is involved in positioning of magnetosomes by an as yet unknown mechanism. It has been speculated that positional information might be provided possibly by interaction with the divisome machinery that regulates proper cell division and determines septum formation (Schüler, 2008; Adams and Errington, 2009). This hypothesis has been further stimulated by the fact that a second *ftsZ*-like gene has been identified in the *mamXY* operon of MSR (Richter *et al.*, 2007). A putative chimeric protein was found within a metagenomic clone, in which a MamK-like domain is coupled to a FtsZ-like domain (Jogler *et al.*, 2009b). A recent study has shown that the second FtsZ-like protein in MSR is not involved in cell division but had rather an effect on biomineralization and, apparently, also on chain assembly (Ding *et al.*, 2009). So far, it still remains to be analysed whether this or the genuine FtsZ has an effect in providing information about midcell position.

Previous studies of MamK_{AMB} localization by Komeili *et al.* revealed that a C-terminal GFP fusion appeared in straight lines extending across most of the cell approximately along its inner curvature, consistent with the magnetosome-associated filaments in both localization and extent (Komeili *et al.*, 2006). CET revealed networks of long filaments 200 to 250 nm in length running parallel along the chain of an AMB WT cell. At any position within the chain, up to seven of these filaments flanked the magnetosome with no obvious spatial pattern (Komeili *et al.*, 2006). In contrast, fluorescence microscopy in our study revealed a more variable localization pattern of MamK_{MSR} depending on the particular GFP fusion and linker length. Variable fluorescence patterns were also detected for other actin-like proteins like ParM and MreB (Jones *et al.*, 2001; Møller-Jensen *et al.*, 2002), as incorporation of EGFP into a polymeric structure might affect MamK tertiary structure. Thus, a longer linker might provide sterical freedom required for its native localization. In addition, different linkers might affect the stability of EGFP fusions, and therefore, the distinct localization of the MamK fusions might also be function-unrelated. Although MamK-EGFP fusions (pAS_K1/2),

which show midcell fluorescence, also seem to complement the deletion of *mamK*, the pole-to-pole localization observed for EGFP-MamK (pAS_K, pEK42) is more consistent with the polar localization of MF bundles observed by CET, and also with the observation by Pradel *et al.* that one extremity of MamK_{AMB} was located at the pole if expressed in *E. coli* (Pradel *et al.*, 2006; 2007). It has been also suggested by these authors that MamK might somehow be involved in magnetoreception, possibly by interaction with other polar components (IcsA) (Pradel *et al.*, 2006). Our finding that extremities of MamK in some MSR cells extend towards arrays of chemoreceptors would support a possible interaction between *mamK* and these structures in signal transduction.

It has been demonstrated previously that MamK interacts with MamJ, but MamJ is not required for MamK filament formation (Scheffel *et al.*, 2006; Scheffel and Schüler, 2007). We found that on the other hand MamK is required for the filamentous localization of MamJ-EGFP (Fig. 2A–J), which is abolished in the MSRΔ*mamK* mutant. Previous studies have suggested that MamJ attaches magnetosomes to filaments formed by MamK by direct interaction (Scheffel and Schüler, 2007). If this would be the only MamJ function, then loss of either MamJ or MamK would be expected to result in essentially identical phenotypes, which is the collapse of chains and agglomeration of magnetosomes. As chain configuration, however, is maintained even in the absence of MamK, but not MamJ, the mode of chain stabilization by MamJ cannot exclusively be accomplished by MamK interaction, but has to involve other, so far unknown mechanisms as well.

MSRΔ*mamK* chains are also shorter, presumably as a consequence of the decreased numbers of magnetite crystals in the mutants. At this point, the reason for this unexpected effect on magnetosome formation is not clear. It has been suggested that MamK could act through establishment of magnetosome biogenesis factors (Komeili, 2007b). This might be, for example, by mediating the recruitment of other proteins required for biomineralization to the MM. A role in the recruitment and positioning of particular proteins has been demonstrated for other Alps and tubulin-like proteins, such as FtsZ, ParM and MreB, in *Bacillus subtilis* and *E. coli* (Salje and Löwe, 2008; Adams and Errington, 2009; Gamba *et al.*, 2009; Vats *et al.*, 2009). However, a preliminary comparative analysis of the MM between the mutant and the WT revealed virtually the same band patterns in SDS-PAGE experiments (data not shown). Intriguingly, our data imply that the number of MM vesicles is higher (21.6) in tomograms of the WT compared with 14.8 in the mutant, and the reduced number of MM vesicles in the mutant might be the reason why less magnetosome crystals are formed in cells devoid of MamK.

Our extensive CET analysis of > 40 WT and mutant cells also revealed several previously unrecognized ultra-structural features with relevance for magnetosomal organelle formation. For example, we have shown that, like in AMB the MM in MSR invaginates from the CM and at least transiently forms a continuum between the two membranes (Komeili *et al.*, 2006), indicating that the mechanisms of intracellular differentiations are similar between these organisms. In addition, we found that in the WT formation of two parallel chains is rather common, which was never observed in MSRΔ*mamK* cells. The reason for the formation of multiple chains in the WT is not entirely clear, but it can be speculated that MamK filaments may have a strong affinity for binding MM vesicles, possibly by its interaction with MamJ and other proteins, and thus tend to gather magnetosomes within their vicinity.

In conclusion, our data argue for a function of MamK in positioning and concatenating magnetosome chains rather than merely providing a rigid scaffold for chain alignment. Our results further suggest that the role of MamK is likely to be more complex and somewhat distinct from previously reported models that were mostly inferred from the single *mamK* deletion in AMB (Komeili *et al.*, 2006; Rioux *et al.*, 2010). At this point, the precise mechanisms by which magnetosome chains are positioned by MamK remains elusive and will require further investigation of interaction with and localization of further constituents of the magnetosome assembly and vesicle formation machinery.

Experimental procedures

Bacterial strains, media and magnetosome isolation

Strains *M. magneticum* AMB-1 (AMB) and *M. gryphiswaldense* MSR-1 (MSR) were grown in modified liquid FSM and LIM (Low iron media, modified FSM) (Heyen and Schüler, 2003; Faivre *et al.*, 2007). Modified magnetic spirillum growth medium (Blakemore *et al.*, 1979; Komeili *et al.*, 2004) (50 μM ferric citrate instead of ferric malate) was alternatively used where indicated. Growth of *E. coli* strain BW29427 (Table 1) was accomplished in lysogeny broth supplemented with 1 mM DL-α ε-diaminopimelic acid (Sigma-Aldrich, Switzerland). Culture conditions for *E. coli* strains were as described (Sambrook and Russell, 2001). Magnetosomes were isolated from microaerobically grown 5l cultures as described elsewhere (Grünberg *et al.*, 2004; Ohuchi and Schüler, 2009). Optical densities and C_{mag} values of MSR cultures were measured turbidimetrically at 565 nm with immotile cells inactivated by the addition of formaldehyde (Fluka, Switzerland) to a final concentration of 0.1% prior to the measurement (Scheffel *et al.*, 2006).

DNA techniques and southern blot

Total DNA from all strains used in this study was isolated as described previously (Marmur, 1961; Grünberg *et al.*, 2001).

Table 1. Plasmids, primers and strains used in this work.

Vector	Details	References	Index
pEK32	4 kb flanking sequences of <i>mamK</i> [13]	This work	[1]
pEK33	<i>mamK_{MSR-1}</i> [15]	This work	[2]
pEK34	<i>mamK_{AMB-1}</i> [15]	This work	[3]
pEK35	<i>mamK_{MS-1}</i> [15]	This work	[4]
pEK36	<i>mamKshort_{MSR-1}</i> [16]	This work	[5]
pEK37	<i>mamK_{AMB-1}</i> [16]	This work	[6]
pEK40	<i>mamK_{MSR-1}</i> [16]	This work	[7]
pEK42	<i>egfp_LCLOGE_{mamKshort_{MSR-1}}</i> [14]	This work	[8]
pAS_K	<i>egfp_LCLOGE_{mamK_{MSR-1}}</i> [14]	(Scheffel, 2007)	[9]
pAS_K1	<i>mamK_GS_egfp</i> [14]	This work	[10]
pAS_K2	<i>egfp_SAI_{mamK}</i> [14]	This work	[11]
pAS_J	<i>mam_J_egfp</i> [14]	This work	[12]
pK19mobGII	–	(Scheffel <i>et al.</i> , 2006)	[13]
pBBR1MCS-2	–	(Katzmann <i>et al.</i> , 1999)	[14]
pBBRP <i>mamDC</i>	–	(Kovach <i>et al.</i> , 1994)	[15]
pBBRP <i>mamAB</i>	–	(Lang <i>et al.</i> , 2009)	[16]
Primer	Sequence (5'-3')	Restriction site	
EkmamK_F02	CATATGGGATGATCTGTTAGC		NdeI
EkmamK_R02	GGATCCTCACTGACCGGAAAC		BamHI
EkmamK_F_kuiz	CATATGAGTGAAGGTGAAGG		NdeI
EkmamK_R02	GGATCCTCACTGACCGGAAAC		BamHI
EK_mamK_AMB1_F	CATATGAGTGAAGGTGAAGCC		NdeI
EK_mamK_AMB1_R2	GGATCCTCACGAGCCGGA		BamHI
EK_mamK_MS1_F	CATATGAGTGAAGGTGAAGCC		NdeI
EK_mamK_MS1_R2	GGATCCTCACGAGCCGGA		BamHI
EK2_K_u_f	TCTAGAGTAGCCGGCCTCGCTCCTGGG		XbaI
EK_K_u_r	CCCGGGATTGCTAACTAGTCAGGT		SmaI/
EK_K_d_f	CTCTATTATCTTATCTTC		SpeI
EK2_K_d_r	ACTAGTCACGTCGAAGGACCCGACTTTTG		SpeI
ASEGFP_f10	CCCGGG GGATCCATTCCGCCCTTCTCCAGTC		BamHI
ASEGFP_r11	GAATTCATGGTGAGCAAGGGCGAG		BamHI
ASmamKs_f3	CTGCCCTGCAGGCACAGCTTGACAGCTCGTCCAT		–
ASmamKe_t2	TGCCCTGCAGGGCGAGCTGTGGATTGATCTGTTA		XbaI
EK_K_f	TCTAGACTACTGACCGGAAACGTCACC		
EK_probek02_r	TTGCTGCTCCCGCCGTTG		
Name	TTGTCCAAGCCATAGCCG		
<i>Magnetospirillum gryphiswaldense</i> , Δ <i>mamK</i>	Relevant genotype or phenotype	(Schultheiss <i>et al.</i> , 2004)	Construction
<i>Magnetospirillum gryphiswaldense</i> MSR-1	MSR-1 E10, Δ <i>mamK</i> , Rif ^r ,	(Scheffel <i>et al.</i> , 2006)	This work
<i>Magnetospirillum gryphiswaldense</i> MSR-1, Δ <i>mamJ</i>	Strept ^r , Rif ^r , Strept ^r derivative of DSM6361 (WT)		
<i>Magnetospirillum gryphiswaldense</i> MSR-1B	Rif ^r , Strept ^r , spontaneous deletion mutant, lacking 40.4 kb within MAI, mag ^r	(Schubbe <i>et al.</i> , 2003; Ullrich <i>et al.</i> , 2005)	
<i>Magnetospirillum magneticum</i> AMB-1	WT ATCC700264	(Kawaguchi <i>et al.</i> , 1992)	
<i>E. coli</i> DH5 α	F- <i>supE</i> 44 DacU169 (80/ <i>lacZ</i> Δ lacU169(Φ 80/ <i>lacZ</i> DM15) <i>hsdR17recA1endA1gyrA96thi-1relA1</i>)	(Bethesda Research Laboratories, 1986)	
<i>E. coli</i> BW29427	<i>thrB1004 pro thi rpsL hsdS lacZ</i> Δ M15 RP4-1360(λ <i>araBAD</i>)567 Δ <i>dapA</i> 1341::[<i>erm pir</i> (wildtyp)] <i>tra</i>	K.A. Datsenko and B.L. Wanner (Purdue University, IN, USA)	

Genetic constructs used to generate the $\text{MSR}\Delta\text{mamK}$ deletion were amplified using standard polymerase chain reaction (PCR) procedures. The primers and plasmids used in this study are shown in Table 1. Primer sequences for amplification of DNA fragments from MSR were deduced from GenBank sequence deposition BX571797. The primer pairs used for the amplification of *mamK* from *Magnetospirillum* strains AMB and MS were deduced from sequence deposition NC_007626 and NZ_AAAP01003824.1 respectively. For sequencing, BigDye terminators v3.1 (Applied Biosystems, Darmstadt, Germany) were used. Sequence data were analysed with Lasergene 6 (DNASTar, Madison, WI) and MacVector 7.2.3 (Oxford Molecular, Oxford, UK) programs. Southern blots were performed by standard procedures as described previously (Ullrich *et al.*, 2005) (Fig. S5).

Construction of an unmarked in-frame *mamK* deletion mutant

Gene deletion was accomplished via homologous recombination of up- and downstream *mamK* flanking sequence in pEK32 with the MSR chromosome. A 2003 bp upstream and a 2009 bp downstream *mamK* flanking region were amplified with primer pairs EK2_K_u_f/EK_K_u_r and EK_K_d_f/EK2_K_d_r. The fragments were fused by cloning into the XbaI and BamHI restriction sites of pK19*mob*GII vector, resulting in pEK32. Plasmids were transferred into *M. gryphiswaldense* by biparental conjugation and screening was performed as previously described (Schultheiss *et al.*, 2004). Screening for the *gusA* marker (Katzen *et al.*, 1999) revealed 8 Kan^r insertion mutants occurring with a frequency of 1.7×10^{-7} on X-Gluc (5-Bromo-4-Chloro-3-Indolyl- β -D-glucuronic acid, 0.5 mM) containing solid FSM plates. After 2 passages for 3 days in 300 μl liquid culture and subsequent 1 day in 10 ml (~5 generations), an incubation for 10 days on solid FSM at 30°C under microoxic conditions was performed. Screening by PCR of 24 white colonies for putative double crossover resolvants revealed eight positive candidates that were *gusA*⁺ and Kan^s . Double crossover mutants were obtained at a final frequency of 2.6×10^{-3} . Successful unmarked in-frame deletion of *mamK* was confirmed by PCR and southern blotting using a 816 bp DNA probe amplifying parts of *mamJ* and *mamK* gene of MSR with primer pairs EK_K_f/EK_probeK02_r (Fig. S5). One clone named $\text{MSR}\Delta\text{mamK}$ was selected for further analysis.

Complementation experiments

A cloned fragment comprising an open-reading frame of 1083 bp that starts with a CTG codon according to the previously deposited database sequence [CAJ30118 (Ullrich *et al.*, 2005)] was not functionally expressed (data not shown). Inspection of the aligned sequences of *mamK* nucleotide sequences of *mamK* orthologs from MSR, AMB (1044 bp, 33 nt mismatches, 90.8% aa identity) and MS (1044 bp, 34 nt mismatches, 90.6% aa identity) revealed a conserved ATG in all three orthologs 39 bp downstream of the predicted CTG start codon in the older database version of *mamK*_{MSR}, which hereafter was considered as the correct start codon, resulting in an open-reading frame of 1044 bp as in the other strains.

The *mamK* gene was either amplified with primer pair EKmamK_F_kurz/EKmamK_R02 and the 1056 bp fragment subsequently cloned into NdeI and BamHI restriction sites of pBBR_{p mamDC} generating pEK36, or with primer pair EKmamK_F02/EKmamK_R02 resulting in a 1083 bp fragment in which the start codon CTG was changed into an ATG. Likewise, the ATG defines the recognition site of 5' NdeI restriction enzyme. Together with the 3' BamHI recognition site the fragment was cloned into pBBR1*p mamAB* (Lang *et al.*, 2009) yielding pEK36 and subsequently transformed into $\text{MSR}\Delta\text{mamK}$ via biparental mating as described (Schultheiss and Schüler, 2003; Schultheiss *et al.*, 2004). The *mamK* of AMB was PCR amplified with primer pairs EK_mamK_AMB1_F/EK_mamK_AMB1_R2 yielding a 1056 bp fragment, which was cloned into NdeI/ BamHI restriction site of pBBR1*p mamAB* or pBBR*p mamDC* , resulting in pEK37 and pEK34 respectively. Amplification and subsequent cloning of MS *mamK* into pBBR1*p mamDC* resulted in pEK35.

Construction of Mam-EGFP fusions

Several different *mamK-egfp* (enhanced GFP) expression fusions were constructed via fusion PCR (Ho *et al.*, 1989). The *mamK* gene of MSR (accession number CAJ30118) and *egfp* (pEGFP-N2, Clontech) were amplified using primers as described, resulting in the C-terminal MamK fusion pAS_K1 (Scheffel, 2007). For construction of the N-terminal fusion with a 6 amino acid linker sequence, primer pairs for *egfp*-gene ASEGFP_f10/ ASEGFP_r11, and for *mamK* ASmamKs_f3/ ASmamKe_r2, were used and resulted in pAS_K vector (Scheffel, 2007).

Gel electrophoresis and Western blot experiments

Protein concentrations were determined with a BCA-Protein Micro assay kit (Pierce) according to the manufacturer's instructions. For one-dimensional SDS-PAGE of magnetosome-associated proteins we used the procedure of Laemmli (Laemmli, 1970). An amount of magnetosome particles or solubilisate equivalent to 6.5 μg of protein was mixed with electrophoresis sample buffer containing 2% (wt/wt) SDS and 5% (wt/vol) 2-mercaptoethanol. After boiling for 5 min, samples were centrifuged for 3 min. The supernatants were loaded onto polyacrylamide gels containing various concentrations of polyacrylamide (8% to 16%). The non-magnetic fraction of whole cells was further processed as described elsewhere (Grünberg *et al.*, 2001), and 6.5 μg protein was used for analysis on SDS gels. Western blot experiments were performed as explained in previous work (Schübbe *et al.*, 2006). The anti-MamK primary antibody was raised by S. Schübbe as described (Schübbe, 2005).

Fluorescence microscopy

MSR WT and $\text{MSR}\Delta\text{mamK}$ bearing the plasmids pAS_J, pAS_K(1,2), were grown in 15 ml polypropylene tubes with sealed screw caps and a culture volume of 10 ml to stationary phase. The cell membranes were stained with the membrane stain FM4-64 (Invitrogen, Karlsruhe, Germany) at a final con-

centration of 16.4 μM , immobilized on agarose pads (FSM salts in H_2O , supplemented with 1% agarose), and imaged with an Olympus BX81 microscope equipped with a 100 UPLSAPO100XO objective (numerical aperture of 1.40) and a Hamamatsu Orca AG camera. Images were captured and analysed using Olympus cell software.

TEM and CET

For TEM analysis, unstained cells were adsorbed on carbon coated copper grids and air-dried (Plano, Wetzlar). Bright field TEM was performed on a FEI Tecnai F20 transmission electron microscope (FEI; Eindhoven, the Netherlands) at an accelerating voltage of 200 kV. Images were captured with a FEI Eagle 4096 \times 4096 pixel CCD camera using EMMenue 4.0 and FEI's Explore 3D.

For CET, a FEI Tecnai F30 Polara transmission electron microscope (FEI; Eindhoven, the Netherlands), equipped with 300 kV field emission gun, a Gatan GIF 2002 Post-Column Energy Filter, and a 2048 \times 2048 pixel Gatan CCD Camera (Gatan; Pleasanton, CA) were used. All data collection was performed at 300 kV, with the energy filter operated in the zero-loss mode (slit width of 20 eV). Tilt series were acquired using Serial EM (Mastronarde, 2005) and FEI's Explore 3D software.

Quantifoil copper grids (Quantifoil Micro Tools GmbH, Jena) were prepared by placing a 5 μl droplet of 10–15 nm colloidal gold clusters (Sigma) on each grid for subsequent alignment purposes. A 5 μl droplet of a fresh MSR culture was added onto the prepared grid, and after blotting was embedded in vitreous ice by plunge freezing into liquid ethane (temperature c. -170°C). Single-axis tilt series for tomography were typically recorded with 2 increments over an angular range of $\pm 65^\circ$. To minimize the electron dose applied to the ice-embedded specimen, data were recorded at low-dose conditions by using automated data acquisition software. The total dose accumulated during the tilt series was kept below 100 $\text{e}/\text{\AA}^2$. To account for the increased specimen thickness at high tilt angles, the exposure time was multiplied by a factor of $1/\cos \alpha$. The object pixel size in unbinned images was 0.661 at a magnification of 34 000 \times , 0.805 at 27 500 \times and 0.979 at 22 500 \times . Images were recorded at nominal defocus values of $-8 \mu\text{m}$ or $-4 \mu\text{m}$.

Data analysis

Three-dimensional reconstructions from tilt series were performed with the weighted back-projection method and further analysis of the tomograms was done using the TOM toolbox (Nickell *et al.*, 2005). Visualizations of the tomograms were done with Amira (<http://www.amiravis.com>) on 2 times binned volumes.

Determination of iron content by atomic absorption spectroscopy

Cells were grown to an optical density of 0.2 and aliquots of 1 ml were taken and pelleted. After a subsequent pellet washing step in 0.5 ml 20 mM HEPES + 5 mM EDTA both the

supernatant (900 μl) and the pellet were supplemented with 10 μl and 100 μl 65% nitric acid respectively. Incubation at 98°C for 2 h dissolved all organic material and magnetosomes, and dilutions of 1:100 and 1:1000 in H_2O were analysed by atomic absorption spectroscopy (Varian AA240) using SpectrAA 240FS software version 5.01 (Varian, Australia) with the following parameters set: wavelength 248.3 nm, slit width 0.2 nm, cathode lamp current 10.0 mA.

Acknowledgements

We are grateful to Günter Pfeifer (MPI of Biochemistry) for help with the TEM. This work was supported by the Max Planck Society and the Deutsche Forschungsgemeinschaft (Schu1080/9-1 and 10-1).

References

- Adams, D.W., and Errington, J. (2009) Bacterial cell division: assembly, maintenance and disassembly of the Z ring. *Nat Rev Microbiol* **7**: 642–653.
- Balkwill, D., Maratea, D., and Blakemore, R.P. (1980) Ultrastructure of a magnetotactic spirillum. *J Bacteriol* **141**: 1399–1408.
- Bethesda Research Laboratories (1986) BRL pUC host: *E. coli* DH5 alpha competent cells. *Focus* **8**: 1–19.
- Blakemore, R., Maratea, D., and Wolfe, R. (1979) Isolation and pure culture of freshwater magnetic spirillum in chemically defined medium. *J Bacteriol* **140**: 720–729.
- Briegleb, A., Ortega, D.R., Tocheva, E.I., Wuichet, K., Li, Z., Chen, S., *et al.* (2009) Universal architecture of bacterial chemoreceptor arrays. *Proc Natl Acad Sci USA* **106**: 17181–17186.
- Carballido-Lopez, R. (2006) The bacterial actin-like cytoskeleton. *Microbiol Mol Biol Rev* **70**: 888–909.
- Carballido-Lopez, R., and Errington, J. (2003) A dynamic bacterial cytoskeleton. *Trends Cell Biol* **13**: 577–583.
- Derman, A.I., Becker, E.C., Truong, B.D., Fujioka, A., Tucey, T.M., Erb, M.L., *et al.* (2009) Phylogenetic analysis identifies many uncharacterized actin-like proteins (Alps) in bacteria: regulated polymerization, dynamic instability and treadmilling in Alp7A. *Mol Microbiol* **73**: 534–552.
- Ding, Y., Li, J., Liu, J., Yang, J., Jiang, W., Tian, J., *et al.* (2009) Deletion of the *ftsZ*-like gene results in the production of superparamagnetic magnetite magnetosomes in *Magnetospirillum gryphiswaldense*. *J Bacteriol* **192**: 1097–1105.
- Dye, N.A., Pincus, Z., Theriot, J.A., Shapiro, L., and Gitai, Z. (2005) Two independent spiral structures control cell shape in *Caulobacter*. *Proc Natl Acad Sci USA* **102**: 18608–18613.
- Faivre, D., Böttger, L.H., Matzanke, B.F., and Schüler, D. (2007) Intracellular magnetite biomineralization in bacteria proceeds by a distinct pathway involving membrane-bound ferritin and an iron(II) species. *Angew Chem Int Ed Engl* **46**: 8495–8499.
- Frankel, R., and Bazylinski, D. (2006) How magnetotactic bacteria make magnetosomes queue up. *Trends Microbiol* **14**: 329–331.
- Gamba, P., Veening, J.-W., Saunders, N.J., Hamoen, L.W.,

- and Daniel, R.A. (2009) Two-step assembly dynamics of the *Bacillus subtilis* divisome. *J Bacteriol* **191**: 4186–4194.
- Gorby, Y.A., Beveridge, T.J., and Blakemore, R. (1988) Characterization of the bacterial magnetosome membrane. *J Bacteriol* **170**: 834–841.
- Grünberg, K., Wawer, C., Tebo, B.M., and Schüler, D. (2001) A large gene cluster encoding several magnetosome proteins is conserved in different species of magnetotactic bacteria. *Appl Environ Microbiol* **67**: 4573–4582.
- Grünberg, K., Müller, E.C., Otto, A., Reszka, R., and Linder, D. (2004) Biochemical and proteomic analysis of the magnetosome membrane in *Magnetospirillum gryphiswaldense*. *Appl Environ Microbiol* **70**: 1040–1050.
- Heyen, U., and Schüler, D. (2003) Growth and magnetosome formation by microaerophilic *Magnetospirillum* strains in an oxygen-controlled fermentor. *Appl Microbiol Biotechnol* **61**: 536–544.
- Ho, S., Hunt, H., Horton, R., Pullen, J., and Pease, L. (1989) Site-directed mutagenesis by overlap extension using the polymerase chain reaction. *Gene* **77**: 51–59.
- Jogler, C., and Schüler, D. (2007) Genetic analysis of magnetosome biomineralization. In *Magnetoreception and Magnetosomes in Bacteria*. Schüler D. (ed.). Berlin, Heidelberg: Springer-Verlag Berlin Heidelberg, pp. 133–161.
- Jogler, C., and Schüler, D. (2009) Genomics, genetics, and cell biology of magnetosome formation. *Annu Rev Microbiol* **63**: 501–521.
- Jogler, C., Kube, M., Schübbe, S., Ullrich, S., Teeling, H., Bazylini, D.A., et al. (2009a) Comparative analysis of magnetosome gene clusters in magnetotactic bacteria provides further evidence for horizontal gene transfer. *Environ Microbiol* **11**: 1267–1277.
- Jogler, C., Lin, W., Meyerdieks, A., Kube, M., Katzmann, E., Flies, C., et al. (2009b) Toward cloning of the magnetotactic metagenome: identification of magnetosome island gene clusters in uncultivated magnetotactic bacteria from different aquatic sediments. *Appl Environ Microbiol* **75**: 3972–3979.
- Jones, L.J., Carballido-Lopez, R., and Errington, J. (2001) Control of cell shape in bacteria: helical, actin-like filaments in *Bacillus subtilis*. *Cell* **104**: 913–922.
- Katzen, F., Becker, A., Ielmini, M.V., Oddo, C.G., and Ielpi, L. (1999) New mobilizable vectors suitable for gene replacement in gram-negative bacteria and their use in mapping of the 3' end of the *Xanthomonas campestris* pv. *campestris* gum operon. *Appl Environ Microbiol* **65**: 278–282.
- Kawaguchi, R., Burgess, J., and Matsunaga, T. (1992) Phylogeny and 16S rRNA sequence of *Magnetospirillum* sp. AMB-1, an aerobic magnetic bacterium. *Nucleic Acids Res* **20**: 1140.
- Kirschvink, J.L. (1982) Paleomagnetic evidence for fossil biogenic magnetite in western Crete. *Earth Planet Sci Lett* **59**: 388–392.
- Kobayashi, A., Kirschvink, J.L., Nash, C.Z., Kopp, R.E., Sauer, D.A., Bertani, L.E., et al. (2006) Experimental observation of magnetosome chain collapse in magnetotactic bacteria: sedimentological, paleomagnetic, and evolutionary implications. *Earth Planet Sci Lett* **245**: 538–550.
- Komeili, A. (2007a) Cell biology of magnetosome formation. In *Magnetoreception and Magnetosomes in Bacteria*. Schüler, D. (ed.). Berlin, Heidelberg: Springer-Verlag Berlin Heidelberg, pp. 163–173.
- Komeili, A. (2007b) Molecular mechanisms of magnetosome formation. *Annu Rev Biochem* **76**: 351–366.
- Komeili, A., Vali, H., Beveridge, T.J., and Newman, D.K. (2004) Magnetosome vesicles are present before magnetite formation, and MamA is required for their activation. *Proc Natl Acad Sci USA* **101**: 3839–3844.
- Komeili, A., Li, Z., Newman, D.K., and Jensen, G.J. (2006) Magnetosomes are cell membrane invaginations organized by the actin-like protein MamK. *Science* **311**: 242–245.
- Kovach, M.E., Phillips, R.W., Elzer, P.H., Roop, R.M., and Peterson, K.M. (1994) pBBR1MCS: a broad-host-range cloning vector. *BioTechniques* **16**: 800–802.
- Laemmli, U.K. (1970) Cleavage of structural proteins during the assembly of the head of bacteriophage T4. *Nature* **227**: 680–685.
- Lang, C., Pollithy, A., and Schüler, D. (2009) Identification of promoters for efficient gene expression in *Magnetospirillum gryphiswaldense*. *Appl Environ Microbiol* **75**: 4206–4210.
- Li, Z., and Jensen, G. (2009) Electron cryotomography: a new view into microbial ultrastructure. *Curr Opin Microbiol* **12**: 1–8.
- Li, J.L., Pan, Y., Chen, G., Liu, Q., Tian, L., and Lin, W. (2009) Magnetite magnetosome and fragmental chain formation of *Magnetospirillum magneticum* AMB-1: transmission electron microscopy and magnetic observations. *Geophys J Int* **177**: 33–42.
- Li, Z., Trimble, M.J., Brun, Y.V., and Jensen, G. (2007) The structure of FtsZ filaments in vivo suggests a force-generating role in cell division. *EMBO J* **26**: 4694–4708.
- Lučić, V., Forster, F., and Baumeister, W. (2005) Structural studies by electron tomography: from cells to molecules. *Annu Rev Biochem* **74**: 833–865.
- Marmur, J. (1961) A procedure for the isolation of deoxyribonucleic acid from microorganisms. *J Mol Biol* **3**: 208–218.
- Mastrorade, D.N. (2005) Automated electron microscope tomography using robust prediction of specimen movements. *J Struct Biol* **152**: 36–51.
- Milne, J.L.S., and Subramaniam, S. (2009) Cryo-electron tomography of bacteria: progress, challenges and future prospects. *Nat Rev Microbiol* **7**: 666–675.
- Møller-Jensen, J., Jensen, R.B., Löwe, J., and Gerdes, K. (2002) Prokaryotic DNA segregation by an actin-like filament. *EMBO J* **21**: 3119–3127.
- Murat, D., Quinlan, A., Vali, H., and Komeili, A. (2010) Comprehensive genetic dissection of the magnetosome gene island reveals the step-wise assembly of a prokaryotic organelle. *Proc Natl Acad Sci USA* **107**: 5593–5598.
- Nakazawa, H., Arakaki, A., Narita-Yamada, S., Yashiro, I., Jinno, K., Aoki, N., et al. (2009) Whole genome sequence of *Desulfovibrio magneticus* strain RS-1 revealed common gene clusters in magnetotactic bacteria. *Genome Res* **19**: 1801–1808.
- Nickell, S., Forster, F., Linaroudis, A., Net, W.D., Beck, F., Hegerl, R., et al. (2005) TOM software toolbox: acquisition and analysis for electron tomography. *J Struct Biol* **149**: 227–234.
- Ohuchi, S., and Schüler, D. (2009) *In vivo* display of a multisubunit enzyme complex on biogenic magnetic nanoparticles. *Appl Environ Microbiol* **75**: 7734–7738.

- Pradel, N., Santini, C., Bernadac, A., Fukumori, Y., and Wu, L. (2006) Biogenesis of actin-like bacterial cytoskeletal filaments destined for positioning prokaryotic magnetic organelles. *Proc Natl Acad Sci USA* **103**: 17485–17489.
- Pradel, N., Santini, C., Bernadac, A., Shih, Y., Goldberg, M., and Wu, L. (2007) Polar positional information in *Escherichia coli* spherical cells. *Biochem Biophys Res Commun* **353**: 493–500.
- Richter, M., Kube, M., Bazylnski, D.A., Lombardot, T., Glöckner, F.O., Reinhardt, R., and Schüler, D. (2007) Comparative genome analysis of four magnetotactic bacteria reveals a complex set of group-specific genes implicated in magnetosome biomineralization and function. *J Bacteriol* **189**: 4899–4910.
- Rioux, J.-B., Philippe, N., Pereira, S., Pignol, D., Wu, L.-F., and Ginet, N. (2010) A second actin-like MamK protein in *Magnetospirillum magneticum* AMB-1 encoded outside the genomic magnetosome island. *PLoS ONE* **5**: e9151.
- Salje, J., and Löwe, J. (2008) Bacterial actin: architecture of the ParMRC plasmid DNA partitioning complex. *EMBO J* **27**: 2230–2238.
- Sambrook, J., and Russel, D. (2001) *Molecular Cloning: A Laboratory Manual*. New York: Cold Spring Harbor Laboratory Press, p. 999.
- Scheffel, A. (2007) Molekulare und strukturelle Untersuchung zur Bildung von Magnetosomen und zur Assemblierung von Magnetosomenketten. *Doctoral thesis*. University of Bremen, 1–194.
- Scheffel, A., and Schüler, D. (2007) The acidic repetitive domain of the *Magnetospirillum gryphiswaldense* MamJ protein displays hypervariability but is not required for magnetosome chain assembly. *J Bacteriol* **189**: 6437–6446.
- Scheffel, A., Gruska, M., Faivre, D., Linaroudis, A., Graumann, P.L., Plitzko, J., and Schüler, D. (2006) An acidic protein aligns magnetosomes along a filamentous structure in magnetotactic bacteria. *Nature* **440**: 110–114.
- Schübbe, S. (2005) Untersuchung zur molekularen Regulation und Organisation der *mam*-Gene in *Magnetospirillum gryphiswaldense* MSR-1. *Doctoral thesis*. University of Bremen, 1–167.
- Schübbe, S., Kube, M., Scheffel, A., Wawer, C., Heyen, U., Meyerdierks, A., et al. (2003) Characterization of a spontaneous nonmagnetic mutant of *Magnetospirillum gryphiswaldense* reveals a large deletion comprising a putative magnetosome island. *J Bacteriol* **185**: 5779–5790.
- Schübbe, S., Würdemann, C., Peplies, J., Heyen, U., Wawer, C., Glöckner, F.O., and Schüler, D. (2006) Transcriptional organization and regulation of magnetosome operons in *Magnetospirillum gryphiswaldense*. *Appl Environ Microbiol* **72**: 5757–5765.
- Schüler, D. (2004a) Molecular analysis of a subcellular compartment: The magnetosome membrane in *Magnetospirillum gryphiswaldense*. *Arch Microbiol* **181**: 1–7.
- Schüler, D. (2004b) Characterization of the magnetosome membrane in *Magnetospirillum gryphiswaldense*. In *Biomineralization*. Baeuerlein, E. (ed.). Weinheim: Wiley-VCH Verlag GmbH, pp. 109–118.
- Schüler, D. (2008) Genetics and cell biology of magnetosome formation in magnetotactic bacteria. *FEMS Microbiol Rev* **32**: 654–672.
- Schüler, D., and Köhler, M. (1992) The isolation of a new magnetic spirillum. *Zentralbl Mikrobiol* **147**: 150–151.
- Schultheiss, D., and Schüler, D. (2003) Development of a genetic system for *Magnetospirillum gryphiswaldense*. *Arch Microbiol* **179**: 89–94.
- Schultheiss, D., Kube, M., and Schüler, D. (2004) Inactivation of the flagellin gene *flaA* in *Magnetospirillum gryphiswaldense* results in nonmagnetotactic mutants lacking flagellar filaments. *Appl Environ Microbiol* **70**: 3624–3631.
- Simpson, E.T. (2008) Electron holography of isolated and interacting magnetic nanocrystals. *Doctoral thesis*. University of Cambridge, 1–197.
- Taoka, A., Asada, R., Sasaki, H., Anzawa, K., Wu, L., and Fukumori, Y. (2006) Spatial localizations of Mam22 and Mam12 in the magnetosomes of *Magnetospirillum magnetotacticum*. *J Bacteriol* **188**: 3805–3812.
- Taoka, A., Asada, R., Wu, L., and Fukumori, Y. (2007) Polymerization of the actin-like protein MamK, which is associated with magnetosomes. *J Bacteriol* **189**: 8737–8740.
- Ullrich, S., Kube, M., Schübbe, S., Reinhardt, R., and Schüler, D. (2005) A hypervariable 130-kilobase genomic region of *Magnetospirillum gryphiswaldense* comprises a magnetosome island which undergoes frequent rearrangements during stationary growth. *J Bacteriol* **187**: 7176–7184.
- Vats, P., Shih, Y.-L., and Rothfield, L. (2009) Assembly of the MreB-associated cytoskeletal ring of *Escherichia coli*. *Mol Microbiol* **72**: 170–182.

Supporting information

Additional supporting information may be found in the online version of this article.

Please note: Wiley-Blackwell are not responsible for the content or functionality of any supporting materials supplied by the authors. Any queries (other than missing material) should be directed to the corresponding author for the article.

2.1.1 Supporting information

Legends to Supplements

S.1: Immunodetection of MamK in fractions of MSR WT and MSR Δ *mamK*. Equal amounts of protein (6.5 μ g) from magnetosomes (MM), membrane (Mem), and soluble (Sol) fraction were separated by SDS-PAGE, transferred to nitrocellulose membrane and detected by an anti-MamK antibody.

S.2: Isolated magnetosomes of MSR WT (*i-ii*) and MSR Δ *mamK* mutant (*iii-iv*). Arrows: magnetosome membrane. Scale bars 25 nm.

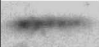
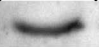
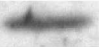
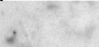
S.3: Immunodetection of ~37 kDa MamK with anti-MamK antibody on whole cell extracts of MSR Δ *mamK*+pEK36, MSR Δ *mamK*+pEK33 and MSR Δ *mamK* (left to right). Equal amounts of protein (6.5 μ g) were transferred to nitrocellulose membrane.

S.4: AMB WT cells grown in modified FSM media. Scale bars 500 nm.

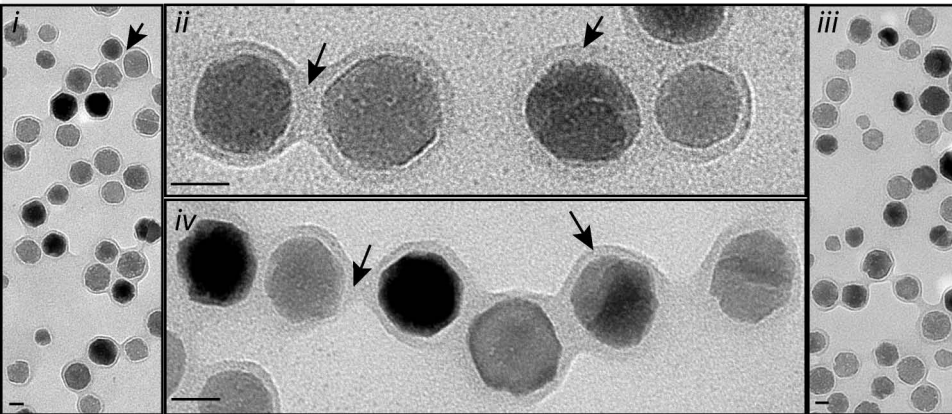
S.5: Southern Blot analysis of Δ *mamK* and WT MSR. Genomic DNA of MSR and MSR Δ *mamK* was digested with *Sac*II and hybridized with a 816 bp DNA probe amplified from a MamJ-MamK fragment. Double crossover resulted in a 3797 bp fragment for MSR Δ *mamK*, whereas two fragments for MSR WT (2937 bp and 1861 bp) were detected.

Movie 1: View through the z-stack of MSR WT tomogram [of late growth phase](#) at 22500 x magnification from Fig. *5i-iii*. The membrane “bleb” visible on the right cell pole results from partial autolysis of the outer membrane.

α - MamK

MSR1 WT			MSR1 $\Delta mamK$		
MM	Mem.	Sol.	MM	Mem.	Sol.
					

M. gryphiswaldense WT



$\Delta mamK$

α - MamK

$\Delta mamK + pEK36$

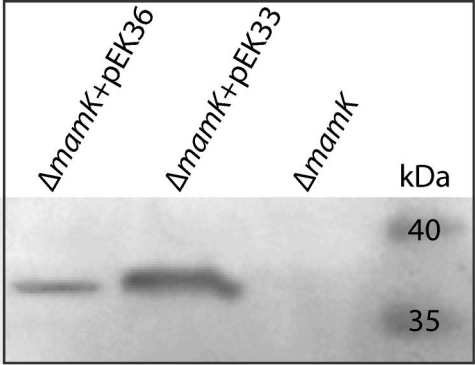
$\Delta mamK + pEK33$

$\Delta mamK$

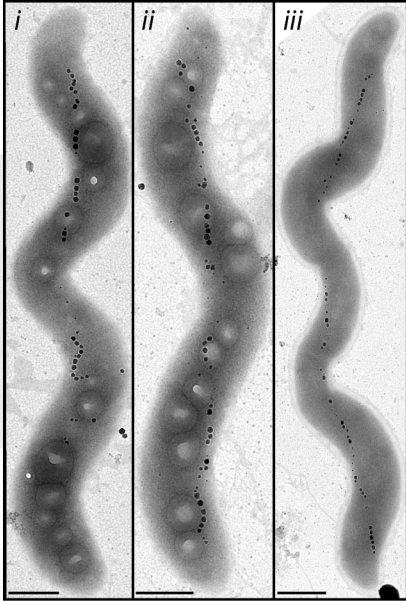
kDa

40

35

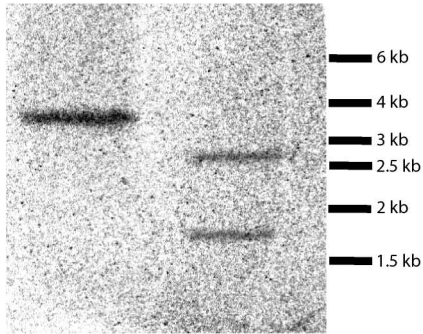


M. magneticum AMB-1



i $\Delta mamK$

WT

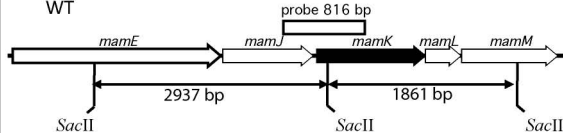


ii

$\Delta mamK$



WT



CHAPTER 3

3.1 Manuscript:

Magnetosome chains are recruited to cellular division sites and split by asymmetric separation

Magnetosome chains are recruited to cellular division sites and split by asymmetric septation

Emanuel Katzmann,^{1,2} Frank D. Müller,¹
Claus Lang,^{1†} Maxim Messerer,¹ Michael Winklhofer,³
Jürgen M. Plitzko² and Dirk Schüler^{1*}

¹Ludwig-Maximilians-Universität München, Department
Biology I, Biozentrum, D-82152 Planegg-Martinsried,
Germany.

²Max Planck Institute of Biochemistry, Department of
Molecular Structural Biology, D-82152
Planegg-Martinsried, Germany.

³Ludwig-Maximilians-Universität München, Department
of Earth and Environmental Sciences, D-80333 Munich,
Germany.

Summary

Magnetotactic bacteria navigate along magnetic field lines using well-ordered chains of membrane-enclosed magnetic crystals, referred to as magnetosomes, which have emerged as model to investigate organelle biogenesis in prokaryotic systems. To become divided and segregated faithfully during cytokinesis, the magnetosome chain has to be properly positioned, cleaved and separated against intrachain magnetostatic forces. Here we demonstrate that magnetotactic bacteria use dedicated mechanisms to control the position and division of the magnetosome chain, thus maintaining magnetic orientation throughout divisional cycle. Using electron and time-lapse microscopy of synchronized cells of *Magnetospirillum gryphiswaldense*, we confirm that magnetosome chains undergo a dynamic pole-to-midcell translocation during cytokinesis. Nascent chains were recruited to division sites also in division-inhibited cells, but not in a *mamK* mutant, indicating an active mechanism depending upon the actin-like cytoskeletal magnetosome filament. Cryo-electron tomography revealed that both the magnetosome chain and the magnetosome filament are split into halves by asymmetric septation and unidirectional indentation, which we interpret in terms of a specific adaptation required to overcome the magnetostatic interactions between

separating daughter chains. Our study demonstrates that magnetosome division and segregation is co-ordinated with cytokinesis and resembles partitioning mechanisms of other organelles and macromolecular complexes in bacteria.

Introduction

Magnetosomes are unique intracellular organelles used by magnetotactic bacteria to navigate along the Earth's magnetic field towards growth-favouring microoxic zones in their aquatic habitats (Jogler and Schüler, 2009). In *Magnetospirillum gryphiswaldense* MSR-1 (in the following referred to as MSR) and related magnetotactic bacteria, magnetosomes are membrane-enveloped sub-100 nm crystals of magnetite (Fe₃O₄) that are aligned in well-ordered chains (Jogler and Schüler, 2009; Murat *et al.*, 2010). Because of their complexity and resemblance to eukaryotic intracellular organelles, magnetosomes have recently emerged as model to investigate organelle biogenesis in prokaryotic systems (Faivre and Schüler, 2008; Murat *et al.*, 2010). Formation of functional magnetosome chains includes (i) the invagination of magnetosome membrane vesicles from the cytoplasmic membrane (Komeili *et al.*, 2006; Katzmann *et al.*, 2010) (ii) transport of iron into the magnetosome membrane vesicles and crystallization of magnetite (Faivre *et al.*, 2007; 2010), and (iii) assembly of crystals into a coherent linear chain along a dedicated cytoskeletal structure, the magnetosome filament (Frankel and Bazylinski, 2006; Komeili *et al.*, 2006; Scheffel *et al.*, 2006; Faivre *et al.*, 2010). It has been shown by a number of recent studies that each step is genetically controlled to achieve one of the highest structural levels found in a bacterial cell (Jogler and Schüler, 2009; Murat *et al.*, 2010).

During cytokinesis, bacterial cells have to duplicate and segregate their cellular content, such as plasmids and chromosomes (Gerdes *et al.*, 2010; Salje *et al.*, 2010). Magnetotactic bacteria face the additional challenge of dividing and equipartitioning the magnetosome chain preferably to pass on the selective advantage of magnetotaxis to both daughter cells. To ensure proper distribution and equal inheritance of functional magnetosome chains during cytokinesis, the magnetosome chain has to be positioned at the cellular division site, where it will be

Accepted 5 October, 2011. *For correspondence. E-mail dirk.schueler@lrz.uni-muenchen.de; Tel. (+49) 89218074502; Fax (+49) 89218074515. †Present address: Department of Biology, Stanford University, Stanford, CA 94305, USA.

split and separated against the cohesive forces caused by magnetostatic interactions between nascent daughter chains. However, it has remained unresolved how this is accomplished and co-ordinated with bacterial cell division.

Several recent observations suggested that magnetosome chain segregation may not occur randomly, but is subject to genetic control. Deletions of two genes were found to affect the assembly and positioning of the magnetosome chain in MSR: Loss of the actin-like MamK protein, which forms the cytoskeletal magnetosome filament, resulted in shorter, fragmented and ectopic (i.e. off-centre) chains (Katzmann *et al.*, 2010), whereas loss of MamJ that is thought to connect magnetosome particles to the magnetosome filament, led to agglomerate magnetosome clusters (Scheffel *et al.*, 2006), which were frequently mispartitioned to daughter cells by 'all-or-nothing' distribution (Scheffel and Schüler, 2007). This implied that the MamK filament might have a crucial role in concatenating and intracellular positioning of the magnetosome chain rather than just providing a rigid scaffold (Katzmann *et al.*, 2010). In addition, it was noted that magnetosomes undergo dynamic localization during chain assembly (Scheffel and Schüler, 2007; Katzmann *et al.*, 2010). Recently, it was suggested that chain structures may perform a sudden 'jump' in position upon completion of cell division (Staniland *et al.*, 2010). In this study, Staniland and colleagues investigated the position of magnetosome chains throughout cell division of MSR by transmission electron microscopy, and based on the low abundance of cells with off-centered chains they concluded that the magnetosome chain may be dynamic and could move rapidly back to the centre of the cell after being cleaved.

Here we provide further evidence that magnetotactic bacteria use dedicated mechanisms for proper positioning and division of the magnetosome chain, rendering both daughter cells capable of magnetic orientation throughout the cell cycle. We demonstrate that magnetosome chain division is spatially and temporally co-ordinated with cytokinesis by recruitment and translocation of nascent chains to cellular division sites, which is followed by splitting of both the magnetosome chain and filament by asymmetric septation and unidirectional indentation. We hypothesize that this unique mechanism of asymmetric cell division and magnetosome chain cleavage represents a specific adaptation, which is required to overcome the substantial cohesive magnetostatic forces within the magnetosome chain during division of cells.

Results

Electron and time-lapse microscopy of the MSR cell cycle

Based on morphological features such as length-to-width ratios and degrees of constriction, electron micrographs

of more than 50 representative cells from synchronized cultures were placed in relative order approximating the progression through cell division. This suggested a sequence of distinct events comprising (i) elongation of cells, (ii) constriction approximately at midcell, (iii) unidirectional bending and (iv) separation of newborn cells. In predivisional wild-type (WT) cells, magnetosome chains were consistently located at midcell, so that the chain became bent and eventually split into two daughter chains of approximately equal particle numbers that segregated evenly to daughter cells (Fig. 1A), similar as described previously (Sato *et al.*, 1995; Yang *et al.*, 2001; Staniland *et al.*, 2010). Notably, at advanced stages of constriction, the proportion of cells with two-stranded chains traversing the division site was increased (Fig. S1). In contrast, $\Delta mamK$ cells had multiple, fragmented and shorter chains that were located randomly along the entire length of the cell at all stages. Even at late division chains often could be found close to cell poles, resulting in uneven segregation of magnetosome crystals (Fig. 1Bvi).

We also investigated dynamics and timing of division in living cells by time-lapse differential interference contrast (DIC) microscopy. While many cells (> 30) ceased growth and underwent spontaneous lysis during observation, in some cells (>10) the entire cycle could be followed for up to three generations. At first, extensive elongation occurred for about 120–180 min with a nearly linear length increase of about 5.4 nm per min (Fig. 2A and B) to reach a final length of about 5 μm . Elongation was followed by a second phase lasting another 40 min, in which cells gradually constricted at midcell. Similar as observed in previous studies in MSR (Staniland *et al.*, 2010) and *M. magneticum* (Yang *et al.*, 2001), this was accompanied by bending around the constriction point up to an angle of about 50°, which eventually resulted in fast separation ('snapping') of the two daughter cells. Acute bending and snapping proceeded very fast in less than 7 min (i.e. the time between two exposures). The entire cell cycle was completed after ~260 min, with a variability of < 30 min between different dividing cells (Figs 1C and 2B, Movie S1). This doubling time is shorter than in previous studies in which doubling times were estimated by averaging one bulk population including unknown proportions of dead and slowly growing cells. In cells dividing for multiple generations, speed of growth and final cell length gradually decreased to 280 min for completion of a full cycle and a maximum length of the mother cells of 4.5 μm during microscopic examination (Fig. 2B). Curiously, most cells elongated asymmetrically, as one of the two poles moved faster and further relative to extracellular reference points close to the cell centre (Fig. 2C–E, Movie S3). This resulted in pairs of daughter cells with lengths differing by 15% on average (maximum difference 60%), which

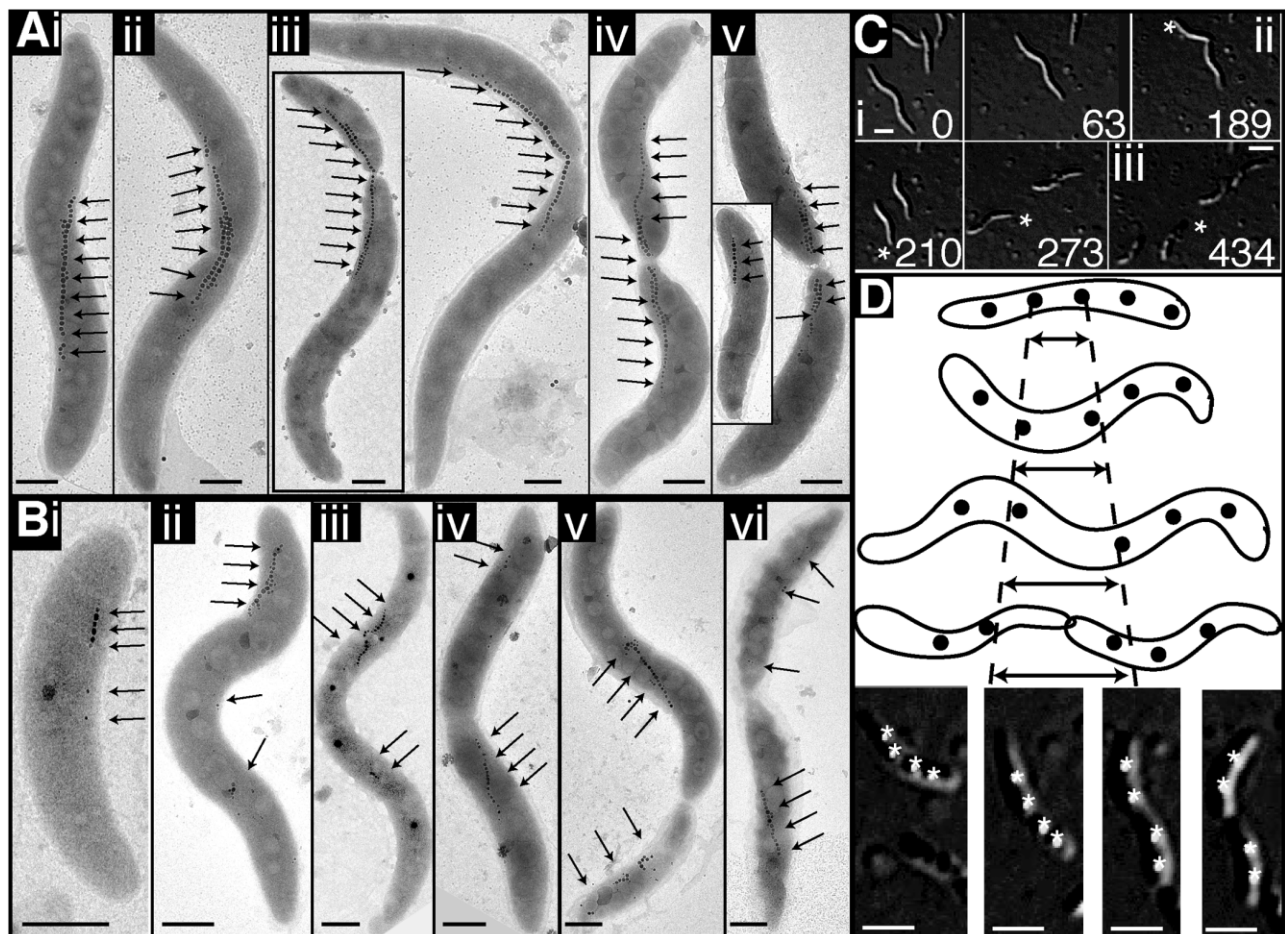


Fig. 1. TEM micrographs of individual WT (A) and $\Delta mamK$ (B) cells arranged by progression through division cycle (i–v/vi). Inset Av: Cell with sub-polar magnetosome chain. Scale bar 500 nm. Arrows indicate positions of magnetosome crystals. C. Selected frames of DIC time-lapse series showing two offspring generations of a dividing WT cell (Movie S1). Scale bar 1 μm . Intervals of exposures are indicated in minutes; i–iii: number of generations; asterisks indicate positions of the same cell. D. Schematic representation (upper panel) of intracellular PHB localization in dividing cells analysed by DIC microscopy (lower panel, Movie S2). Asterisk: positions of PHB granules. Scale bar 1 μm .

was also apparent from the analysis of several electron micrographs (e.g. inset Fig. 1Aiii and Bv).

In electron micrographs, strictly polar localization of magnetosome chains was only rarely observed in fully separated WT cells (inset Fig. 1Av), again suggesting a fast translocation of chains to midcell after division. This could be explained by either (i) fast cell growth at the new pole, or (ii) intracellular movement of magnetosome chains away from the new pole as suggested recently (Staniland *et al.*, 2010). To identify zones of active cellular growth, we tracked the relative movement of intracellular polyhydroxybutyrate (PHB) granules in elongating cells. While PHB granules became rapidly separated at midcell, intergranular spacing remained invariant in polar regions (Fig. 1D and Movie S2). Assuming a transiently fixed position of granules relative to the adjacent cell wall (Williams, 1959), this argues against a polar mode of growth, but is consistent with elongation of the central sidewalls, much

like in most rod-shaped bacteria having MreB (Margolin, 2009).

Recruitment of magnetosome chains to future division sites is mediated by MamK

As the previous observations implied an active magnetosome chain translocation from new poles to midcell during cytokinesis, we asked if chain localization is governed by spatial information provided by division sites in division-inhibited cells. The β -lactam antibiotic cephalixin inhibits the septum-specific penicillin-binding-protein 3 (FtsI). This allows major parts of the divisome to assemble, whereas final septation and cell separation are blocked (Pogliano *et al.*, 1997). Treatment of MSR with 10 $\mu\text{g ml}^{-1}$ cephalixin reversibly caused highly elongated (up to 62 μm) cells that still were magnetotactic as indicated by slow swimming and magnetic

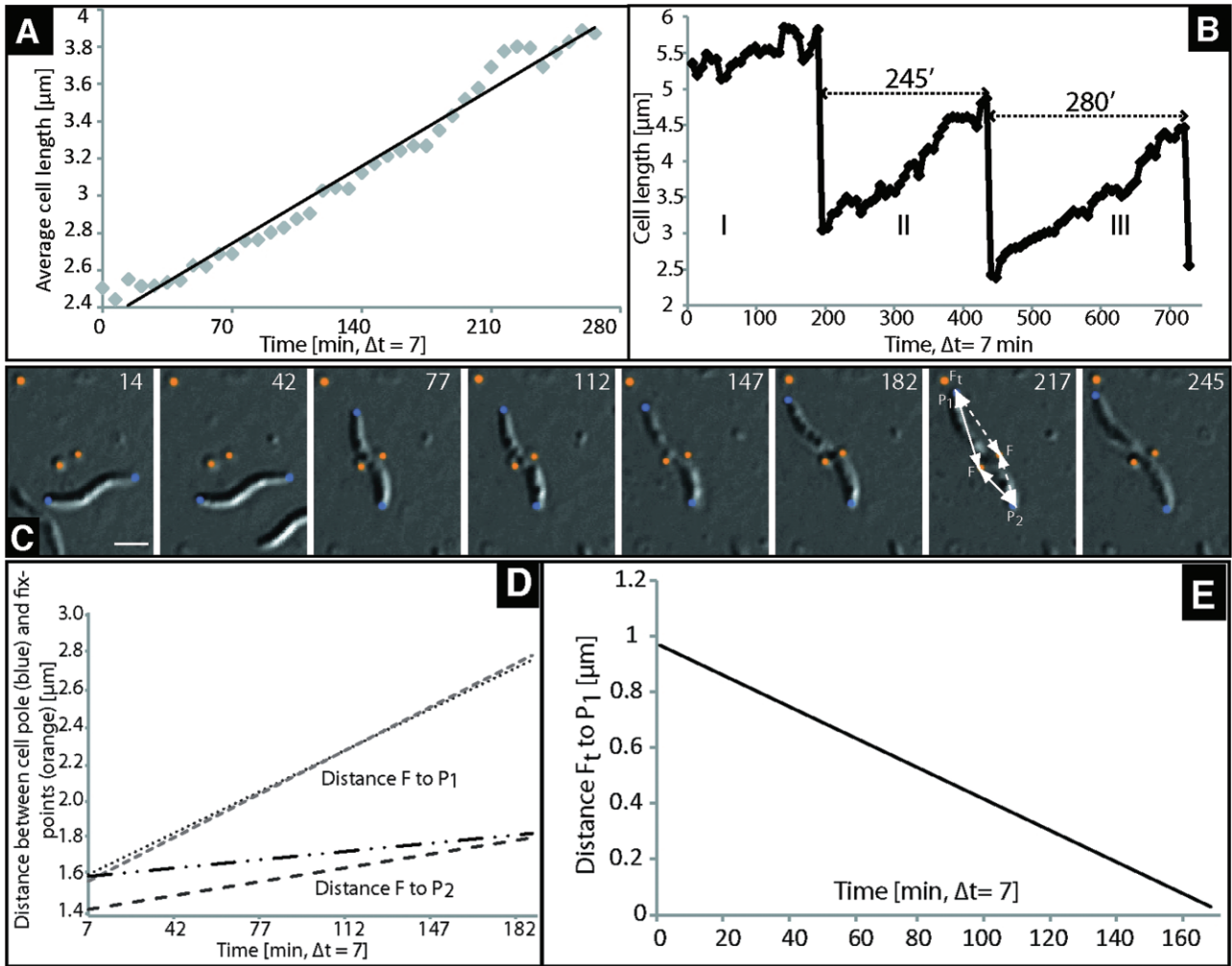


Fig. 2. A. Increase of average cell lengths estimated from time-lapse microscopy of 12 cells over 280 min (equivalent to one generation). B. Time-course of lengths of a single cell and their offspring followed over two generations. Generation times varied from 240 up to 280 min for completion of a full cycle and maximum length of the mother cells from 5.8 down to 4.5 μm . Number I, II and III correspond to DIC series in Fig. 1C. C. Individual frames from DIC series of Fig. 1C followed over 245 min showing uneven elongation of a single cell. Scale bar 1 μm . Orange dots: Fixed external reference points on agar surface. Blue points: cell poles. D. Plot of distances between both cell poles (blue, P1 and P2) and reference points (orange, F and Ft) at cell centre of cell in C over time. E. Plot of distances between cell pole P1 and external reference point Ft (orange) for cell in C over time.

response. 16 h after cephalixin addition cells were on average 25.6 μm in length and exhibited up to seven stalled constriction sites, which were spaced by about one typical cell length (3.5–4 μm) and considered to be equivalent to three consecutive generations (Fig. 3A–C). Cryo-TEM of WT cells revealed magnetosomes adjacent to cytoskeletal magnetosome filaments, which traversed through the aseptate stalled constriction sites (Fig. 3D). This was also shown by fluorescence microscopy of cephalixin-treated cells expressing an eGFP-MamK fusion. Fluorescence was confined to a filamentous signal running through the elongated cells, indicating that MamK filaments traverse the division plane but are not split. DAPI staining of the cephalixin-treated cells

suggested that non-separated daughter cells contained properly segregated chromosomes (Fig. 3G), which indicates that division and separation of magnetosome chains is independent from chromosome segregation.

Many cephalixin-treated WT cells had one long central chain (~10 μm , up to 224 crystals; Fig. S2), which sometimes extended through neighbouring constriction sites. Frequently, 1–3 additional shorter chains (10–30 crystals) were located away from the oldest (i.e. central) division site, which were spaced by large gaps from the primary chain and coincided with younger constrictions. In contrast, cephalixin-treated cells of ΔmamK contained up to 19 highly fragmented short subchains (3–38 particles), which were scattered along filamentous

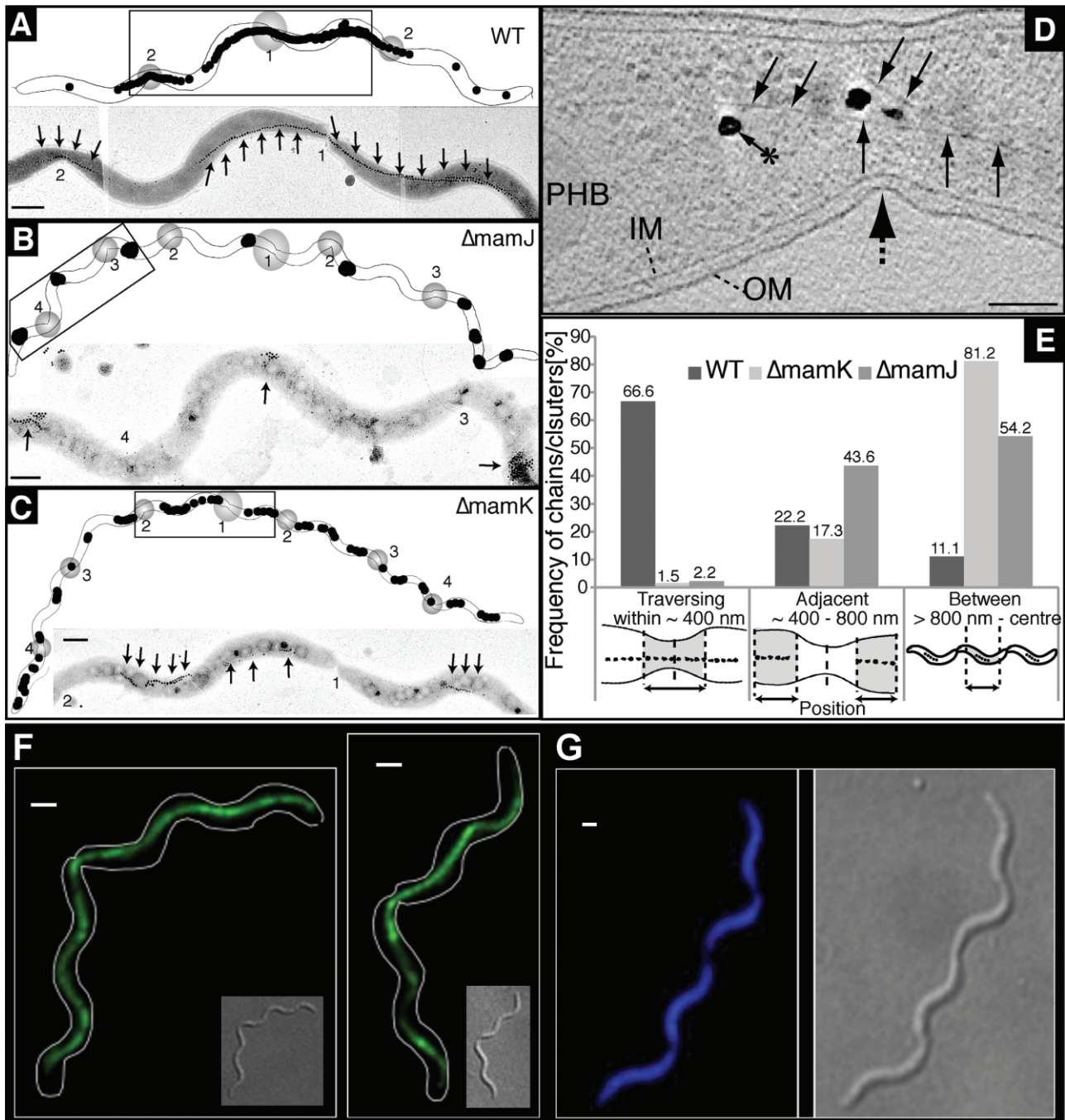


Fig. 3. Cephalixin inhibition in WT, $\Delta mamJ$ and $\Delta mamK$.

A–C. Schematic representations (upper panels) and corresponding TEM micrograph sections (boxes, lower panels) of WT, $\Delta mamK$ and $\Delta mamJ$ cells treated with $10 \mu\text{g ml}^{-1}$ cephalixin for 16 h. Circles: stalled constriction sites. Big circle: site of first division (oldest). Numbers indicate generations after cephalixin addition. Magnetite particles are highlighted in black (not to scale). Arrows indicate positions of magnetosome chains/clusters. Scale bar 500 nm.

D. Cryo-TEM micrograph of a cephalixin-treated WT cell exhibiting unidirectional constriction (dashed arrow) of the inner and outer membrane (IM, OM). Magnetosome filaments: black arrows, magnetite crystals: arrow with asterisk.

E. Frequency of positions of magnetosome chains or clusters in cephalixin-treated cells of WT, $\Delta mamK$ and $\Delta mamJ$. Magnetosome chain and cluster positions were scored as traversing, adjacent, or between constriction sites as described in the *Experimental procedures* section.

F. Cephalixin-treated WT cells expressing eGFP-MamK (green). Invaginations at midcell indicate blocked septa.

G. DAPI staining of a cephalixin-treated cell. Scale Bars: 1 μm .

cells (Fig. 3C). The positions of chains or clusters were scored in cephalaxin-treated cells of WT, $\Delta mamK$, and $\Delta mamJ$ mutants as: (i) traversing (ii) adjacent, or (iii) between the nearest constriction. In the WT most chains were traversing (66.6%), whereas less were adjacent (22.2%) or between (11.1%) constriction sites (Fig. 3E). In $\Delta mamK$, only few chains were traversing (1.5%), or adjacent (17.3%), whereas the majority (81.2%) was between constrictions (Fig. 3E). In $\Delta mamJ$, only 2.2% of clusters were traversing, whereas similar numbers (43.6% and 54.2%) were either adjacent or between respectively. Comparing those frequencies with their proportions from total cell lengths (traversing: ~10%, adjacent: ~20%, between: ~70%) revealed a strong correlation of magnetosome chain positions with constrictions in the WT, whereas in $\Delta mamJ$ the clusters were distributed more or less randomly along the cell length. In contrast, there was a negative bias against traversing or adjacent positions of the fragmented chains in $\Delta mamK$.

To analyse whether nascent magnetosome chains originated and concatenated from division sites, or alternatively became recruited subsequent to synthesis of particles, we also followed assembly and positioning of chains after induction of magnetite biomineralization in division-inhibited cells. If 50 μ M iron citrate was added to iron-starved, cephalaxin-inhibited WT cells, magnetosome synthesis could be first detected by magnetic response after about 180 min (Figs 4 and S3). TEM revealed freshly nucleated small crystallites evenly scattered along the entire filament after 180–240 min. After 300 min individual crystals began to concatenate into short precursory chains, resembling the subchains of *Magnetospirillum magneticum*, for which extremely weak magnetostatic interaction fields were estimated (Li *et al.*, 2009). Positions of these precursor chains gradually shifted towards the blocked division sites (Figs 4 and S3). After 480 min, the majority of larger crystals was found in close proximity to constrictions, whereas smaller crystals (< 20 nm) were predominantly localized between them (Figs 4 and S3). Taken together, these results corroborate the notion that magnetosome chains localize dynamically, and indicate that magnetosome chains are recruited to future division sites subsequent to their synthesis by an active mechanism, which is dependent on the presence of MamK.

Magnetosome chain and magnetosome filament are cleaved by asymmetric septation driven by an arc-like Z-ring

Because the unidirectional bending and snapping of cells observed in time-lapse studies and TEM analyses indicated a putative asymmetry in divisome formation and

division, structures involved in cellular and magnetosome chain division were further investigated by cryo-electron tomography (CET), which allows three-dimensional reconstruction of cells in an *in vivo* state having preserved all biological structures (Li and Jensen, 2009). About 30 synchronized cells at different stages of division were analysed by CET. We detected a local constriction of the cell envelope at midcell, which progressed down to an annular ring of 250 nm (Fig. 5A). Intriguingly, gradual constriction was followed by unidirectional asymmetric inward growth of the peptidoglycan layer. Even in late stages of division, when the division site was already narrowed to 100 nm, both the magnetosome chain and filament were still intact and ran through the division plane. In 80% of cells, constriction started at a position preferentially opposite to chain and filament, leading to an asymmetric, wedge-like indentation of both structures. After further progression of division, single- or double-stranded magnetosome chains became split and eventually separated by acute bending and asymmetric ingrowth of the septum (Fig. 5Bi–iii). In a very late stage also the cytoskeletal magnetosome filament became bisected (Fig. 5Aiv). Interestingly, flagella already became subterminally inserted in cells before completion of division (Fig. 5Av). Although magnetosome filaments and empty magnetosome membrane vesicles were present in the vicinity of septa, we failed to detect magnetite crystals close to poles immediately after septum closure and separation (Fig. 5Av, Bii), again suggesting that magnetosome chains had rapidly moved away from the poles towards future midcells (Fig. 5Av).

The apparently fixed, preferentially distal localization of the division wedge relative to magnetosome chain and filament raised the question whether the observed asymmetry depends on the presence of chains. We therefore analysed different mutants of MSR deficient in magnetosome synthesis or chain formation. Asymmetric septation and cleavage did not depend on the presence of either MamK (forming the magnetosome filament) or MamJ (connecting magnetosomes to the filament), as isogenic mutants of both genes displayed the same wedge-like septal growth as observed in the WT (Fig. 6). This was also observed in strain MSR-1B in which magnetite crystals, magnetosome membrane vesicles and the magnetosome filament are absent due to deletion of a large part of the magnetosome island (MAI) (Ullrich *et al.*, 2005). This suggests that the wedge-like asymmetric division is independent from the presence of magnetosome chain and filament and must be controlled by determinants encoded elsewhere in the genome.

Careful examination of individual sections from several tomograms of dividing WT cells revealed thin filaments 5–10 nm beneath the cytoplasmic membrane. These short (50–100 nm) filaments extended at constriction sites

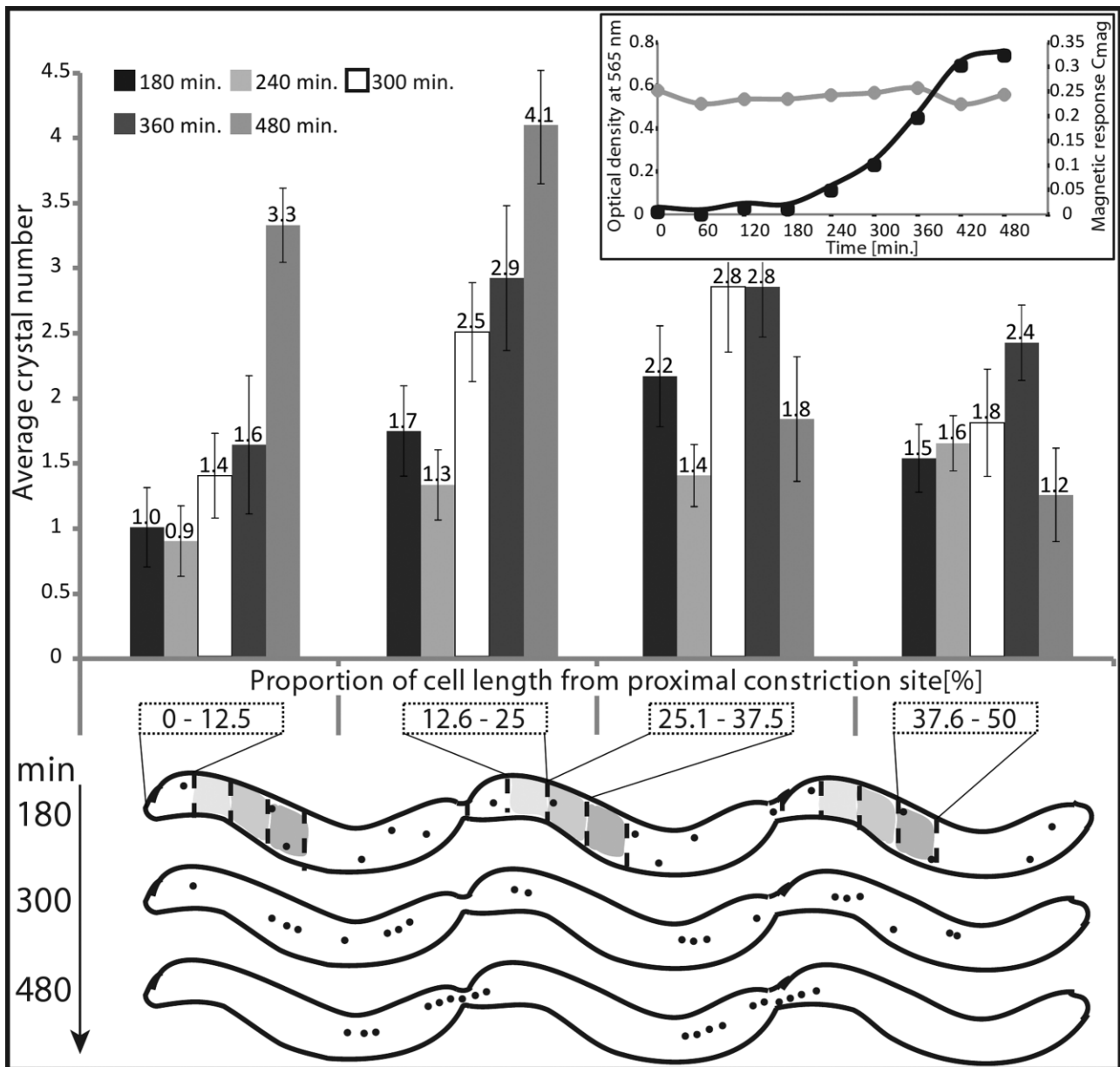


Fig. 4. Dynamic localization of magnetite crystals after induction of magnetite biomineralization in iron-starved, non-magnetic cephalaxin-inhibited cells as analysed by TEM. Inset upper right: Growth curve of iron-starved WT cells after 16 h inhibition and subsequent 50 μ M iron induction. Optical density (grey) and magnetic response (Cmag, black) are shown. Lower part: Schematic representation of magnetite crystal (black dots) positions within elongated cells at different time points after iron induction and their corresponding relative distances from proximal constriction sites i.e. at relative cell lengths 12.5% from proximal constrictions.

parallel to the division plane. When single images were aligned into a stack, arc-like structures were found adjacent to each other when progressing in z-direction (Fig. 5C and D). The resulting arrangement of the arc-like filaments resembled a tight spiral or pinch as previously observed in *Caulobacter crescentus*, in which arc-like Z-ring structures were predicted (Li *et al.*, 2007). Sub-membrane localization of the filaments resulted in an 'M'-like overall shape (Fig. 5C and D). Based on these

characteristics and its resemblance to the ring described by Li *et al.* (Li *et al.*, 2007), we conclude that this asymmetrical arc-like structure is likely identical with the Z-ring.

Discussion

In this study we present a comprehensive analysis of the cell cycle and cytokinesis in magnetotactic bacteria. Our data suggest that magnetosome chain localization and

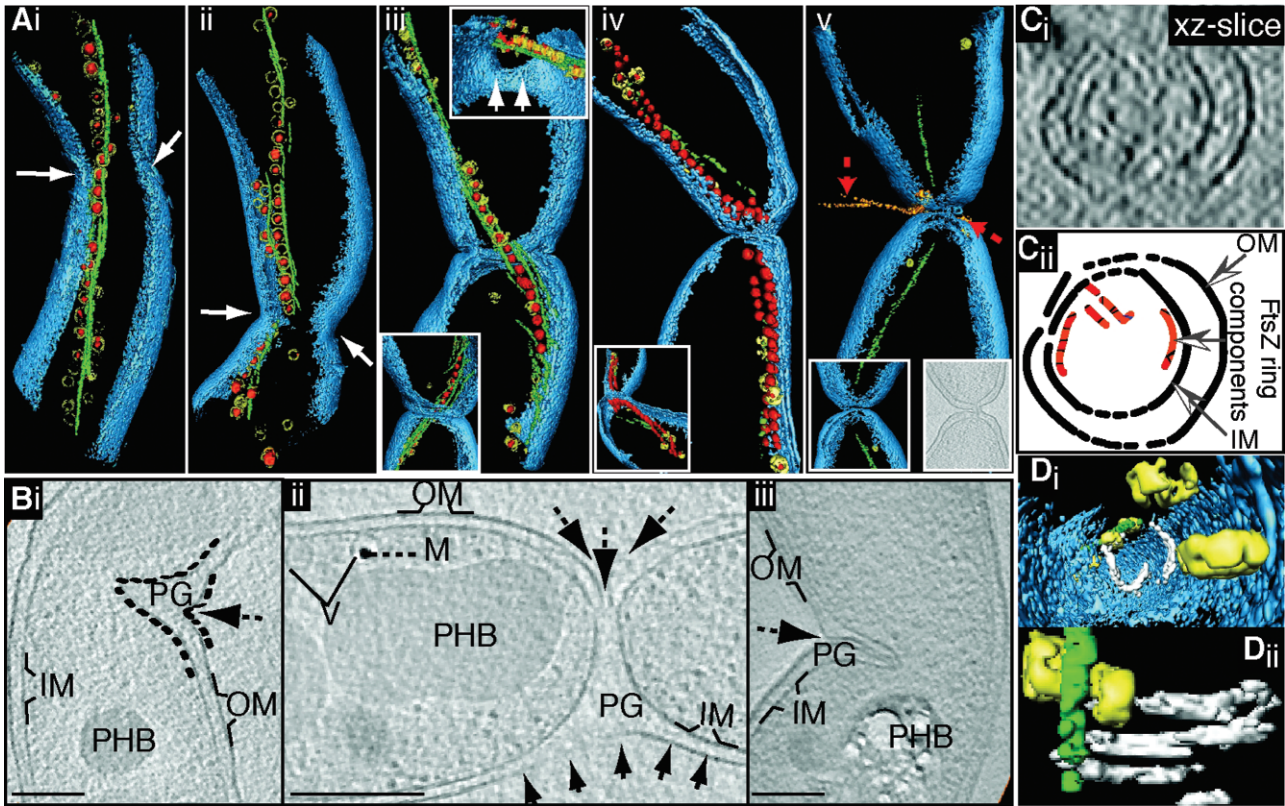


Fig. 5. Segmented tomograms and sections of a tilt series from synchronized MSR cells acquired by CET. Representative tomograms are arranged by progression through cell division.
 A. Cell envelope (blue) with constrictions (white arrows). Red: magnetite crystals, yellow: magnetosome membrane and magnetosome filament (green). Insets Aiii–v: different perspective of the tomogram. Inset Av (right): section of tomogram with still connected daughter cells. Orange: flagella (red arrows).
 B. Individual sections of tomograms illustrating the asymmetric peptidoglycan (PG) wedge caused by inward growth (dashed arrows) of the outer membrane (OM). Inner membrane (IM), vesicles (V), magnetite crystals (M), and PHB granules are indicated. Scale bar 100 nm.
 C. Analysis of Z-ring by CET. i: xz – slice of a WT cell through the constriction site and its schematic segmentation (ii). Dashed line represents the missing wedge, FtsZ ring components in different colours.
 D. Tomogram of C segmented at constriction site. Individual Z-arcs (white) show pinch-like localization (ii) just beneath the cell envelope (blue). magnetosome filament: green; magnetosome vesicles: yellow.

segregation is well co-ordinated with cell division by positioning the chains to the future division site subsequent to magnetosome synthesis, which in line with previous speculations (Staniland *et al.*, 2010) is followed by dynamic translocation of chains to midcell after division, carried out according to the scheme in Fig. 7A. In this process, the actin-like MamK protein has a key role as its presence is required for proper magnetosome chain positioning and segregation. The recruitment of chains to stalled constrictions in division-inhibited cells demonstrated that division site recognition is independent from septum formation. So far it remains unknown how division-site positioning is then determined at the molecular level. Apart from the possibility of a geometric cue provided by altered membrane curvature around the constriction site, positional information for division site formation is determined by the Z-ring, preceding the assembly of the multiprotein divisome complex during cytokinesis

(den Blaauwen *et al.*, 2008; Goley *et al.*, 2011). It could be envisioned that magnetosome chain localization at midcell might be controlled by early assembling components of the divisome complex (Fig. 7A), perhaps by direct interaction with the magnetosome filament as it has been speculated based on the discovery of a chimeric protein in which a *mamK* domain is fused to an *ftsZ* domain (Jogler *et al.*, 2009; Katzmann *et al.*, 2010).

After being cleaved at midcell, daughter chains have to be translocated from new cell poles to midcell. The apparent absence of strictly polar magnetosome chain positions in fully separated cells of the WT in our and a previous study (Staniland *et al.*, 2010) suggests that this translocation occurs very fast, i.e. within several minutes or less. Because results of our time-lapse experiments argue against (mono)polar growth, this has to be accomplished by active movement although the molecular mechanism behind this relocalization is not fully clear.

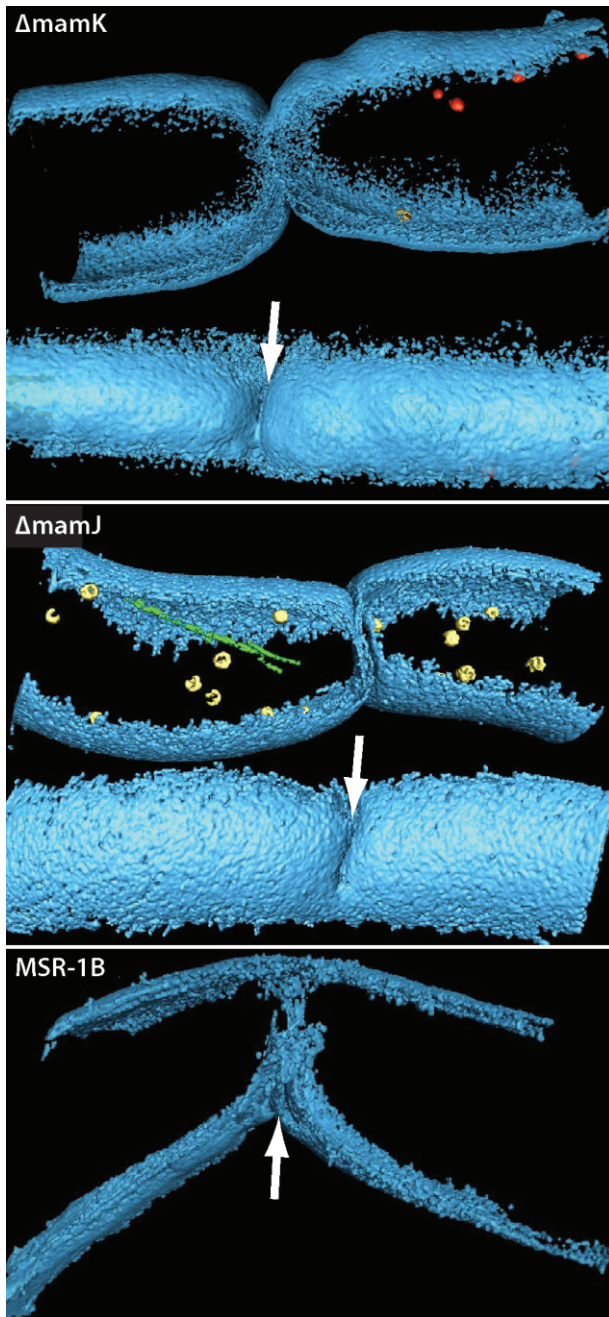


Fig. 6. Segmentations of cryo-electron tomograms of $\Delta mamJ$, $\Delta mamK$ and MSR-1B cells at their constriction sites. White arrows indicate the asymmetric, wedge-like constriction. Blue: cell envelope, red: magnetite, yellow: magnetosome membrane, green: MamK filament.

There is an increasing number of examples that rapid intracellular movement of organelles, DNA molecules, and protein complexes in bacterial cells is achieved by cytomotive cytoskeletal filaments (Löwe and Amos, 2009; Gerdes *et al.*, 2010; Savage *et al.*, 2010). For instance, actin-like protein filaments can govern intracellular positioning by providing a track for other proteins

to move along (Salje *et al.*, 2010). In the related *C. crescentus* disintegration of the polar FtsZ complex is followed by assembly of a Z-ring in proximity of the cell centre, which depends on the activity of the cell division regulator MipZ that is also present in magnetospirilla (Thanbichler and Shapiro, 2006). Assuming a similar mechanism of Z-ring positioning in MSR, we speculate that magnetosome chains may follow the localization of the Z-ring by and along the MamK cytoskeletal filaments (Fig. 7A).

Protein filaments can also lead to force generation by attaching to a structure and actively moving it as a result of filament growth or shrinkage (Salje *et al.*, 2010). For example, the *parMRC* system uses bundles of actin-like ParM filaments to push plasmids to opposite poles of the cell, whereupon they are stably inherited on cell division (Salje *et al.*, 2010). ParM filaments are dynamically unstable unless bound to plasmids, and thus undergo cycles of growing and shrinking to search the cell space for plasmids. A similar mechanism may well apply to magnetosome chain segregation by the actin-like MamK magnetosome filaments. Instead of pushing, 'treadmilling', i.e. polar depolymerization and shrinkage of MamK filaments anchored at midcell via divisive interaction might generate pulling forces that move magnetosome chains towards future division site (Fig. 6). This mechanism would be also consistent with the results of previous experiments, which revealed that the assembly of MamK filaments expressed in *Escherichia coli* is a highly dynamic and kinetically asymmetrical process and that MamK filaments also displayed intrinsic polarity (Pradel *et al.*, 2006). It was also noted in this study that most MamK filaments seemed to be ended at the cellular septa, and it was suggested that short filamentous cables might nucleate at these points and make new filaments in the daughter cells. The assumption that MamK anchored at division sites may actively recruit magnetosome subchains also could explain the abundance of two-stranded chains at constriction sites in the WT, but not in $\Delta mamK$ (Katzmann *et al.*, 2010), because both ends of shrinking MamK filaments could efficiently bind precursor chains synthesized in both of the opposite halves of the predivisional cell, and then concatenate and bidirectionally move them to midcell.

Our time-lapse and electron microscopic analysis revealed that cell division in MSR displays asymmetry along two directions: (i) newborn daughter cells frequently had uneven lengths, and (ii) unidirectional bending, snapping, and septation occurred asymmetrically along the division plane. It has been suggested that length asymmetry might be a feature common to many alphaproteobacteria due to the presence of CtrA regulator, which co-ordinates the cell cycle with asymmetric division in *Caulobacter* (Hallez *et al.*, 2004), and is also present in

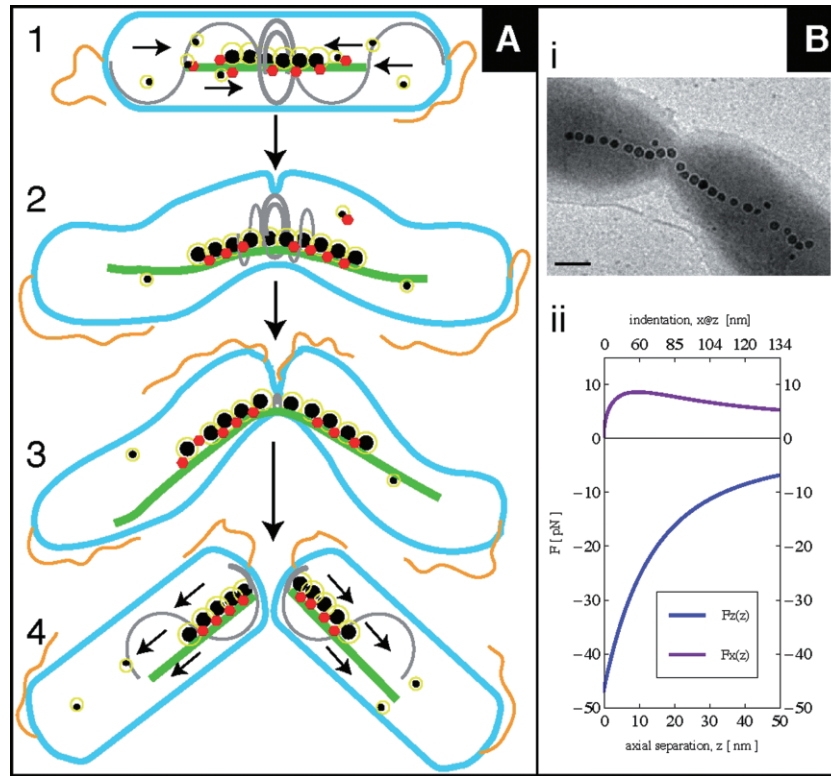


Fig. 7. A. Proposed mechanism of magnetosome chain positioning and division. (1) During cell elongation the magnetosome filament formed by MamK is anchored at midcell to the divisome. By dynamic shrinking of the filament, magnetite crystals bound to the filaments by MamJ, and nascent subchains become concatenated and recruited to midcell. (2) Contraction of the Z arc (grey) results in gradual asymmetric constriction followed by unidirectional inward growth of peptidoglycan. (3) The wedge-like septum causes lateral indentation and acute bending of the magnetosome chain, thereby allowing the adjacent daughter chains to separate against their magnetostatic attraction. Eventually, snapping results in cleavage of the magnetosome chain and filament and breaks the daughter cells apart. (4) Following the divisome to new midcell as determined by the Z arc, split magnetosome chains are rapidly translocated by the magnetosome filament from the new poles of daughter cells towards the future division sites. Blue: cell envelope, green: MamK filament; red: MamJ, black: magnetite crystals, yellow: magnetosome membrane; orange: flagella.

B. Representative TEM image of a dividing MSR cell with lateral indentation of the magnetosome chain (between stage 2 and 3). Scale bar 100 nm. Plots illustrating forces opposing lateral indentation (magenta) and axial separation (blue) during chain division, showing that, owing to its leverage, indentation requires a comparatively small force for magnetosome chain separation.

magnetospirilla (Brilli *et al.*, 2010). However, it requires further clarification if the observed asymmetric division in MSR also reflects functional asymmetry and differentiation as suggested for other Alphaproteobacteria (Halez *et al.*, 2004).

Cryo-electron tomography analysis indicated a preferred position of the Z-ring and septum distal to the magnetosome chain and the filament. This suggests a controlled mechanism of asymmetric division, which was independent from the presence of magnetosomes, the magnetosome filament, and any genes of the *mamAB*, *mms6* and *mamGFDC* operons of the MAI. Asymmetric constriction and septation might be induced by the arc-shaped Z-ring that we identified by CET. Arc-like FtsZ rings seem to be correlated with asymmetric division in distinct *E. coli ftsZ* mutants (Addinall and Lutkenhaus, 1996) and in cyanelle plastids of some protists, in which the Z-ring extends from one-fourth to one-half way around

the cell and is located over a very asymmetrically forming septum (Sato *et al.*, 2007). In MSR, a FtsZ homologue (FtsZm) is encoded within the *mamXY* operon of the MAI (Richter *et al.*, 2007). Although no effect on cell division was reported so far for its deletion in MSR (Ding *et al.*, 2009), it is tempting to speculate that asymmetric ring structures might result from the absence of the binding domain to the membrane tether FtsA in FtsZm. This in turn might cause partial detachment of such a mixed ring from the inner membrane, and consequently, the asymmetric positioning of PG-synthesizing proteins such as FtsI (Fig. 5).

Although bending has been observed in the division of non-magnetic spirilla (Williams, 1959) and magnetic spirilla (Yang *et al.*, 2001; Staniland *et al.*, 2010), asymmetric, wedge-like constriction and septation to our knowledge has not been described before and hence appears to represent a novel and possibly unique mode of

bacterial cell division. This raises the question whether this mechanism reflects a specific adaptation of magnetotactic bacteria in order to split their magnetosome chains. To physically underpin this proposition, we considered the magnetic attraction forces among magnetite crystals in a chain. In MSR, the magnetic attraction is about 40 pN in a one-stranded magnetosome chain (see blue force curve in inset of Fig. 7Bii) and nearly twice as strong in a two-stranded magnetosome chain, but because magnetite crystals in MSR are relatively small and of roughly equidimensional habitus, these figures define rather the lower limit of magnetic attraction forces in a magnetosome chain. Larger crystals of hexagonal prismatic morphology in other magnetotactic bacteria like the magnetic vibrio MV-1 are magnetically held together by attraction forces that well exceed 100 pN (Shcherbakov *et al.*, 1997). On top of this, the linear continuity of the cytoskeletal MamK filament to which magnetosomes are attached, must be interrupted too, which requires either additional mechanical forces or cleavage by localized depolymerization (Vats and Rothfield, 2007). We are not aware of a mechanism during cell division that would be capable of producing extensional forces of at least 40 pN acting from the constriction site bidirectionally along the cell axis (Erickson *et al.*, 2010). However, through lateral indentation of a magnetosome chain (Fig. 7Bi), the mechanic force required to split the chain could be greatly reduced (from greater than 45 pN to less than 10 pN in the example shown in Fig. 7Bii), owing to leverage. For this mechanism to work, the magnetosome chain must have space to bend away from the indenter. Asymmetric septation is consistent with this geometric requirement.

Recently, it has been demonstrated that intracellular positioning and segregation of bacterial organelles and macromolecular complexes, such as plasmids, chemoreceptors, carboxysomes, and PHB granules (Thompson *et al.*, 2006; Galán *et al.*, 2010; Savage *et al.*, 2010) is governed by dedicated and co-ordinated mechanisms. In conclusion, this study shows that such a mechanism very likely exists also for the highly controlled positioning, division and equipartitioning of bacterial magnetosomes.

Experimental procedures

Bacterial strains, media and growth conditions

Escherichia coli strain DH5 α cells (Invitrogen, Karlsruhe, Germany) were used as hosts for cloning. The *dap*⁻ *E. coli* strain BW29427 was used as donor for transformation of *M. gryphiswaldense* MSR-1 (WT) by conjugation. *E. coli* cultures were grown in lysogeny broth (LB) medium at 37°C shaking supplemented with kanamycin (50 $\mu\text{g ml}^{-1}$) and 1 mM 2,6-diaminopimelic acid (Sigma-Aldrich, Switzerland) if appropriate. *M. gryphiswaldense* strains were routinely grown microaerobically at 30°C under moderate shaking (120 r.p.m.) in modified FSM medium or in LIM (Low iron

media, modified FSM) as described (Heyen and Schüler, 2003; Faivre *et al.*, 2007; Lang and Schüler, 2008). For cultivation on solid media, agar was added to 1.5% (wt/vol). Kanamycin was supplied to a final concentration of 5 $\mu\text{g ml}^{-1}$ where necessary. Cephalixin treatment to inhibit cell division was carried out in 1 ml culture volume in 6-well plates under microaerobic conditions. The minimal inhibitory concentration (MIC) of cephalixin for *M. gryphiswaldense* was determined to be 10 $\mu\text{g ml}^{-1}$ by growth experiments with various concentrations of cephalixin accompanied by microscopic inspection of cell morphology, motility and viability (reversibility of the inhibitory effect after removal of the antibiotic). Optical densities and C_{mag} values of MSR cultures were measured turbidimetrically at 565 nm with immotile cells inactivated by the addition of formaldehyde (Fluka, Switzerland) to a final concentration of 0.1% before the measurement. For cell cycle synchronization cells were grown to stationary growth phase in 10 ml FSM hungate vials. Then half of the culture was withdrawn and diluted by fresh modified FSM medium. Cells were grown for 8–12 h at 25°C. The dilution and subsequent growth steps were repeated 4–6 times until >80% of the cell culture were in division process as verified by light microscopy.

Iron induction experiments

Growth of cephalixin (10 $\mu\text{g ml}^{-1}$) inhibited cells was performed in microaerobic environment in 24 well plates and 1 ml culture volume over night. For induction of magnetite biomineralization Fe(III)-citrate was supplemented to cells, which were iron starved at aerobic conditions and passaged 4 \times in LIM, at a final iron concentration of 50 μM (Scheffel *et al.*, 2006; Faivre *et al.*, 2007).

Transmission electron microscopy (TEM) and CET

For conventional TEM analysis, unstained cells were absorbed on carbon coated copper grids (Plano, Wetzlar). Bright field TEM was performed on FEI Tecnai F20 transmission electron microscope (FEI; Eindhoven, The Netherlands) at an accelerating voltage of 200 kV. Images were captured with Eagle 4096 \times 4096 pixel CCD camera using EMMenue 4.0 (Tietz, Gauting, Germany) and FEI software. For cryotomography FEI Tecnai F30 Polara transmission electron microscope (FEI; Eindhoven, The Netherlands), equipped with 300 kV field emission gun; Gatan GIF 2002 Post-Column Energy Filters; and 2.048 \times 2.048 pixel Multiscan CCD Camera (Gatan; Pleasanton, CA, USA) was used. All data collection was performed at 300 kV, with the energy filter operated in the zero-loss mode (slit width of 20 eV). Tilt series were acquired using Serial EM and FEI software. Quantifoil copper grids (Quantifoil Micro Tools GmbH, Jena) were prepared by placing a 5 μl droplet of 10–15 nm colloidal gold clusters (Sigma) on each grid for subsequent alignment purposes. Additionally a 5 μl droplet of logarithmic MSR-1 culture was added onto the prepared grid, and after blotting embedded in vitreous ice by plunge freezing into liquid ethane (temperature *c.* -170°C). The specimen was tilted typically about one axis with 1.5° increments over a total angular range of +/-65°. To minimize the electron dose

applied to the ice-embedded specimen, data were recorded under low-dose conditions by using automated data acquisition software. The total dose accumulated during the tilt series was kept below $200 \text{ e}/\text{\AA}^2$. To account for the increased specimen thickness at high tilt angles, the exposure time was multiplied by a factor of $1/\cos \alpha$. The pixel size in unbinned images was 0.661 at $34\,000$ magnification, 0.805 at $27\,500$ magnification and 0.979 at $22\,500$ magnification. Images were recorded at nominal $-8 \mu\text{m}$ or $-4 \mu\text{m}$ defocus.

CET data analysis

Three-dimensional reconstructions from tilt series were performed with the weighted back-projection method and further analysis of the tomograms was done using the TOM toolbox (Nickell *et al.*, 2005). Visualizations of the tomograms were done with Amira (<http://www.amira.com>) on 2 times binned volumes.

Microscopy and time-lapse experiments

Magnetospirillum gryphiswaldense strains bearing the plasmid pEK42 were grown in 15 ml polypropylene tubes with sealed screw caps and a culture volume of 11 ml to early mid-log phase. A droplet ($\sim 10 \mu\text{l}$) of this culture was fixed to an FSM-agar pad (FSM salts supplemented with 1% agarose) and covered with a coverslip. For staining of nucleic acids, cells were incubated with 10 ng ml^{-1} DAPI for 10 min and immobilized as above. The immobilized cells were imaged with an Olympus BX81 microscope equipped with a $100\times$ UPLSAPO100XO objective with a numerical aperture of 1.40 and an Orca-ER camera (Hamamatsu). For time-lapse microscopy, cells were fixed on agarose pads and the coverslips with the immobilized cells were placed into a Ludin chamber (Life Imaging Services, Basel, Switzerland) filled with FSM. Cells were imaged with above mentioned microscope and set up. The cell^M autofocus option was set to a range of $5 \mu\text{m}$ with widths of 1.67 and $0.2 \mu\text{m}$ for big and small steps respectively. Exposures were recorded every 7 min for 100 cycles and processed using Olympus Xcellence and the GNU Image Manipulation Program (GIMP) software.

Scoring of intracellular magnetosome chain positions

Positions of magnetosome chains in cephalaxin-inhibited cells were scored (by the position of the outermost particle of a magnetosome chain/magnetosome cluster nearest to a constriction site) as either (i) traversing: within 400 nm periphery of constrictions (equivalent to the extension of membrane curvature) (ii) adjacent: within $\sim 400\text{--}800 \text{ nm}$ away from nearest constriction (iii) between: more than 800 nm away from the nearest constriction.

Theoretical modelling of forces in a magnetosome chain

Magnetite crystals in magnetosome chains of MSR like those in *M. magnetotacticum* are magnetic single domains (Dunin-Borkowski *et al.*, 1998) and have a roughly isometric habitus, which allows us to mathematically describe them as homoge-

enously magnetized spheres, tractable with the dipole formula. Our model magnetosome chain consists of n identical magnetosomes, each containing a ferrimagnetic core of diameter D , surrounded by a non-magnetic shell of thickness h representing the lipid-bilayer membrane of the magnetosome vesicle. Each crystal is magnetized along the chain axis and carries a magnetization equal to the saturation magnetization of magnetite at room temperature ($M_s = 470 \text{ G}$). The magnetic dipolar interaction energy of the chain is given by

$$W_n = -\left(\frac{\pi M_s D^3}{6}\right)^2 \sum_{j=1}^n \sum_{k=1}^{j-1} \frac{2}{|r_j - r_k|^3}, \quad (1)$$

where r_i and r_j are the position vectors of magnetosomes j and k respectively. In a close-packed linear chain, we have $|r_j - r_k| = |j - k|(D + 2h)$, where $D + 2h$ is the centre-to-centre distance between any two adjacent particles. Inserting a gap of clear axial distance $z = \gamma(D + 2h)$ between the two innermost magnetosomes (i.e. $j = n/2$ and $k = n/2 + 1$), we obtain the following expression for the magnetostatic interaction energy between two linear magnetosome chain halves separated by a gap z along the chain axis:

$$W(z) = -2\left(\frac{\pi M_s}{6}\right)^2 \frac{D^3}{(1 + 2h/D)^3} \left(\sum_{j=1}^{n/2} \frac{j}{(j + \gamma)^3} + \sum_{j=n/2+1}^{n-1} \frac{(n-j)}{(j + \gamma)^3} \right). \quad (2)$$

The (axial) force F_z holding the two magnetosome chain halves together is easily obtained by taking the derivative of $W(z)$, i.e.

$$F_z(z) = -\frac{dW}{dz} = -\frac{dW}{d\gamma} \cdot \frac{d\gamma}{dz}. \quad (3)$$

$F_z(z)$ is always attractive (negative sign) and is of maximum magnitude at close contact ($z = 0$). For typical magnetosome chain geometries in MSR ($D = 42.5 \text{ nm}$, $h = 4 \text{ nm}$, $n = 10$), $F_z(0)$ is about 40 pN . $F_z(z)$ converges quickly with chain length n , that is, $F_z(z)$ changes by as little as 2.5% when going from $n = 6$ to $n = 20$. To derive the mechanical force required for magnetosome chain division by lateral indentation (perpendicular to the chain axis), we let the indentation force F_x act on the central part of the magnetosome chain and assume that each chain half is bent into a circular arc, curving away from the indenter while the two (outer) ends of the chain are kept fixed in position (cf. Fig. 7Bi). Then from elementary geometrical considerations, we can express the lateral indentation distance as $x = R(1 - \cos \alpha)$ and the axial separation between the two chain halves as $z = 2R(\alpha - \sin \alpha)$, where $R = (L/2)/\alpha$ is the radius of curvature, $L/2 = (n/2) \cdot (D + 2h)$ is the (arc) length of each magnetosome chain half, and α is the deflection angle (Fig. S4). A relationship between indentation x and separation z can be obtained by elimination of α , which in first order yields $z \cong 8x^2/(3L)$. This non-linear lever rule $z(x)$ can now be used to determine the force required for lateral indentation

$$F_x(z) = \frac{dW}{dx} = \frac{dW}{dz} \cdot \frac{dz}{dx} \cong -4\sqrt{\frac{2\gamma}{3n}} F_z(z), \quad (4)$$

which vanishes at $\gamma = 0$ ($z = 0$), that is, lateral indentation does not require an activation force as opposed to axially

pulling two magnetosome chain halves apart from each other. The maximum of $F_x(z)$ occurs near $\gamma = 1/7$ and is $\sqrt{1/(2n)}$ times smaller in magnitude compared to $F_z(0)$ (cf. Fig. 7Bii).

Acknowledgements

We thank Günter Pfeifer for his continued help with TEM and CET. This research was supported by grants DFG Schu1080/9–1 to D.S. and DFG Wi1828/4–1 to M.W.

References

- Addinall, S.G., and Lutkenhaus, J. (1996) FtsZ-spirals and -arcs determine the shape of the invaginating septa in some mutants of *Escherichia coli*. *Mol Microbiol* **22**: 231–237.
- den Blaauwen, T., Pedro, M.D., Nguyen-Distèche, M., and Ayala, J.A. (2008) Morphogenesis of rod-shaped sacculi. *FEMS Microbiol Rev* **32**: 321–344.
- Brilli, M., Fondi, M., Fani, R., Mengoni, A., Ferri, L., Bazzicalupo, M., and Biondi, E.G. (2010) The diversity and evolution of cell cycle regulation in alpha-proteobacteria: a comparative genomic analysis. *BMC Syst Biol* **4**: 1–16.
- Ding, Y., Li, J., Liu, J., Yang, J., Jiang, W., Tian, J., et al. (2009) Deletion of the ftsZ-like gene results in the production of superparamagnetic magnetite magnetosomes in *Magnetospirillum gryphiswaldense*. *J Bacteriol* **192**: 1097–1105.
- Dunin-Borkowski, R.E., McCartney, M.R., Frankel, R.B., Bazylinski, D.A., Posfai, M., and Buseck, P.R. (1998) Magnetic microstructure of magnetotactic bacteria by electron holography. *Science* **282**: 1868–1870.
- Erickson, H., Anderson, D., and Osawa, M. (2010) FtsZ in bacterial cytokinesis: cytoskeleton and force generator all in one. *Microbiol Mol Biol Rev* **74**: 504–528.
- Faivre, D., and Schüler, D. (2008) Magnetotactic bacteria and magnetosomes. *Chem Rev* **108**: 4875–4898.
- Faivre, D., Böttger, L.H., Matzanke, B.F., and Schüler, D. (2007) Intracellular magnetite biomineralization in bacteria proceeds by a distinct pathway involving membrane-bound ferritin and an iron(II) species. *Angew Chem Int Ed Engl* **46**: 8495–8499.
- Faivre, D., Fischer, A., Garcia-Rubio, I., Mastrogiacomo, G., and Gehring, A.U. (2010) Development of cellular magnetic dipoles in magnetotactic bacteria. *Biophys J* **99**: 1268–1273.
- Frankel, R., and Bazylinski, D. (2006) How magnetotactic bacteria make magnetosomes queue up. *Trends Microbiol* **14**: 329–331.
- Galán, B., Dinjaski, N., Maestro, B., de Eugenio, L., Escapa, I., Sanz, J., et al. (2010) Nucleoid-associated PhaF phasin drives intracellular location and segregation of polyhydroxyalkanoate granules in *Pseudomonas putida* KT2442. *Mol Microbiol* **79**: 402–418.
- Gerdes, K., Howard, M., and Szardenings, F. (2010) Pushing and pulling in prokaryotic DNA segregation. *Cell* **141**: 927–942.
- Goley, E.D., Yeh, Y.-C., Hong, S.-H., Fero, M.J., Abeliuk, E., McAdams, H.H., and Shapiro, L. (2011) Assembly of the *Caulobacter* cell division machine. *Mol Microbiol* **80**: 1680–1698.
- Hallez, R., Bellefontaine, A., Letesson, J., and De Bolle, X. (2004) Morphological and functional asymmetry in alpha-proteobacteria. *Trends Microbiol* **12**: 361–365.
- Heyen, U., and Schüler, D. (2003) Growth and magnetosome formation by microaerophilic *Magnetospirillum* strains in an oxygen-controlled fermentor. *Appl Microbiol Biotechnol* **61**: 536–544.
- Jogler, C., and Schüler, D. (2009) Genomics, genetics, and cell biology of magnetosome formation. *Annu Rev Microbiol* **63**: 501–521.
- Jogler, C., Lin, W., Meyerdieks, A., Kube, M., Katzmann, E., Flies, C., et al. (2009) Toward cloning of the magnetotactic metagenome: identification of magnetosome island gene clusters in uncultivated magnetotactic bacteria from different aquatic sediments. *Appl Environ Microbiol* **75**: 3972–3979.
- Katzmann, E., Scheffel, A., Gruska, M., Pitzko, J.M., and Schüler, D. (2010) Loss of the actin-like protein MamK has pleiotropic effects on magnetosome formation and chain assembly in *Magnetospirillum gryphiswaldense*. *Mol Microbiol* **77**: 208–224.
- Komeili, A., Li, Z., Newman, D., and Jensen, G. (2006) Magnetosomes are cell membrane invaginations organized by the actin-like protein MamK. *Science* **311**: 242–245.
- Lang, C., and Schüler, D. (2008) Expression of green fluorescent protein fused to magnetosome proteins in microaerophilic magnetotactic bacteria. *Appl Environ Microbiol* **74**: 4944–4953.
- Li, J., Pan, Y., Chen, G., Liu, Q., Tian, L., and Lin, W. (2009) Magnetite magnetosome and fragmental chain formation of *Magnetospirillum magneticum* AMB-1: transmission electron microscopy and magnetic observations. *Geophys J Int* **177**: 33–42.
- Li, Z., and Jensen, G.J. (2009) Electron cryotomography: a new view into microbial ultrastructure. *Curr Opin Microbiol* **12**: 1–8.
- Li, Z., Trimble, M.J., Brun, Y.V., and Jensen, G.J. (2007) The structure of FtsZ filaments *in vivo* suggests a force-generating role in cell division. *EMBO J* **26**: 4694–4708.
- Löwe, J., and Amos, L.A. (2009) Evolution of cytomotive filaments: the cytoskeleton from prokaryotes to eukaryotes. *Int J Biochem Cell Biol* **41**: 323–329.
- Margolin, W. (2009) Sculpting the bacterial cell. *Curr Biol* **19**: 812–822.
- Murat, D., Byrne, M., and Komeili, A. (2010) Cell Biology of Prokaryotic Organelles. *Cold Spring Harb Perspect Biol* **2**: 1–18.
- Nickell, S., Förster, F., Linaroudis, A., Net, W., Beck, F., Hegerl, R., et al. (2005) TOM software toolbox: acquisition and analysis for electron tomography. *J Struct Biol* **149**: 227–234.
- Pogliano, J., Pogliano, K., Weiss, D.S., Losick, R., and Beckwith, J. (1997) Inactivation of FtsI inhibits constriction of the FtsZ cytokinetic ring and delays the assembly of FtsZ rings at potential division sites. *Proc Natl Acad Sci USA* **94**: 559.
- Pradel, N., Santini, C.-L., Bernadac, A., Fukumori, Y., and Wu, L.-F. (2006) Biogenesis of actin-like bacterial cytoskeletal filaments destined for positioning prokaryotic magnetic organelles. *Proc Natl Acad Sci USA* **103**: 17485–17489.

- Richter, M., Kube, M., Bazylinski, D.A., Lombardot, T., Glöckner, F.O., Reinhardt, R., and Schüler, D. (2007) Comparative genome analysis of four magnetotactic bacteria reveals a complex set of group-specific genes implicated in magnetosome biomineralization and function. *J Bacteriol* **189**: 4899–4910.
- Salje, J., Gayathri, P., and Löwe, J. (2010) The ParMRC system: molecular mechanisms of plasmid segregation by actin-like filaments. *Nat Rev Microbiol* **8**: 683–692.
- Sato, M., Nishikawa, T., Kajitani, H., and Kawano, S. (2007) Conserved relationship between FtsZ and peptidoglycan in the cyanelles of *Cyanophora paradoxa* similar to that in bacterial cell division. *Planta* **227**: 177–187.
- Sato, R., Miyagi, T., Kamiya, S., Sakaguchi, T., Thornhill, R., and Matsunaga, T. (1995) Synchronous culture of *Magnetospirillum* sp. AMB-1 by repeated cold treatment. *FEMS Microbiol Let* **128**: 15–19.
- Savage, D., Afonso, B., Chen, A., and Silver, P.A. (2010) Spatially ordered dynamics of the bacterial carbon fixation machinery. *Science* **327**: 1258–1261.
- Scheffel, A., and Schüler, D. (2007) The acidic repetitive domain of the *Magnetospirillum gryphiswaldense* MamJ protein displays hypervariability but is not required for magnetosome chain assembly. *J Bacteriol* **189**: 6437–6446.
- Scheffel, A., Gruska, M., Faivre, D., Linaroudis, A., Graumann, P.L., Plietzko, J.M., and Schüler, D. (2006) An acidic protein aligns magnetosomes along a filamentous structure in magnetotactic bacteria. *Nature* **440**: 110–114.
- Shcherbakov, V., Winklhofer, M., Hanzlik, M., and Petersen, N. (1997) Elastic stability of chains of magnetosomes in magnetotactic bacteria. *Eur Biophys J* **26**: 319–326.
- Staniland, S.S., Moisescu, C., and Benning, L.G. (2010) Cell division in magnetotactic bacteria splits magnetosome chain in half. *J Basic Microbiol* **50**: 392–396.
- Thanbichler, M., and Shapiro, L. (2006) MipZ, a spatial regulator coordinating chromosome segregation with cell division in *Caulobacter*. *Cell* **126**: 147–162.
- Thompson, S.R., Wadhams, G.H., and Armitage, J.P. (2006) The positioning of cytoplasmic protein clusters in bacteria. *Proc Natl Acad Sci USA* **103**: 8209–8214.
- Ullrich, S., Kube, M., Schübbe, S., Reinhardt, R., and Schüler, D. (2005) A hypervariable 130-kilobase genomic region of *Magnetospirillum gryphiswaldense* comprises a magnetosome island which undergoes frequent rearrangements during stationary growth. *J Bacteriol* **187**: 7176–7184.
- Vats, P., and Rothfield, L. (2007) Duplication and segregation of the actin (MreB) cytoskeleton during the prokaryotic cell cycle. *PNAS* **104**: 17795–17800.
- Williams, M.A. (1959) Cell elongation and division in *Spirillum anulus*. *J Bacteriol* **78**: 374–377.
- Yang, C., Takeyama, H., Tanaka, T., Hasegawa, A., and Matsunaga, T. (2001) Synthesis of bacterial magnetic particles during cell cycle of *Magnetospirillum magneticum* AMB-1. *Appl Biochem Biotechnol* **91–93**: 155–160.

Supporting information

Additional supporting information may be found in the online version of this article.

Please note: Wiley-Blackwell are not responsible for the content or functionality of any supporting materials supplied by the authors. Any queries (other than missing material) should be directed to the corresponding author for the article.

3.1.1 Supporting information

Supplemental Material

Magnetosome chains are recruited to cellular division sites and split by asymmetric septation

Emanuel Katzmann, Frank D. Müller, Claus Lang, Maxim Messerer, Michael Winklhofer, Jürgen M. Plitzko and Dirk Schüler

Figure Legends:

Figure S1: Electron micrographs of WT cells depicting the heterogeneity of chain conformations at constriction sites (single, double or parallel chains) during cytokinesis in early and late stages (subpolar chains). Asterisk marks the TEM micrograph in Figure 7B. Scale bar 500nm.

Figure S2: Frequency of cephalixin inhibited WT, $\Delta mamK$ and $\Delta mamJ$ cells having 10-50, 50-100 and more than 100 crystals per chain or cluster.

Figure S3: TEM micrographs (upper part) and corresponding schematic representations (lower part) of positions of magnetosome crystals (arrows) in iron-induced, cephalixin-treated cells. Circles: stalled constriction sites. Big circle: site of first division (oldest). Numbers indicate generations after cephalixin addition. Magnetite crystals are black. Scale bar 1 μm .

Figure S4: Sketch showing MC division by lateral indentation. The MC is initially straight (horizontal thick dashes). Upon indentation by the lateral force F_x (red arrow), each MC half deforms into a circular arc (thick solid line). Note that to achieve a given separation z , a much larger indentation distance x is required. As a consequence, the force required to separate the two MC halves through lateral indentation is much smaller than the force required for axially pulling apart the two MC halves (lever rule).

MovieS1: Time-lapse movie of a MSR cell undergoing two cycles of division followed followed for 441 min by DIC microscopy.

MovieS2: Time-lapse movie of a single dividing MSR cell with PHB granules (yellow marks) indicating cell elongation at midcell.

MovieS3: Time-lapse movie of a 31 growing and dividing MSR cell trapped between two fixed extracellular reference points (orange, F or Ft) in the agar surface and a third reference point at the P1 pole (Figure 2C). Asymmetric longitudinal growth can be seen by comparing distances P1 to Ft/F and P2 to F (Figure 2D-E), resulting in two daughter cells with different lengths.

Table S1:

Plasmids and primers used in this study

Plasmid	Genotype/description	Reference/ source
pBBR1MCS-2	mobilizable broad-host-range vector; backbone for gene expression in <i>E. coli</i> and <i>M. gryphiswaldense</i> , Km	(Kovach <i>et al</i> , 1995)
pEK42	source of <i>eGFP-mamK</i>	(Katzmann <i>et al</i> , 2010)

Kovach ME, Elzer PH, Hill DS, Robertson GT, Farris MA, Roop RM, Peterson KM (1995) Four new derivatives of the broad-host-range cloning vector pBBR1MCS, carrying different antibiotic-resistance cassettes. *Gene* **166**: 175-176

Katzmann E, Scheffel A, Gruska M, Plitzko JM, Schüler D (2010) Loss of the actin--like protein MamK has pleiotropic effects on magnetosome formation and chain assembly in *Magnetospirillum gryphiswaldense*. *Mol Microbiol* **77**: 208-224

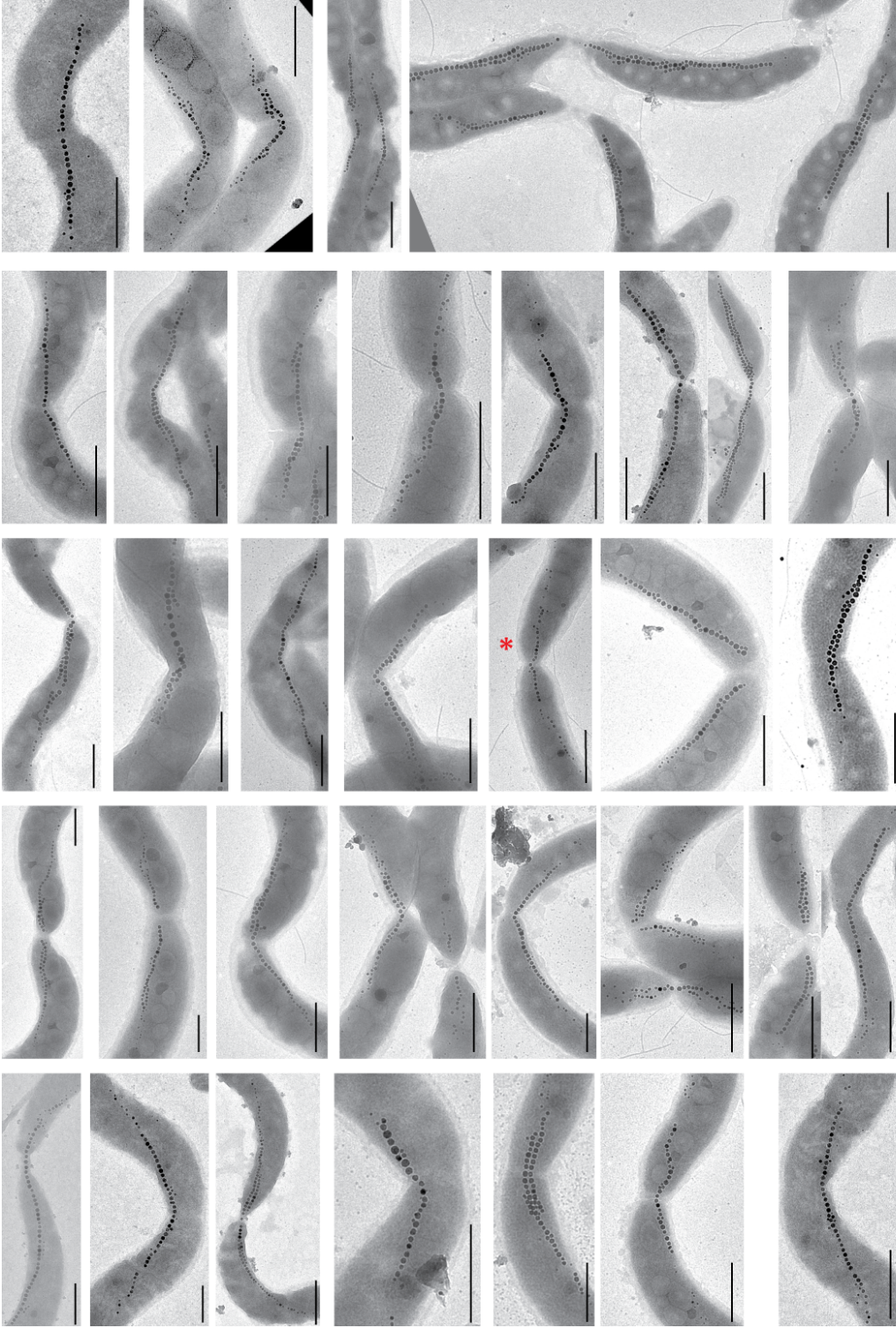


Figure S1

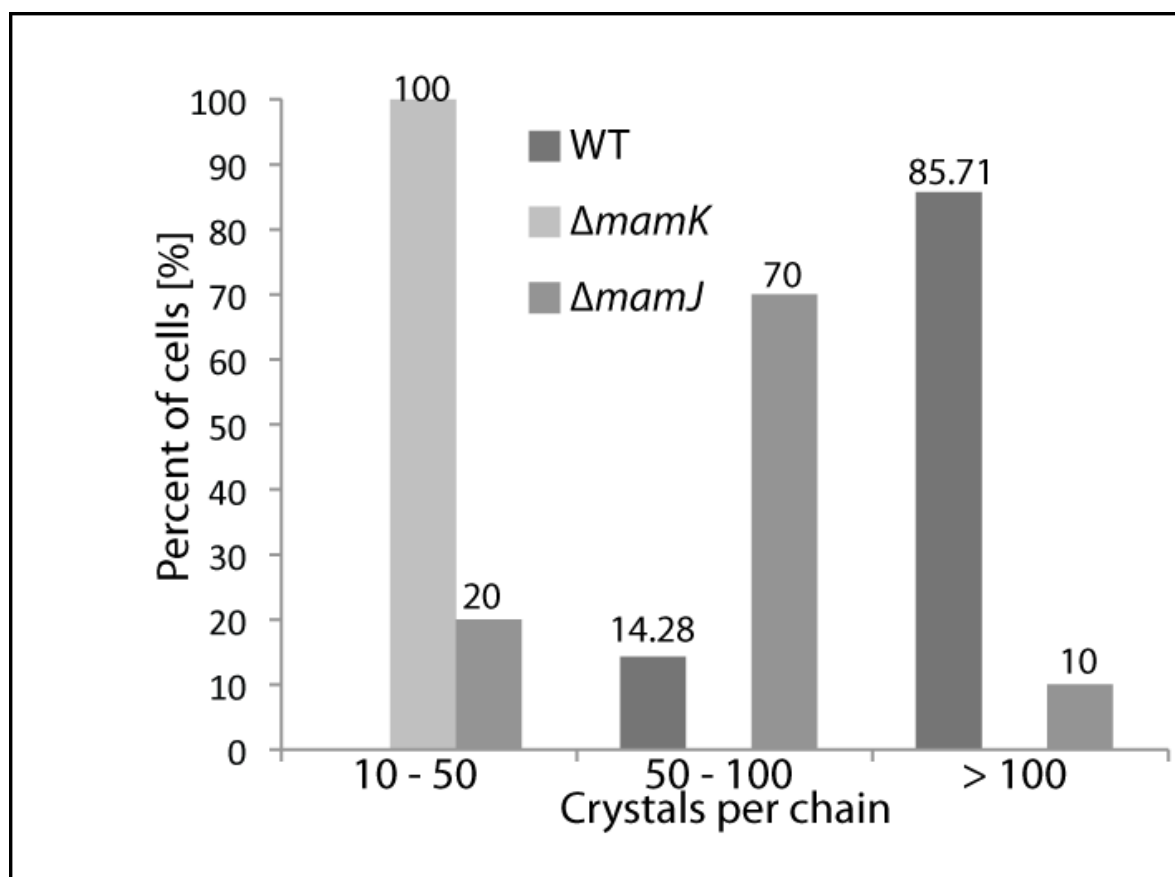


Figure S2

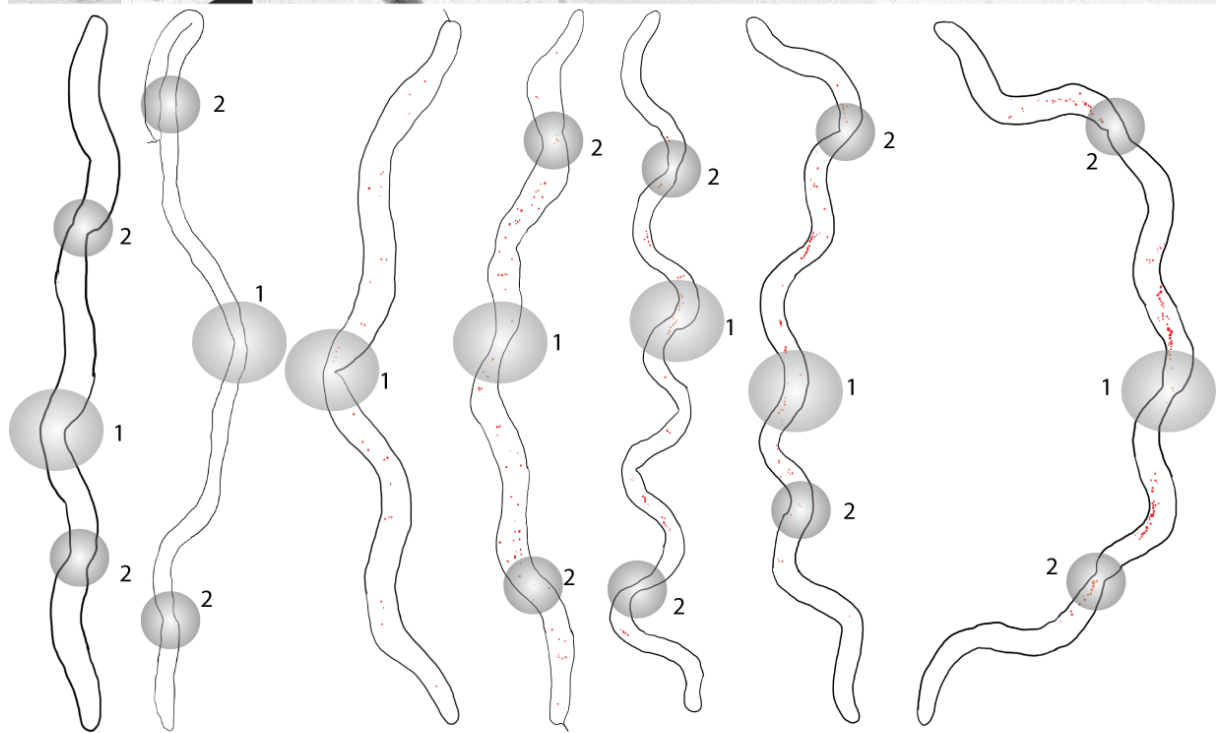
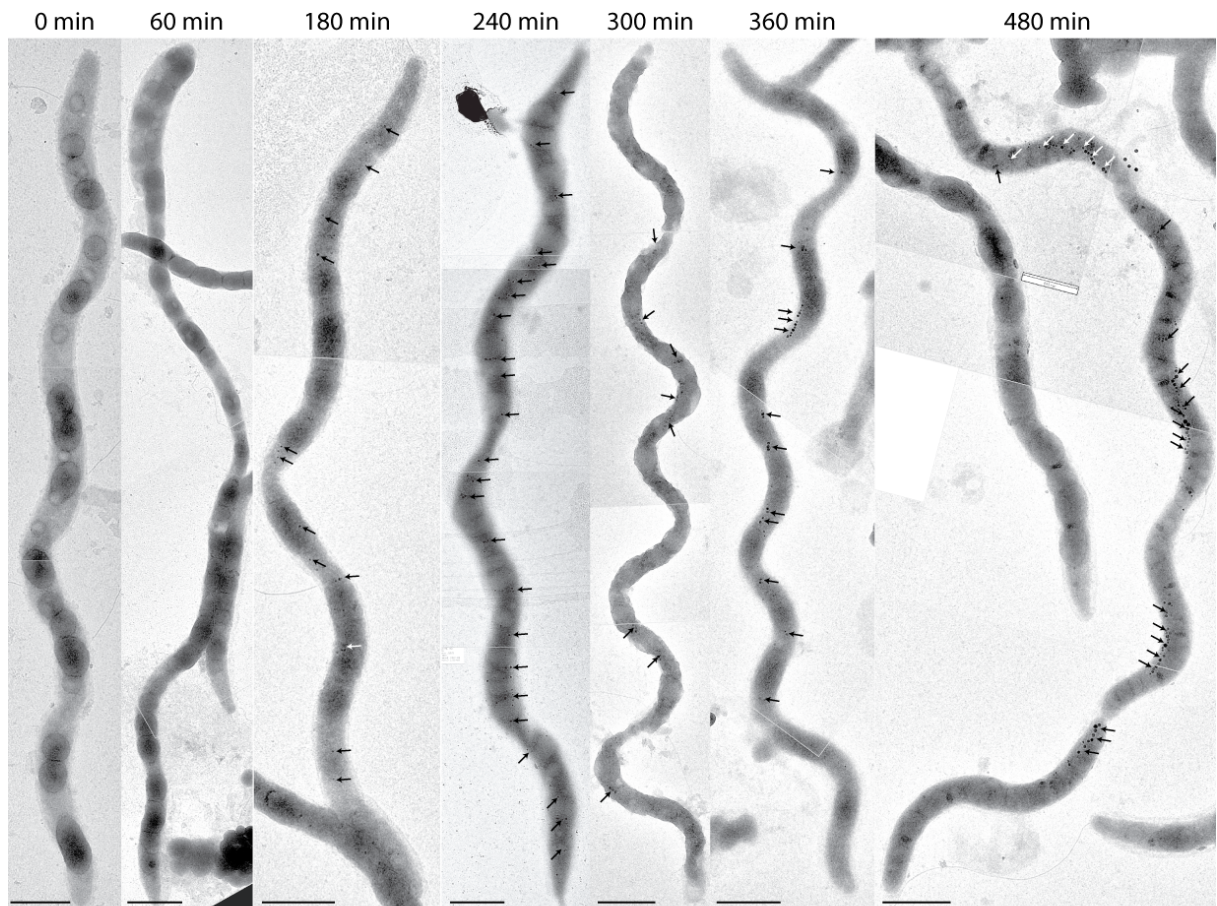


Figure S3

CHAPTER 4

Discussion

The magnetosome chain (MC) of magnetotactic bacteria (MTB) is one of the highest ordered structures found in bacteria. To maintain this high structural integrity, proteins with specific functions are necessary. Two proteins were speculated to contribute to chain integrity, but the mechanism to assemble, position and segregate these structures remained unknown. In this work novel insights into the structure, kinetics and partition mechanism of *M. gryph.* were presented and will be discussed in the following.

The actin-like MamK protein enables the formation of long, straight MCs with central position in *M. gryph.* Moreover, it is localising and concatenating magnetosomes towards the future division site to assure equal distribution of the MC and thus chain integrity throughout the cell cycle. To finally split and overcome the magnetic attraction forces of the chain, a new mechanism by means of bending of the entire cell and asymmetric septum formation, acting as indenter, is described. This mechanism allows minimisation of the forces required for MC division.

4.1 Temperature and oxidative stress affect chain formation

Beside the biotic, also the effect of abiotic factors on MC formation was studied. Therefore, temperature, oxygen and media composition were changed and magnetite formation of *M. gryph.* WT cells was analysed after 1 to 8 days by TEM with respect to magnetite crystal shape and arrangement. The strongest influence on magnetite formation and MC integrity was observed at the highest temperature and aerobic conditions. These led to small magnetite crystals with twinned or fringed morphologies and the occurrence of 'pseudo-chains' (unpublished data) (Figure 8).

In contrast, regular cuboctahedric crystal morphologies with diameters of ~35 – 45 nm aligned in long (> 30 particles) MCs were observed at anaerobic conditions and low temperatures (Figure 8). Noteworthy, the cell length moderately decreased when temperatures were increased.

In conclusion, abiotic factors only have a minor effect on bacterial growth, but have a major effect on magnetite biomineralisation and chain assembly (unpublished data).

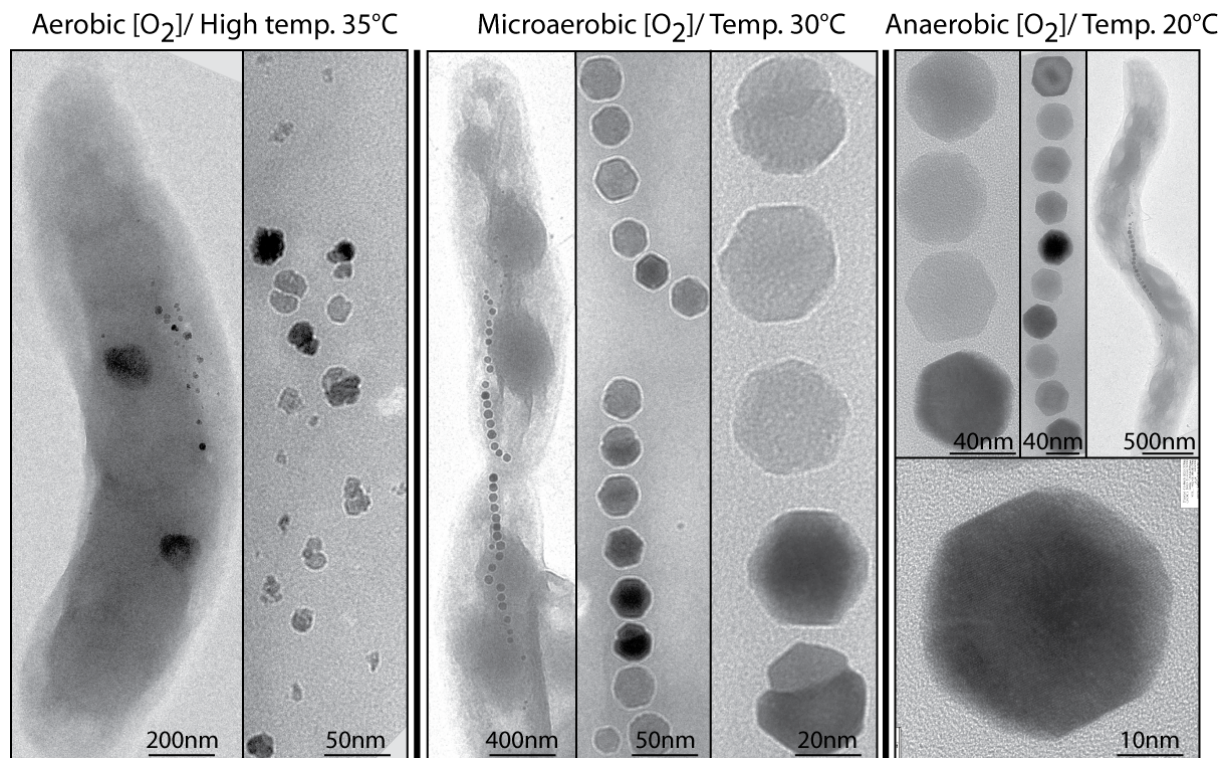


Figure 8: TEM micrographs of *M. gryph.* WT cells, magnetosome chains and magnetite crystals at various oxygen and temperature conditions (unpublished data).

4.2 *M. gryph.* grows from midcell and divides into asymmetric daughter cells.

To study how cell growth influences magnetosome chain assembly, time-lapse cell cycle analyses of *M. gryph.* by differential interference contrast microscopy (DIC) were performed and revealed (i) growth of the cell from the midcell when internal PHB granules were tracked and (ii) asymmetry in daughter cell length.

The incorporation of cell wall material at the area of the future division site (midcell) argues against a polar growth mode as described for other alphaproteobacteria. However, both growth mechanisms are observed within bacteria as a polar growth mode was described in detail in a recent study on *Agrobacterium tumefaciens*, which lacks the MreBCD and Pbp2 cluster (97, 98). Elongation of the central sidewalls, i. e. growth from midcell, was described for *E. coli* and *Caulobacter crescentus* both containing MreB. MreB is the critical key player for peptidoglycan synthesis, and beside FtsZ (tubulin-like protein, forms the Z-ring/arcs) during division, another classification

criterion for growth modes in bacteria. Bacteria devoid of MreB like the cocci *Staphylococcus aureus* with only septal growth and *Corynebacterium glutamicum* with polar cell elongation show a distinct branch (99) compared to *M. gryph.*, where MreB as well as FtsZ are present in the genome. In this work *M. gryph.* growth could be followed in time-lapse experiments for up to three generations. An average cell cycle lasted ~ 260 min with an elongation speed of $5.4 \text{ nm} \cdot \text{min}^{-1}$ and a final pre-divisional cell length of 4 - 5 μm . Unexpectedly, this growth process turned out to be asymmetric in terms of unequal daughter size, since separated *M. gryph.* daughter cells length differed by 15% on average.

Asymmetry in cell length has been also described in four other alphaproteobacteria (*C. crescentus*, *Sinorhizobium meliloti*, *A. tumefaciens* and *Brucella abortus*)(100). Cells of *E. coli* differed by 1 - 4% and *C. crescentus* offspring by 10% in cell length (88, 101). One explanation for this asymmetry might result from the applied artificial growth conditions, which have been demonstrated to generate shorter *E. coli* cells (102) and in this work also faster generation times in *M. gryph.* compared to environmental conditions (103). Other studies associated asymmetric offspring with bacterial aging by which cell material is anchored to the mother cell and left behind by asymmetric protein segregation and division (104). This results could imply that *M. gryph.* might prevent cell damage as consequence of oxidative stress during sample preparation.

However, a more likely explanation relies on the fact that the position of the division site is regulated by specific proteins. In *C. crescentus* a gradient of the negative regulator MipZ is responsible to localize the divisome at its correct position. Depletion of MipZ, however, led to off-centred septa formation resulting in mini swarmer and elongated stalk cells (88). Since MipZ is also present in *M. gryph.* it is likely to be the determinant of divisome localisation. Thus, the observed asymmetry in daughter cell length of *M. gryph.* might be explained by an altered MipZ expression, since Z-ring formation occurs at the area of lowest MipZ concentration (88). If this concentration gradient is shifted away from midcell it would result in an off-centred (asymmetric) Z-ring localisation.

4.3 MamK participates in magnetosome chain recruitment and segregation

MamK was first implicated in building the filamentous scaffold to which individual magnetosomes are arranged into chains (1, 2).

First, the identity of the filamentous structures detected by Scheffel *et al.* (2006) could be confirmed to MamK, since it was no longer detectable in $\Delta mamK$ *M. gryph.* described in this study. However, deletion of *mamK* in *M. gryph.* had pleiotropic effects. Second, shorter magnetosome chains were observed and third the chain fragments were delocalised from their midcell position as typical for WT cells. In WT 92% of the cells showed magnetosome chains (MC) at midcell, whereas this was observed for only 43% of $\Delta mamK$ cells. In a previous study on the closely related *M. magnet.* MamK was shown to form a filament to which the individual magnetite particles are associated. Further, actin-like *mamK* deletion were described to result in groups of 3 - 4 magnetosomes scattered throughout the entire cell (1). Both MamK proteins are highly similar (94.3% identity) and functionally equivalent as shown by cross complementation. In addition, growth conditions had only minor effects, thus discrepancies in magnetosome arrangement between the two mutants are likely due to a different genetic context. Both organisms only share 52% of the overall gene content, which fortifies this assumption. A more recent study by Rioux *et al.* (2010) challenged the ambiguity of the $\Delta mamK$ phenotype and deduced MamK role by Komeili *et al.* (2006) in *M. magnet.*, since they discovered a small cluster of magnetosome genes outside the magnetosome island (MAI), termed islet, in which a second version of MamK (MamK-like) was found. Similar to MamK_{*M. magnet.*} the MamK-like protein was able to form filamentous bundles *in vitro* with a protein identity to MamK_{*M. magnet.*} of 54.5%, which argues for a potential functional redundancy. Taken together, these results indicate that the phenotype described for $\Delta mamK$ *M. magnet.* is not caused by the absence of any filamentous MamK and its conclusive function in *M. magnet.* could only be derived by analysis of a $\Delta mamK mamK$ -like double mutant.

In contrast, in *M. gryph.* deletion of *mamK* resulted in an unequivocal phenotype, since only a single copy of *mamK* was found in the genome. The observed pleiotropic effects of *mamK* deletion may likely be explained by a different MamK function in concatenating and positioning of magnetosomes and the MC, instead of merely providing a backbone or scaffold to which the individual particles are attached to.

This raises new questions: (i) chains, although shorter are still present in $\Delta mamK$ *M. gryph.* against their tendency to agglomerate by magnetic interactions and there must be other scaffolding factors instead of MamK contributing to MC assembly and stability. Magnetostatic interactions on the one hand and transient attachment to the inner membrane on the other hand might cause chain-like arrangement of magnetosomes in absence of MamK. However, magnetostatic interactions are only effective over short ranges if the particles are already in close contact (< 50 nm). The contribution of this forces to wider spaced crystals can be doubted (57). In addition recent *in silico* studies of MC formation in which magnetic and biological interactions were simulated support the assumption that magnetostatic interactions alone are not sufficient for the line up of magnetosomes in *M. gryph.* (105).

Another protein with experimentally confirmed function for MC integrity is MamJ, which was previously demonstrated to interact weakly with MamK and itself (60). Re-examination of the $\Delta mamJ$ mutant during this study by CET revealed previously unknown deletion effects. A non-magnetic iron starved $\Delta mamJ$ cell showed empty vesicles and fragmented parts of MamK filaments. However, the empty vesicles were not clustered, as observed for magnetic cells, instead a spiral-like vesicle arrangement was detected closely below the cytoplasmic membrane. These spirals resembled somewhat the localisation pattern of an eGFP-MreB fusion protein expressed in *M. gryph.* in this study (unpublished data). Recent experimental evidences, however, controversially discuss the helical MreB pattern and the suggested localisation models largely depend on the examination technique (75, 76, 106). Anyway, CET images only display a static snapshot of vesicle organization omitting the cellular dynamics and preliminary protein composition analysis by 2D gel electrophoresis and subsequent mass spectrometry (MALDI) of WT and $\Delta mamK$ magnetosome membranes detected significantly less amounts of MreB ($1/3$) in $\Delta mamK$ (unpublished data).

Interestingly, the previously uncharacterised protein MamY was recently observed to localise in a filamentous pattern when labelled with mCherry (24). Like in $\Delta mamK$ deletion of *mamY* also resulted in an aberrant MC localisation in *M. gryph.* The fact that MamY is neither an actin-like protein nor was it found in any other organism beside magnetotactic spirilla, implicated a putative link between cell (spirilla) shape and MC localisation. A double deletion of *mamY* and *mamK* resulted in a phenotype resembling somewhat the phenotype observed for $\Delta mamJ$ (personal communication O. Raschdorf) with ring-like MC and clustered magnetosomes. Thus, it can be speculated that MamY

might be the protein responsible for the chain-like localisation patterns observed in $\Delta mamK$ *M. gryph*. Further experiments and characterisation of MamY mutants or interaction studies e.g. with cytoskeletal elements like MreB or proteins of the magnetosome membrane will allow to draw a more conclusive picture of its contribution to MC formation.

4.4 Cleavage, midcell-recruitment and relocalisation of the magnetosome chain is mediated by MamK.

To distribute the magnetosome chain (MC) equally between the daughter cells of *M. gryph*, the MC has to be localised at the future division site.

In cells in which final septation was inhibited by cephalaxin, the majority of MCs (66.6%) were running through the individual constriction sites of the filamentous cells, whereas in $\Delta mamK$ cells the majority of MCs was located at positions between individual constrictions (81.2%). This was also seen for cells in which magnetosome formation became induced by addition of iron after division inhibition. Both experiments suggest a concatenation of magnetosomes at the arrested division sites and are consistent with an active, dynamic role of MamK in the recruitment of MCs during *M. gryph* cell cycle.

How is this recruitment mediated? Two hypotheses are conceivable: (i) MamK provides only a 'track' along which the magnetosomes are transported or (ii) MamK generates the force by dynamic polymerisation events. An active movement of the magnetosomes along filamentous structures like MamK, where it serves as a 'track' along which the magnetosomes can assemble into chains would imply a bacterial system analogous to the eukaryotic microtubulin-walking kinesin motor proteins. However, since no bacterial kinesin-like motor proteins have been identified so far, one has to assume that the bacterial Alps described are the precursors of this motor proteins but perform such a task in a less complex way.

More likely is the second hypothesis, because it is known that actin-like proteins can rapidly assemble and disassemble into filaments, which are describe as 'cytomotive' like filaments of ParM (see detailed mode of ParM action in introduction section)(80, 81). Directly after cell division MamK could act similar to the cytomotive ParM but only polymerize into longer filaments away from the new cell pole if it is assumed that parts

of MamK are inherited after division as it was demonstrated in *E. coli* by Pradel *et al.* (2006) and proven for *M. gryph.* in tomograms in this study (103). In accordance with these observations and the here described unidirectional, asymmetric cell growth of *M. gryph.* both facts could be an explanation of how the MC localizes at midcell.

Still, the positional information for MamK to localise specifically at the division site remains to be determined. Preliminary results of this study obtained by a bacterial Two-Hybrid system indicated strong interactions between MamK and FtsA, MamJ - FtsA and weaker to MreB (unpublished data). As conclusion, FtsA, which is known to tether the Z-ring (formed by FtsZ) at the membrane and to recruit downstream proteins for divisome assembly is a promising candidate for midcell mediated MamK i.e. MC localisation (103, 107). However, this has to be verified in future studies.

4.5 Magnetosome chain and magnetosome filament are cleaved by asymmetric septation and snapping

In addition to proper assembly and positioning MTB face the challenge to ensure that the magnetosome chain (MC) becomes split against the magnetic interaction forces and distributed towards the offspring to allow magnetotactic orientation behaviour throughout the cell cycle. The observed unidirectional bending and snapping of *M. gryph.* cells during cell division suggested an asymmetric formation of the divisome. To examine this process in greater detail CET studies on dividing *M. gryph.* cells were performed.

This work revealed that (i) bending of the entire cell around the division site is followed by (ii) a fast snapping caused by on-going constriction and thus destabilisation of the cell envelope. The constriction, however, was observed to be (iii) asymmetric in terms of a wedge-like, unidirectional indentation of the inner membrane distal (opposite) of the MC. This asymmetric indentation and the resulting bending allows the cell to effectively 'break' the MC, thus to overcome the magnetostatic interactions. This pre-divisional cell bending or buckling seems to be restricted to some spirilla-shaped bacteria like *Spirillum anulus*, *M. magnet.*, *M. gryph.* and MS-1 (3, 19, 108) and the clue might be the helical cell shape.

What are the possible mechanisms causing the asymmetric division?

The forces to overcome the magnetic attraction within a MC for magnetic spirilla like *M. gryph.* were calculated (by Michael Winklhofer, LMU Geophysics) to be at least 40 pN. There are no mechanisms described to generate forces of this strength in bacteria that are sufficient to separate magnetite crystals within a MC. Interestingly, *M. gryph.* could drastically reduce the required forces if an indentation mechanism, as was observed for the MC by combined microscopic approaches, was included in the force calculations.

In this study CET analysis of *M. gryph.* revealed Z-arcs of FtsZ with pinch-like filaments localised beneath the cell envelope at the constriction site, which were also observed in *C. crescentus* (93) and support the model of 'iterative pinching' for cell division described by Erickson *et al.* (1997) (109). This Z-arc filaments resulted in a 'M'-like shape and are likely to compose the Z-ring of *M. gryph.* (103). The Z-arcs and a wedge-like peptidoglycan inward growth together reduced the forces to overcome magnetostatic interactions by the cosine of the bending angle, thus splitting becomes possible by FtsZ constriction. In contrast, the concentric Z-ring of *E. coli* exerts only a force between 3 to 8 pN, which is sufficient for cell division i.e. membrane bending (85, 110) but is one order of magnitude lower than necessary to split adjacent magnetic particles, where forces are calculated to exceed 40 pN in case of the cuboctahedric crystals of *M. gryph.* (103, 111). This mechanism is applicable for magnetotactic spirilla with cuboctahedric magnetite crystal chains and their typical cell shape but might become even more difficult for big (> 50 nm in diameter) cuboid magnetite crystals of cocci. Beside their stronger magnetic interaction forces the interparticle distance in magnetic cocci is reduced to ~ 5 nm. Both aspects and the missing leverage effect due to spherical cell morphology suggests other or modified MC division mechanisms compared to spirilla-shaped *M. gryph.* Interestingly, TEM micrographs of the magnetic ovoid bacterium MO-1 showed a bending of the MC due to an inward growth and constriction of the Z-ring from one side, which led to two daughter chains with identical magnetosome numbers (112). However, an asymmetric Z-ring formation was so far only described for the cyanelle of the protist *Cyanophora paradoxa* and shown but not commented in a CET projection of dividing *E. coli* by Wang *et al.* (2011) (113, 114). Further, CET examination in this study on the non-magnetic mutant *M. gryph.* MSR-1B showed the same cell bending as detected in WT, indicating that bending is not caused by proteins encoded within the MAI, but might be rather a cell shape-typical feature of division.

Another hypothesis was that asymmetric Z-ring presence might be due to a second *ftsZ*-like gene (*ftsZm*) in the genome of *M. gryph*. However, preliminary CET analysis, as part of this work, indicated that the septum formation in Δ *ftsZm* *M. gryph*. occurs still asymmetric from the site opposite the MC as observed for *M. gryph*. WT.

To study how the wedge-like indentation is formed and affects the MC, a detailed analysis of the division site in *M. gryph*. revealed an invaginated peptidoglycan layer. A Tol-Pal complex examined in *E. coli* and *C. crescentus* was observed to induce outer membrane constriction during late cell division (87, 115). Expression of the Tol-Pal complex, present in the genome of *M. gryph*., most likely accounts for the observed pattern. The stress caused by the wedge-like indentation might bend the MamK filament or weaken its cohesiveness and result in a knick or break, which has to be examined. Despite these ambiguities wedge-like indentation and subsequent filament splitting together with magnetosome displacement, allows the cell in a low energy process, the efficient fission of the magnetosome chain.

4.6 Ultrastructural analysis of the magnetosome

A side observation during CET analysis raised interesting questions: where does the magnetite nucleate within the vesicle and what is the state of the membrane during the magnetite growth? Both presented models for magnetosome chain formation differ in the state of their magnetosomes: permanent membrane association in *M. magnet*. vs. transient membrane association in *M. gryph*. Since magnetosomes of *M. magnet*. are permanently membrane bound it is tempting to speculate that their vesicles can grow via lipid incorporation derived from the inner membrane. But this raises several questions on how the specific chemical environment is preserved within a magnetosome without mixing both compartments (periplasm – vesicle)? Examination of CET tomograms of *M. gryph*. revealed a number of membrane unbound magnetosome vesicles of different sizes. Interesting were vesicles with a small diameter (ca. 20 - 30 nm), likely to represent immature versions. These detached vesicles were partially filled with tiny magnetite crystals (< 20 nm), and assuming these crystals will grow further, this would occur independent from a vesicle contact to the periplasm. Beside the vesicles detached from the inner membrane also attached vesicles were detected. However, this observation was confirming the transient membrane association hypothesis of magnetosomes in *M. gryph*.

Another mode for magnetite crystal growth without a permanent membrane contact was suggested by Faivre *et al.* in which vesicles are first membrane bound iron loaded and then independently of their localisation biomineralise magnetite (116).

In this study, the magnetosome vesicle diameter was observed to be uncorrelated with magnetite crystal size or even abundance, since mature vesicles with a tiny or no magnetite crystal at all could be detected infrequently in tomograms of *M. gryph.* This implies a magnetite crystal growth independent from magnetosome vesicle growth. If in return the magnetosome vesicle diameter is constraining the magnetite crystal size needs further clarification.

In projections of CET tomograms all immature magnetite crystals were closely associated with the magnetosome membrane, but never found detached. This could provide a first hint on where the magnetite nucleates within an empty vesicle (Figure 9). Interestingly, vesicles containing two opposing immature magnetite crystals were also observed infrequently (Figure 9, arrows).

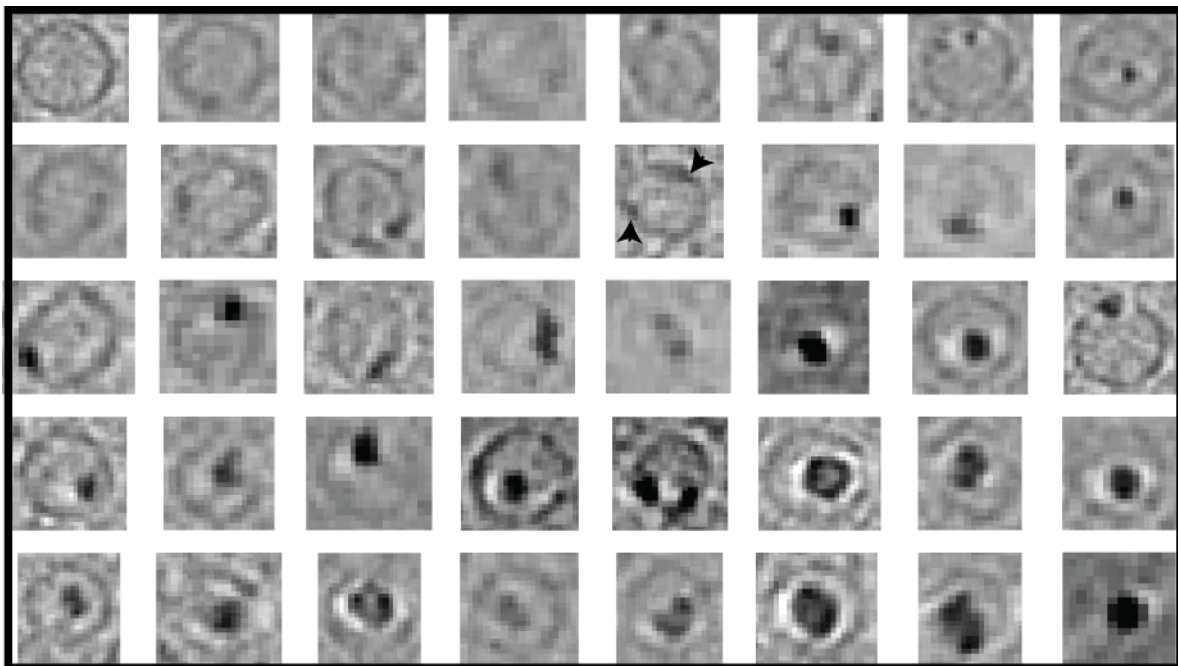


Figure 9: Projections of individual tomogram sections in x-y direction. Magnetosome vesicles arranged by progression of magnetite biomineralisation: absence of magnetite (upper left) to mature magnetosomes (lower right). Black Arrow heads indicate crystal twinning onset. Vesicle diameter is ~ 40nm.

This configuration of independent dual nucleation spots within one vesicle was suggested by Devouard *et al.* (1998) to be the initial situation for crystal twinning. Twinning character as a crystal growth defect was not described up to date in its onset

steps but was frequently observed for mature magnetite in various MTB (Figure 9)(117).

4.7 An improved model of magnetosome chain assembly

Both previous models are combined results of studies performed by Scheffel *et al.* and Komeili *et al.* (1, 2), which were based on experimental data mainly derived by knockout mutagenesis, cryo-electron tomography and magnetosome *de novo* synthesis within non-magnetic cells of *M. gryph.* and *M. magnet.* However, the examination of the *M. gryph.* $\Delta mamK$ mutant during this study revealed several differences to the *M. magnet.* $\Delta mamK$ mutant and a more precise role of MamK, which directs towards a different mode of magnetosome chain (MC) formation in both organisms.

Examination of *M. magnet.* cells with conventional TEM revealed that the MC had larger gaps between individual crystals and that the entire MC extended close to both cell poles in contrast to the tightly packed central chain of *M. gryph.* Both previous models differed in two aspects: (i) the immature magnetosomes were localised either scattered (*M. gryph.*) or arranged to a chain (*M. magnet.*) and (ii) are either permanently cytoplasmic membrane (CM) bound in *M. magnet.* or in a transient CM attached or detached state in *M. gryph.* This work showed that magnetosomes in *M. gryph.* can be occasionally found membrane bound as a result of invagination of the CM, which was not demonstrated until this work. Besides, the majority of mature magnetosomes were either close to the CM without any obvious connection or clearly separated, away from CM, as also observed in the related *Rhodobacter spheroides*. *R. spheroides* has the ability to form intracellular vesicles in order to increase its surface area to absorb and utilise solar energy (118). Membrane detached vesicles were not observed in *M. magnet.* (personal communication A. Komeili) and points towards a different mode of MC assembly between both organisms or simply escaped detection. Anyway, it can not be excluded that future work will prove the one or the other observation to be general for both organisms. There is only a limited set of techniques available to visualize the state of magnetosomes with respect to their membrane dependent localisation but rapid

advances in microscopy techniques might resolve discrepancies between *M. magnet.* and *M. gryph.* vesicle formation. However, what both models had in common was the MamK associated localisation of the magnetosomes and invagination as origin of the magnetosome membrane.

In addition, both models lacked the dynamic component, which must be present at least for *M. gryph.* due to the fact of inherited magnetosomes (3, 103). The sorting and positioning function of MamK, as well as its either direct or indirect segregation with the division apparatus resulted in a new model of MC formation combining *de novo* magnetite crystal synthesis with the new dynamic distribution of MCs between daughter cells in *M. gryph.*

In this revised model (i) small, immature magnetosomes are derived through invagination and grow scattered throughout the entire cell. (ii) Reversible polymerisation i. e. cytomotive action of MamK at the cell centre and poles, assembly of the arc-like Z-ring together with other magnetosomal as well as cytoskeletal proteins captures free magnetosomes during proceeding crystal and cell growth at the cell centre. (iii) Diametral alignment of the MC depends on MamJ, which interacts with MamK and on a speculative interaction of magnetosomal MamY with convex areas of the inner membrane. (iv) On-going asymmetric constriction of the division machinery and unidirectional peptidoglycan inward growth causes cell bending and the wedge-like indentation splits the MC against their magnetostatic attraction at its centre. Daughter cell elongation (v), relaxation and filamentous growth of the FtsZ towards the new midcell, i.e. low MipZ concentrations, is followed by MamK polymerisation and MC segregation (Figure 10).

The precise mechanism of how the magnetosome sub chains are localised by MamK towards midcell is still not fully understood and will be subject for future studies.

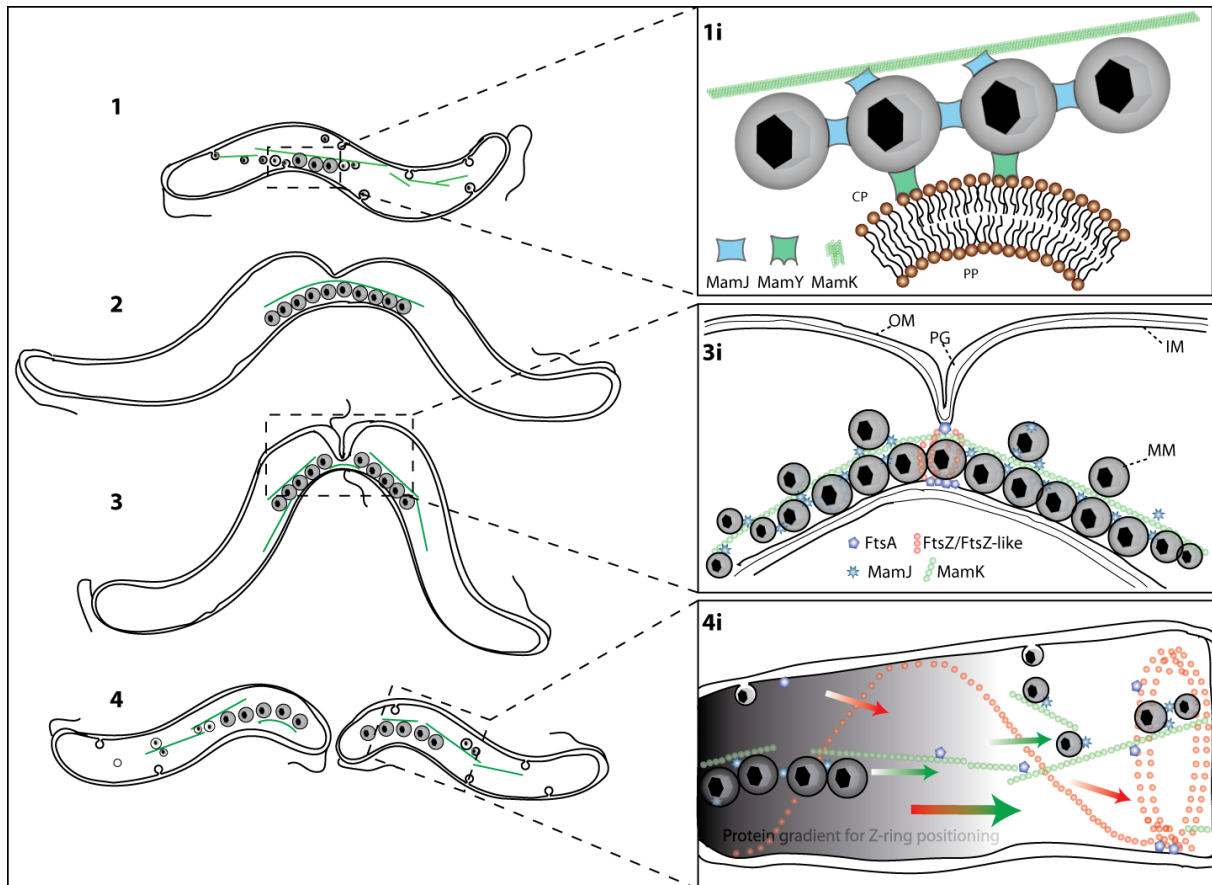


Figure 10: Model of magnetosome chain (MC) formation and cell division in *M. gryph*. (1): Cell growth and magnetosome formation via invagination with subsequent chain assembly along MamK filaments. (1i): Magnetosome chain integrity is maintained through *i* MamK filaments (green), *ii* MamJ dimerization as well as *iii* interaction with MamK. Diametral MC anchoring might be accomplished by the putatively curvature sensing MamY protein (PP, periplasm, CP, cytoplasm). (2 - 3): The mature, central magnetosome chain bends in the adult cell through asymmetric indentation of the outer and inner membrane resulting in buckling of the entire cell. (3i): Close up of the division plane with wedge-like inward growth of the inner and outer membrane (IM, OM). The magnetosome chain is indented and kept at its central position through interaction with MamK (green) and condensed proteins of the divisome (purple - FtsA, red - FtsZ/FtsZ-like ring). (4): Acute buckling and progressive wedge formation splits the magnetosome chain and filament together with the cell and results in two daughter cells with polar, inherited sub chain fragments. (4i): Formation of the new Z-ring at the cell centre (red) together with MamK filament formation (green) results in a segregation movement (red-green arrows) of the inherited magnetosomes towards the cell centre. Segregation is putatively coordinated by gradients (black to white background) of the negative regulators MipZ (MGR4222) of *M. gryph*.

Outlook

This work resulted in a new model of magnetosome chain (MC) formation and division of *Magnetospirillum gryphiswaldense* including some hypothetical elements, which should be verified in future experimental work.

One element is the anchor of the MC within the cell. MamK, as cytoskeletal element, assembles the magnetosomes into chains but the entire chain (magnetosomes and filament) must remain with the cell envelope to ensure proper transmission of the magnetic force into a torque of the entire cell body. The contribution of membrane bound magnetosomes within the MC, especially due to the spirilla-shaped cell body, should be examined. So far, MamK could be visualized at polar regions but no direct contact to the inner polar membrane or else was observed. What is described was the ending of filaments near arrays of chemoreceptors. Possible experiments could use fusion proteins of both putative interaction partners with fluorophores. Techniques like split eYFP or FRET (fluorescence resonance energy transfer) should be used, since they also account for the dynamic character of MamK. Along with this, the occurrence of shorter MCs within the $\Delta mamK$ mutant implies other factors critical for chain formation e.g. the MamY protein. This protein has to be studied in greater detail to elucidate the role of its exclusive abundance in spirilla-shaped MTBs and to reassess its speculated magnetosome membrane (MM) anchor and membrane curvature sensing function.

A second unknown element is how the inherited magnetosomes of the split parental MC are localised towards midcell? This work revealed a connection between the divisome and MamK but the precise interaction mechanism or driving force to midcell remains to be solved.

To examine how the magnetosomes are distributed between dividing *M. gryph.* cells *in vivo*, more detailed time-lapse experiments should be performed. A possible experiment would be a dual marker approach with labelled magnetosomal MamC-GFP constitutively expressed together with an inducible mCherry fused to another protein of the MM, which is activated after cell division. A green signal would indicate the inherited magnetosomes, whereas yellow (overlay of green and red) colour defines newly synthesized particles.

The next step is to examine the role of MipZ in *M. gryph.* as it is a negative regulator of FtsZ polymerization and defines the position of the Z-ring in the related *C. crescentus*. Moreover, it marks the old pole in predivisional *C. crescentus* cells and moves to the new pole along with the duplicated chromosome before cell division (119). An approach of high resolution light microscopy (120) in combination with time-lapse imaging could reveal how the magnetosomes and magnetosome filament localise at midcell.

Less is known about the structure of the MM and its attached proteins. On-going use of cryo-electron tomography (CET) to study MM genesis and structure at a higher resolution will help to understand the complexity of magnetosome formation and arrangement. Since this technique allows to resolve macromolecular complexes attached to the MM, it might also reveal the detailed mode of MamK – MM binding. Moreover, the initial interaction studies between MamK and MamJ with the bacterial Two-Hybrid system were not fully conclusive, since in some cases only a weak or transient contact could be detected. Additional work has to be performed in order to reveal the exact mode of action between both proteins.

Important for cell shape is the cytoskeletal protein MreB, which is also involved in cell elongation. MreB was shown to interact weakly with MamJ as well as with MamK (unpublished data). It has to be examined if this protein might be able to transport magnetosomes for example through its cell elongation function or in a more specific manner towards midcell. The use of light microscopic techniques such as TIRF would be the method of choice.

References

1. A. Komeili, Z. Li, D. Newman, G. Jensen (2006) Magnetosomes Are Cell Membrane Invaginations Organized by the Actin-Like Protein MamK. *Science* 311: 242.
2. A. Scheffel *et al.* (2006) An acidic protein aligns magnetosomes along a filamentous structure in magnetotactic bacteria. *Nature* 440: 110.
3. S. S. Staniland, C. Moiescu, L. G. Benning (2010) Cell division in magnetotactic bacteria splits magnetosome chain in half. *J Basic Microbiol* 50: 392.
4. A. van Leeuwenhoek (1677) Concerning Little Animals by Him Observed in Rain-Well-Sea and Snow Water; as Also in Water Wherein Pepper Had Lain Infused. *Philosophical Transactions* 12: 821.
5. S. Bellini (2009) Further studies on "Magnetosensitive bacteria". *CJOL*: 1.
6. R. Blakemore (1975) Magnetotactic bacteria. *Science* 190: 377.
7. S. Kolinko *et al.* (2011) Single-cell analysis reveals a novel uncultivated magnetotactic bacterium within the candidate division OP3. *Environ Microbiol* 14: 1709.
8. C. B. Flies *et al.* (2005) Diversity and vertical distribution of magnetotactic bacteria along chemical gradients in freshwater microcosms. *FEMS Microbiol Ecol* 52: 185.
9. S. L. Simmons, K. J. Edwards, in *Magnetoreception and Magnetosomes in Bacteria*, D. Schüler, Ed. (Springer, Heidelberg, 2006), vol. 3, pp. 77-102.
10. R. Blakemore, R. Frankel (1981) Magnetic navigation in bacteria. *Sci Am* 245: 42.
11. R. Frankel, R. Blakemore (1980) Navigational compass in magnetic bacteria. *J Magnetism Magnet Mat* 15-18: 1562.
12. D. Schüler (2008) Genetics and cell biology of magnetosome formation in magnetotactic bacteria. *Fems Microbiol Rev* 32: 654.
13. C. Jogler *et al.* (2010) Conservation of proteobacterial magnetosome genes and structures in an uncultivated member of the deep-branching *Nitrospira* phylum. *Proc Natl Acad Sci* 108: 1134.
14. R. Frankel, D. Bazylinski, M. Johnson, B. Taylor (1997) Magneto-Aerotaxis in Marine Coccoid Bacteria. *Biophys J* 73: 994.

15. S. Ullrich, M. Kube, S. Schübbe, R. Reinhardt, D. Schüler (2005) A hypervariable 130-kilobase genomic region of *Magnetospirillum gryphiswaldense* comprises a magnetosome island which undergoes frequent rearrangements during stationary growth. *J Bacteriol* 187: 7176.
16. K. Grünberg *et al.* (2004) Biochemical and proteomic analysis of the magnetosome membrane in *Magnetospirillum gryphiswaldense*. *Appl Environ Microbiol* 70: 1040.
17. D. Murat, A. Quinlan, H. Vali, A. Komeili (2010) Comprehensive genetic dissection of the magnetosome gene island reveals the step-wise assembly of a prokaryotic organelle. *Proc Natl Acad Sci* 107: 5593.
18. A. Lohße *et al.* (2011) Functional Analysis of the Magnetosome Island in *Magnetospirillum gryphiswaldense*: The *mamAB* Operon Is Sufficient for Magnetite Biomineralization. *PLoS ONE* 6: 1.
19. C. Yang, H. Takeyama, T. Tanaka, A. Hasegawa, T. Matsunaga (2001) Synthesis of bacterial magnetic particles during cell cycle of *Magnetospirillum magneticum* AMB-1. *Appl Biochem Biotechnol* 91-93: 155.
20. D. Schüler, M. Köhler (1992) The isolation of a new magnetic spirillum. *Zentralbl Mikrobiol* 147: 150.
21. U. Heyen, D. Schüler (2003) Growth and magnetosome formation by microaerophilic *Magnetospirillum* strains in an oxygen-controlled fermentor. *Appl Microbiol Biotechnol* 61: 536.
22. K. Schleifer *et al.* (1991) The genus *Magnetospirillum* gen. nov., description of *Magnetospirillum gryphiswaldense* sp. nov. and transfer of *Aquaspirillum magnetotacticum* to *Magnetospirillum magnetotacticum* comb. nov. *Syst Appl Microbiol* 14: 379.
23. M. Richter *et al.* (2007) Comparative Genome Analysis of Four Magnetotactic Bacteria Reveals a Complex Set of Group-Specific Genes Implicated in Magnetosome Biomineralization and Function. *J Bacteriol* 189: 4899.
24. O. Raschdorf, Diploma thesis, LMU Munich Biocenter (2011).
25. D. Schultheiss, D. Schüler (2003) Development of a genetic system for *Magnetospirillum gryphiswaldense*. *Arch Microbiol* 179: 89.
26. T. Matsunaga, T. Sakaguchi, F. Tadokoro (1991) Magnetite formation by a magnetic bacterium capable of growing aerobically. *Appl Microbiol Biotechnol* 35: 651.

27. A. Scheffel, A. Gärdes, K. Grünberg, G. Wanner, D. Schüler (2008) The major magnetosome proteins MamGFDC are not essential for magnetite biomineralization in *Magnetospirillum gryphiswaldense* but regulate the size of magnetosome crystals. *J Bacteriol* 190: 377.
28. M. Tanaka, E. Mazuyama, A. Arakaki, T. Matsunaga (2011) MMS6 Protein Regulates Crystal Morphology during Nano-sized Magnetite Biomineralization *in Vivo*. *J Biol Chem* 286: 6386.
29. D. Murat, M. Byrne, A. Komeili (2010) Cell Biology of Prokaryotic Organelles. Cold Spring Harb Perspect Biol 2: 1.
30. Y. Gorby, T. Beveridge, R. Blakemore (1988) Characterization of the Bacterial Magnetosome Membrane. *J Bacteriol* 170: 834.
31. M. Byrne *et al.* (2010) *Desulfovibrio magneticus* RS-1 contains an iron- and phosphorus-rich organelle distinct from its bullet-shaped magnetosomes. *Proc Natl Acad Sci* 107: 12263.
32. T. Matsunaga, M. Nemoto, A. Arakaki, M. Tanaka (2009) Proteomic analysis of irregular, bullet-shaped magnetosomes in the sulphate-reducing magnetotactic bacterium *Desulfovibrio magneticus* RS-1. *Proteomics* 9: 3341.
33. A. P. Taylor, J. C. Barry (2004) Magnetosomal matrix: Ultrafine structure may template biomineralization of magnetosomes. *J Microsc* 213: 180.
34. F. Meldrum, S. Mann, B. Heywood, R. Frankel, D. Bazylinski (1993) Electron-Microscopy Study of Magnetosomes in 2 Cultured Vibrioid Magnetotactic Bacteria. *Proc R Soc Lond* 251: 237.
35. M. Tanaka *et al.* (2006) Origin of magnetosome membrane: Proteomic analysis of magnetosome membrane and comparison with cytoplasmic membrane. *Proteomics* 6: 5234.
36. R. Frankel, G. Papaefthymiou, R. Blakemore, W. O'Brian (1983) Fe_3O_4 Precipitation in Magnetotactic Bacteria. *Biochim Biophys Acta* 763: 147.
37. E. Katzmann, Diploma thesis, Universität Bremen (2007).
38. M. Tanaka, A. Arakaki, T. Matsunaga (2010) Identification and functional characterization of liposome tubulation protein from magnetotactic bacteria. *Mol Microbiol* 76: 480.
39. R. Blakemore (1982) Magnetotactic bacteria. *Annu Rev Microbiol* 36: 217.
40. J. Baumgartner, D. Faivre (2011) Magnetite Biomineralization in Bacteria. *Prog Mol Subcell Biol* 30: 1.

41. D. Schüler (1999) Formation of magnetosomes in magnetotactic bacteria. *J Mol Microbiol Biotechnol* 1: 79.
42. C. Rong *et al.* (2008) Ferrous iron transport protein B gene (*feoB1*) plays an accessory role in magnetosome formation in *Magnetospirillum gryphiswaldense* strain MSR-1. *Res Microbiol* 159: 530.
43. D. Schüler, E. Baeuerlein (1996) Iron-limited growth and kinetics of iron uptake in *Magnetospirillum gryphiswaldense*. *Arch Microbiol* 166: 301.
44. D. Schüler, E. Baeuerlein (1998) Dynamics of iron uptake and Fe₃O₄ biomineralization during aerobic and microaerobic growth of *Magnetospirillum gryphiswaldense*. *J Bacteriol* 180: 159.
45. R. Uebe, Doctoral thesis, Ludwig-Maximilians-Universität (2011).
46. R. Uebe *et al.* (2011) The cation diffusion facilitator proteins MamB and MamM of *Magnetospirillum gryphiswaldense* have distinct and complex functions, and are involved in magnetite biomineralization and magnetosome membrane assembly. *Mol Microbiol* 82: 818.
47. D. Faivre, D. Schüler (2008) Magnetotactic bacteria and magnetosomes. *Chemical Reviews* 108: 4875.
48. R. Frankel, R. Blakemore (1979) Magnetite in Freshwater Magnetotactic Bacteria. *Science* 203: 1355.
49. J. Kirschvink (1980) South-seeking magnetic bacteria. *J Exp Biol* 86: 345.
50. J. Kirschvink, J. Gould (1981) Biogenic magnetite as a basis for magnetic field detection in animals. *Biosystems* 13: 181.
51. C. Keim, F. Abreu, U. Lins, H. Lins de Barros, M. Farina (2004) Cell organization and ultrastructure of a magnetotactic multicellular organism. *J Struct Biol* 145: 254.
52. L. G. Abraçado *et al.* (2011) Magnetosome chain superstructure in uncultured magnetotactic bacteria. *Phys Biol* 7: 1.
53. H. Vali, J. Kirschvink, R. Frankel, R. Blakemore, in *Iron Biominerals*. (1990), pp. 97-115.
54. M. Hanzlik, M. Winklhofer, N. Petersen (1996) Spatial arrangement of chains of magnetosomes in magnetotactic bacteria. *Earth Planet Sci Lett* 145: 125.
55. R. Dunin-Borkowski *et al.* (1998) Magnetic microstructure of magnetotactic bacteria by electron holography. *Science* 282: 1868.

56. R. B. Frankel (1984) Magnetic guidance of organisms. *Ann Rev Biophys Bioeng* 13: 85.
57. E. T. Simpson, Doctoral thesis, University of Cambridge (2008).
58. S. Ofer *et al.* (1984) Magnetosome dynamics in magnetotactic bacteria. *Biophys J* 46: 57.
59. J.-B. Rioux *et al.* (2010) A second actin-like MamK protein in *Magnetospirillum magneticum* AMB-1 encoded outside the genomic magnetosome island. *PLoS ONE* 5: e9151.
60. A. Scheffel, D. Schüler (2007) The acidic repetitive domain of the *Magnetospirillum gryphiswaldense* MamJ protein displays hypervariability but is not required for magnetosome chain assembly. *J Bacteriol* 189: 6437.
61. O. Draper *et al.* (2011) MamK, a bacterial actin, forms dynamic filaments in vivo that are regulated by the acidic proteins MamJ and LimJ. *Mol Microbiol* 82: 342.
62. A. Derman *et al.* (2009) Phylogenetic Analysis Identifies Many Uncharacterized Actin-like Proteins (Alps) in Bacteria: Regulated Polymerization, Dynamic Instability, and Treadmilling in Alp7A. *Mol Microbiol* 73: 534.
63. A. Guljamow *et al.* (2007) Horizontal gene transfer of two cytoskeletal elements from a eukaryote to a cyanobacterium. *Curr Biol* 17: R757.
64. S. Schübbe *et al.* (2006) Transcriptional organization and regulation of magnetosome operons in *Magnetospirillum gryphiswaldense*. *Appl Environ Microbiol* 72: 5757.
65. N. Pradel, C.-L. Santini, A. Bernadac, Y. Fukumori, L.-F. Wu (2006) Biogenesis of actin-like bacterial cytoskeletal filaments destined for positioning prokaryotic magnetic organelles. *Proc Natl Acad Sci* 103: 17485.
66. N. Pradel *et al.* (2007) Polar positional information in *Escherichia coli* spherical cells. *Biochem Biophys Res Commun* 353: 493.
67. A. Taoka, R. Asada, L.-F. Wu, Y. Fukumori (2007) Polymerization of the actin-like protein MamK, which is associated with magnetosomes. *J Bacteriol* 189: 8737.
68. A. Marchler-Bauer *et al.* (2009) CDD: specific functional annotation with the Conserved Domain Database. *Nucleic Acids Res* 37: D205.
69. M. Doi *et al.* (1988) Determinations of the DNA sequence of the *mreB* gene and of the gene products of the *mre* region that function in formation of the rod shape of *Escherichia coli* cells. *J Bacteriol* 170: 4619.

70. F. Van den Ent, L. Amos, J. Löwe (2001) Prokaryotic origin of the actin cytoskeleton. *Nature*.
71. L. Jones, R. Carballido-Lopez, J. Errington (2001) Control of cell shape in bacteria: helical, actin-like filaments in *Bacillus subtilis*. *Cell* 104: 913.
72. D. Popp *et al.* (2010) Filament structure, organization, and dynamics in MreB sheets. *J Biol Chem* 285: 15858.
73. P. L. Graumann (2007) Cytoskeletal elements in bacteria. *Annu Rev Microbiol* 61: 589.
74. M. T. Swulius *et al.* (2011) Long helical filaments are not seen encircling cells in electron cryotomograms of rod-shaped bacteria. *Biochem Biophys Res Commun* 407: 650.
75. J. Domínguez-Escobar *et al.* (2011) Processive Movement of MreB-Associated Cell Wall Biosynthetic Complexes in Bacteria. *Science* 333: 225.
76. E. C. Garner *et al.* (2011) Coupled, Circumferential Motions of the Cell Wall Synthesis Machinery and MreB Filaments in *B. subtilis*. *Science* 333: 222.
77. J. Salje, F. Van Den Ent, P. De Boer, J. Löwe (2011) Direct Membrane Binding by Bacterial Actin MreB. *Mol Cell* 43: 478.
78. P. Vats, Y.-L. Shih, L. Rothfield (2009) Assembly of the MreB-associated cytoskeletal ring of *Escherichia coli*. *Mol Microbiol* 72: 170.
79. S. Austin, A. Wierzbicki (1983) Two Mini-F-Encoded Proteins Are Essential for Equipartition. *Plasmid* 10: 73.
80. J. Salje, P. Gayathri, J. Löwe (2010) The ParMRC system: molecular mechanisms of plasmid segregation by actin-like filaments. *Nat Rev Microbiol* 8: 683.
81. J. Löwe, L. A. Amos (2009) Evolution of cytomotive filaments: The cytoskeleton from prokaryotes to eukaryotes. *Int J Biochem Cell Biol* 41: 323.
82. E. Garner, C. Campbell, R. D. Mullins (2004) Dynamic instability in a DNA-segregating prokaryotic actin homolog. *Science*.
83. Y. Hirota, A. Ryter, F. Jacob (1968) Thermosensitive mutants of *E. coli* affected in the processes of DNA synthesis and cellular division. *Cold Spring Harb Symp Quant Biol* 33: 677.
84. E. Bi, J. Lutkenhaus (1991) FtsZ ring structure associated with division in *Escherichia coli*. *Nature* 354: 161.
85. H. P. Erickson, D. E. Anderson, M. Osawa (2010) FtsZ in Bacterial Cytokinesis: Cytoskeleton and Force Generator All in One. *Microbiol Mol Biol Rev* 74: 504.

86. E. D. Goley *et al.* (2011) Assembly of the *Caulobacter* cell division machine. *Mol Microbiol* 80: 1680.
87. Y. Yeh, L. Comolli, K. H. Downin, L. Shapiro, H. H. McAdams (2010) The *Caulobacter* Tol-Pal Complex Is Essential For Outer Membrane Integrity and the Positioning of a Polar Localization Factor. *J Bacteriol* 192: 4847.
88. M. Thanbichler, L. Shapiro (2006) MipZ, a spatial regulator coordinating chromosome segregation with cell division in *Caulobacter*. *Cell* 126: 147.
89. D. Savage, B. Afonso, A. Chen, P. A. Silver (2010) Spatially ordered dynamics of the bacterial carbon fixation machinery. *Science* 327: 1258.
90. B. Galán *et al.* (2010) Nucleoid-associated PhaF phasin drives intracellular location and segregation of polyhydroxyalkanoate granules in *Pseudomonas putida* KT2442. *Mol Microbiol* 79: 402.
91. J. Kürner, A. S. Frangakis, W. Baumeister (2005) Cryo-electron tomography reveals the cytoskeletal structure of *Spiroplasma melliferum*. *Science* 307: 436.
92. G. P. Henderson, L. Gan, G. J. Jensen, P. Digard (2007) 3-D Ultrastructure of *O. tauri*: Electron Cryotomography of an Entire Eukaryotic Cell. *PLoS ONE* 2: e749.
93. Z. Li, M. J. Trimble, Y. V. Brun, G. J. Jensen (2007) The structure of FtsZ filaments *in vivo* suggests a force-generating role in cell division. *EMBO J* 26: 4694.
94. L. Gan, S. Chen, G. J. Jensen (2008) Molecular organization of Gram-negative peptidoglycan. *Proc Natl Acad Sci* 105: 18953.
95. J. Salje, B. Zuber, J. Löwe (2009) Electron cryomicroscopy of *E. coli* reveals filament bundles involved in plasmid DNA segregation. *Science* 323: 509.
96. L. Gan, G. J. Jensen (2011) Electron tomography of cells. *Quart Rev Biophys*: 1.
97. P. J. B. Brown *et al.* (2012) Polar growth in the Alphaproteobacterial order *Rhizobiales*. *Proc Natl Acad Sci* 109: 1697.
98. T. den Blaauwen, M. A. de Pedro, M. Nguyen-Disteche, J. A. Ayala (2008) Morphogenesis of rod-shaped sacculi. *FEMS Microbiol Rev* 32: 321.
99. W. Margolin (2009) Sculpting the Bacterial Cell. *Curr Biol* 19: 812.
100. R. Hallez, A. Bellefontaine, J. Letesson, X. De Bolle (2004) Morphological and functional asymmetry in alpha-proteobacteria. *Trends Microbiol* 12: 361.
101. K. Young (2010) Bacterial shape: two-dimensional questions and possibilities. *Annu Rev Microbiol* 64: 223.
102. F. Trueba (1982) On the precision and accuracy achieved by *Escherichia coli* cells at fission about their middle. *Arch Microbiol* 131: 55.

103. E. Katzmann *et al.* (2011) Magnetosome chains are recruited to cellular division sites and split by asymmetric septation. *Mol Microbiol* 82: 1316.
104. A. B. Lindner, R. Madden, A. Demarez, E. J. Stewart, F. Taddei (2008) Asymmetric segregation of protein aggregates is associated with cellular aging and rejuvenation. *Proc Natl Acad Sci* 105: 3076.
105. S. Klumpp, D. Faivre (2012) Interplay of Magnetic Interactions and Active Movements in the Formation of Magnetosome Chains. *PLoS ONE* 7: e33562.
106. S. Wang, L. Furchtgott, K. C. Huang, J. W. Shaevitz (2012) Helical insertion of peptidoglycan produces chiral ordering of the bacterial cell wall. *Proc Natl Acad Sci* 109: E595.
107. S. Pichoff, J. Lutkenhaus (2005) Tethering the Z ring to the membrane through a conserved membrane targeting sequence in FtsA. *Mol Microbiol* 55: 1722.
108. M. A. Williams (1959) Cell elongation and division in *Spirillum anulus*. *J Bacteriol* 78: 374.
109. H. Erickson (1997) FtsZ, a tubulin homologue in prokaryote cell division. *Trends Cell Biol* 7: 362.
110. J. F. Allard, E. N. Cytrynbaum (2009) Force generation by a dynamic Z-ring in *Escherichia coli* cell division. *Proc Natl Acad Sci* 106: 145.
111. V. Shcherbakov, M. Winklhofer, M. Hanzlik, N. Petersen (1997) Elastic stability of chains of magnetosomes in magnetotactic bacteria. *Eur Biophys J* 26: 319.
112. C. Lefèvre, A. Bernadac, K. Yu-Zhang, N. Pradel, L.-F. Wu (2009) Isolation and characterization of a magnetotactic bacterial culture from the Mediterranean Sea. *Environ Microbiol* 11: 1646.
113. M. Sato, T. Nishikawa, H. Kajitani, S. Kawano (2007) Conserved relationship between FtsZ and peptidoglycan in the cyanelles of *Cyanophora paradoxa* similar to that in bacterial cell division. *Planta* 227: 177.
114. Q. Wang, C. P. Mercogliano, J. Löwe (2011) A Ferritin-Based Label for Cellular Electron Cryotomography. *Structure* 19: 147.
115. A. Bernadac, M. Gavioli, J. C. Lazzaroni, S. Raina, R. Lloubès (1998) *Escherichia coli* tol-pal mutants form outer membrane vesicles. *J Bacteriol* 180: 4872.
116. D. Faivre, L. H. Böttger, B. F. Matzanke, D. Schüler (2007) Intracellular magnetite biomineralization in bacteria proceeds by a distinct pathway involving membrane-bound ferritin and an iron(II) species. *Angew Chem Int Ed Engl* 46: 8495.

117. B. Devouard *et al.* (1998) Magnetite from magnetotactic bacteria: Size distributions and twinning. *Am Mineral* 83: 1387.
118. J. D. Tucker *et al.* (2010) Membrane invagination in *Rhodobacter sphaeroides* is initiated at curved regions of the cytoplasmic membrane, then forms both budded and fully detached spherical vesicles. *Mol Microbiol* 76: 833.
119. W. B. Schofield, H. C. Lim, C. Jacobs-Wagner (2010) Cell cycle coordination and regulation of bacterial chromosome segregation dynamics by polarly localized proteins. *EMBO J* 29: 3068.
120. R. Kasper, B. Huang (2011) SnapShot: Light microscopy. *Cell* 147: 1198.e1.

Acknowledgements

There are a couple of colleagues I would like to thank for guiding me through these inspiring years of my Ph.D. work. However, first of all I would like to thank *Magnetospirillum gryphiswaldense* for still fascinating me and by that being the motivation to perform this study.

That I was able to work with *M. gryph.* is due to my supervisor Prof. Dirk Schüler and I am deeply grateful for his support, advice and the scientific freedom he gave me during my work. Not to mention the invaluable discussions and one or the other sausage during the summer BBQs in his garden.

Lots of credit is given to my 2nd lab and collaborators at the Max Planck Institute of Biochemistry in the department for Molecular Structural Biology of Prof. Wolfgang Baumeister and in particular to Dr. Jürgen M. Plitzko for giving me the chance to perform cryo-electron tomography in the 'bunker' and valuable discussions together with the 'fairy godmother' Günter Pfeifer and my helpful colleagues Manuela Gruska, Stefan Bohn, Lars-Anders Carlson and Matthias Eibauer.

Dr. Michael Winklhofer who introduced me to the physical aspects of magnetotactic bacteria from the Geophysics of the LMU owes my sincere gratitude.

Next I would like to thank the thesis committee, especially Prof. Dr. Marc Bramkamp for being the second examiner of this thesis.

Of course this work would have been only half as fruitful without the former and current colleagues of the 'Magnetolab' and for all the fun we had in- and outside the lab. Especially I would like to thank André Scheffel, who convinced me to do this Ph.D. work. Thanks also goes to René, Claus and Felix in terms of scientific and non-scientific aspects (e.g. 2nd price at the Kicker tournament or regular mountaineering in the alps).

Last but not least I would like to thank my parents, who fully understand my scientific work, Helena and Georg for bringing me back down to earth on a regular basis.

Eidesstattliche Erklärung

Hiermit erkläre ich an Eides statt, dass die vorliegende Dissertation von mir selbständig und ohne unerlaubte Hilfe angefertigt wurde. Des weiteren erkläre ich, dass ich nicht anderweitig ohne Erfolg versucht habe, eine Dissertation einzureichen oder mich der Doktorprüfung zu unterziehen. Die vorliegende Dissertation liegt weder ganz, noch in wesentlichen Teilen einer anderen Prüfungskommission vor.

Emanuel Katzmann, München